

Some Notes on Neurovascular Coupling Models

Tim David

December 4, 2015

0.1 NVU Version control details

- version 1.0: Farr and David [21]
- version 1.1: above + Dormanns et al [14],[15]**STABLE VERSION**
- version 1.11: version 1.1 + astrocytic Ca^{2+} + EET (mediation of BK channel) pathway **NOT YET IMPLEMENTED** but is a topic branch
- version 1.12: version 1.11 + TRPV4 channel **NOT YET IMPLEMENTED** but is a topic branch

it is not yet clear whether the work by de Ruijter in developing the TRPV4 includes VOCCs. We have never had VOCCs in the astrocyte. The astrocytic membrane potential is generated by the GHK equation rather than an o.d.e. Additionally the figure showing the model does NOT include the EET pathway.

- version 1.2: version 1.12 plus nitric oxide model **NOT YET IMPLEMENTED**

up to this point NVS versions exist beyond which we will need to put code through NVS

- version 2.0: Elshin/Chang model of neuron and extracellular space **NOT YET IMPLEMENTED**

check Elshin's model coupled with correct version 1.1

- version 2.1: version 2.0 + neuron Ca^{2+}
- version 2.2: version 2.1 + version 1.2 **NOT YET IMPLEMENTED**

0.2 parBRAIN Version control details

- version 1.0: Simple NVU (variation of CO_2 by modulation of the metabolic rate)
- version 1.1: NVU version 1.1 without diffusion (**published in Frontiers**) **MASTER Branch**
- version 1.11: above plus diffusion in the PVS only **topic branch**
- version 1.12: version 1.11 + nitric oxide
- version 2.0: NVU version 2.0 model into parBRAIN using NVS.**NOT YET IMPLEMENTED**
- version 2.1: diffusion in ECS **NOT YET IMPLEMENTED**

Todo list

it is not yet clear whether the work by de Ruijter in developing the TRPV4 includes VOCCs. We have never had VOCCs in the astrocyte. The astrocytic membrane potential is generated by the GHK equation rather than an o.d.e. Additionally the figure showing the model does NOT include the EET pathway.	1
up to this point NVS versions exist beyond which we will need to put code through NVS	1
check Elshin's model coupled with correct version 1.1	1
Tests need to be made which determine whether this shift is important or not	5
need to check if the VOCCs are modelled. If not then we need to do it	13
the results in the figures seem to be in contrast to the text. Joerik states that the constant nernst potential model is best for astrocytic Ca^{2+} and the figures show that the conductance of the TRPV4 channel is a sensitive parameter. However there are no results which indicate whether a reduction/increase in Ca^{2+} produces a corresponding dilation/constriction in the perfusing radius.	13
ref needed here for the book chapter from which the model has been taken	14
equations required here	14
look at paper by Andrews et al [2] and [1] for experimental evidence on endothelial NO production.	21
up to this point NVS versions exist beyond we will need to put code through NVS	25
has the above been implemented in the nitric oxide model ?	26
check Elshin's model coupled with correct version 1.1	26
need to explain the difference between extracellular space and synaptic cleft	26
check dilation dynamics of ver 2.0 are the same compared to ver 1.2 . . .	27
what is the nernst potential at this stage for potassium?	32
need Chang reference	32
need to define a proper link for the $[\text{ion}]_e$ conservation equation now that the buffer term is not needed	32
proper oxygen model that fits with Cloutier is crucial see section 2.2.1 and section 1.4	34
black-box Beard and link to Cloutier or black-box Cloutier and link to Beard	35

email sasha.bulik@charite.de for the code	35
look at integrating mitochondrial models into a single model linked with	
NVU	35
need to find this reference	38
can we use this, by implementing a spatially averaged value of concentra-	
tions in the NVU model?	41
can we use the method of [?] to model slow disease states such as plaque	
growth and Alzheimer's?	43
What is the fast variable in Alzheimer's?	43
put in details of Berwick lab	46
look at GABA interneurons and the glutamatergic pyramidal neurons	
forming a COX-1 type pathway via AA and EETs. In contrast to	
the K ⁺ pathway that we currently support.	47
Rejuvinate the BACE1/hypoxic hypothesis for another HRC grant appli-	
cation	49
investigate energy model of mitochondrial oxygen consumption of [?]	
perhaps we should compare with the model of ?]	49

Chapter 1

NVU

1.1 Background

Latest version Functional hyperemia is an important metabolic autoregulation mechanism by which increased neuronal activity is matched by a rapid and regional increase in blood supply. This mechanism is facilitated by a process known as ‘neurovascular coupling’, the orchestrated communication system involving neurons, astrocytes and arterioles. Over the past five years the Canterbury group has developed an increasingly complex model of neurovascular coupling. This started with the work of Hannah Farr [21] and it has been updated with the work of Dormanns et al [14]. These notes are intended to document historical and future development.

1.1.1 some general references

The following are some papers that those of us have either forgotten how things work or we are new to the area **should read !** [29], [24], [23], [22], [?], [? 40], [71] and of course [35]. A review article looking at the blood brain barrier dysfunction as a cause of Alzheimer’s is well worth reading [19].

1.2 Model version 0

This model was based on the work of Farr and David [21] who investigated the experiments and hypothesis of Filosa and other workers [22]. The model is a compartmental one where neuron, astrocyte and coupled smooth muscle and endothelial cell make up the full model. Here the basic premise was that neuronal activity mediated glutamate release into the synaptic cleft. The mGluR receptors release via the membrane bound G-protein phospholypase C and subsequently IP₃. The IP₃ receptors on the sarcoplasmic reticulum in the astrocyte release cytosolic Ca²⁺. Increased concentration of cytosolic Ca²⁺ mediates the EET pathway. In addition the Na/K ATPase pump allows synaptic cleft K⁺ to

be pumped into the astrocyte. Both K^+ and EET mediate the opening of the BK ion channel situated on the end feet of the astrocyte which is adjacent to the perivascular space. This space divides the end feet from the SMC. K^+ in the PVS allows the opening of the inwardly rectified K^+ ion channel situated on the SMC (in contrast to the model of Koenigsberger et al [46] which did not include a K_{IR} channel). The pathways are shown schematically in Figure 1.1. The dilation/contraction of the arteriole is determined by using the model of Hai and Murphy [35] and second order o.d.e modelling the mass acceleration of a unit mass of vessel tissue. The acceleration term is small and neglected (this means that one boundary condition is not able to be specified). The force produced by the phosphorylated myosin and activated phosphorylated myosin provides data for the Young's modulus of the tissue. The model successfully accounts for several observations seen in experiment. The model is capable of simulating the approximate 15% arteriolar dilation caused by a 60-s neuronal activation (modelled as a release of potassium and glutamate into the synaptic cleft). This model also successfully emulates the paradoxical experimental finding that vasoconstriction follows vasodilation when the astrocytic calcium concentration (or perivascular potassium concentration) is increased further. It is suggested that the interaction of the changing smooth muscle cell membrane potential and the changing potassium-dependent resting potential of the K_{IR} channel are responsible for this effect. Finally, the model demonstrates that a well controlled mechanism of potassium buffering is potentially important for successful neurovascular coupling.

1.2.1 Notes

This model was successful but fairly simple. Indeed the neuron model was non-existent and only relied on synaptic K^+ release and the action of mGluR to provide Ca^{2+} and EET concentrations in the astrocyte. K^+ concentration was not considered in the astrocyte as it was deemed that influx at the "head" was balanced by efflux at the "feet" with the BK channel. VOCCs are not modelled for the astrocyte [7]

There is a pump in the astrocyte and Ca^{2+} in the ER was obtained by allowing the rate of change of cytosolic Ca^{2+} to be equal and opposite to the store Ca^{2+} (with a volume change variable to maintain proper concentration). EET was assumed to "shift" the equilibrium state of the open probability for the BK channel. A simple shift to the membrane potential component of the equilibrium was used. This is based on experiments from Lu et al [?] where a variation in EET derived DHET provided a proportional variation in the half-maximal probability. It is noted that the DHET concentration was very small (of the order of 5 nM).

Tests need to be made which determine whether this shift is important or not

The K_{IR} channel's Nernst potential is a function of extracellular potassium

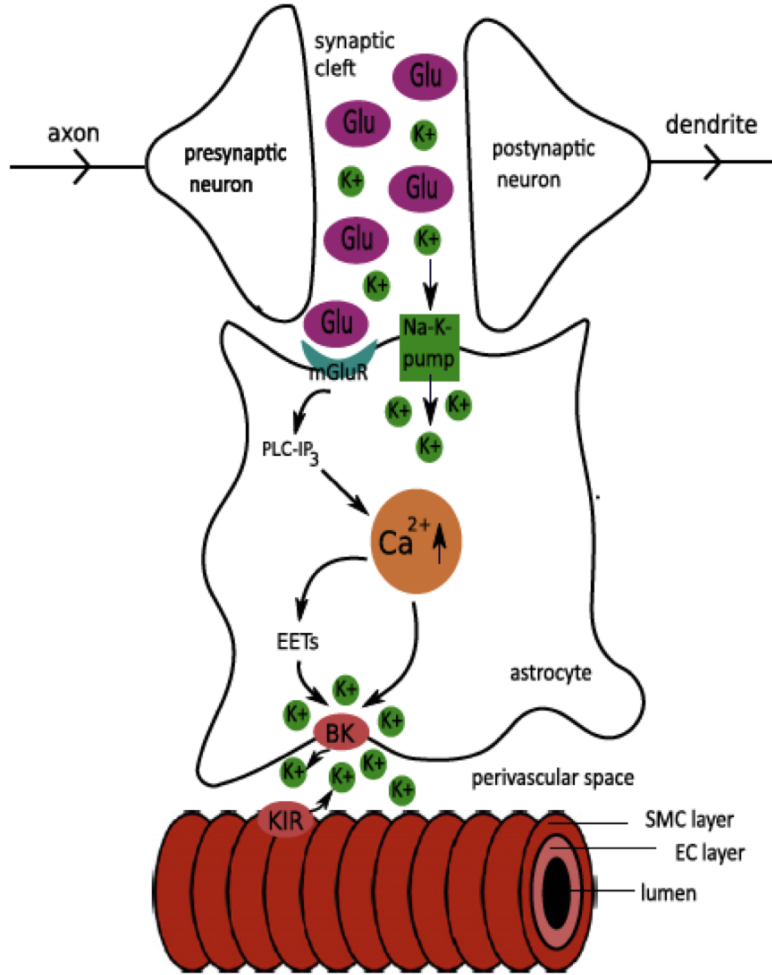


Figure 1.1: Overview of the complete NVC Model due to Farr and David [21].

(in this case the concentration in the PVS), Farr and David modelled it using the data from Quayle et al [?] as a log/linear relationship. The maximum conductance of the channel was a simple square root function of extracellular K^+ . This would be changed in version 1.0 (see section 1.3).

The dilation took some time to reach peak value of radius change. This was thought to be due to the reaction constants for the Hai and Murphy model.

Although the results were encouraging in comparison with the experimental data of Edwards [18] they were qualitative at best. Increasing perivascular potassium did reverse the dilation but the figures in the paper seemed contradictory. For example Figure 2 shows a change in perivascular potassium from 4.2 to 5.2 mM and the corresponding radius changes from 16 to approximately

20 μ m. Yet Figure 4 shows that changes in radius only occur for potassium concentrations of 8 mM and above.

1.3 Versions 1.*

1.3.1 version 1.0:

Farr and David [21]

After much discussion it was decided to completely rebuild NVU with new neuron and astrocyte models based on the work of Ostby et al [57]. A schematic of the pathways is given in Figure 1.2. As in version 0 the model did not include any detail in the internal concentrations of ions etc in the neuron but simply a release of K⁺ and Na⁺ into the synaptic cleft and its re-distribution back to the neuron via the NaKATPase pump. The time-dependent input for the neuronal activity is treated as a pulse like release of K⁺ into the synaptic cleft and a simultaneous equal influx of Na⁺ from the neuron following activity using an input signal, f(t). In contrast to Farr and David conservation equations are developed in the astrocyte and the SMC and ECs for K⁺, Na⁺, Cl and HCO₃. All Nernst potentials for the K⁺, Na⁺, Cl and HCO₃ channels are log functions of the ratio of external to internal concentrations where the external concentration is defined as the concentration in the synaptic cleft. This is important as the concentrations in the cleft vary over time and especially when the neuron is active.

One of the main questions that this model version answered was whether Ca²⁺ was a necessary and sufficient component for neurovascular coupling as proposed by [22, 24]. The model utilises only the K⁺ pathway, excluding both Ca²⁺ and the subsequent AA/EET/20-HETE components in the astrocyte. The second question related to the possible action of ATP as an agonist in flowing blood on the endothelium and smooth muscle cells. Experiments indicated that the P2Y receptor on the luminal side of the endothelium would, if activated by ATP, mediate the production of IP₃ in the endothelial cell. IP₃ flowing through the myo-endothelial gap junction into the SMC will allow cytosolic Ca²⁺ to be released from the SR. Due to the calcium dependent receptors on the SR the cytosolic Ca²⁺ will mediate further release of Ca²⁺ into the cytosol, a process known as calcium induced calcium release (CICR) [31]. Results showed that this effect was dramatic and the paper by Dommanns et al. [15] indicated that increased reaction of ATP on the endothelial surface reduced the dilation of the perfusing arteriole due to the SMC oscillating and providing an increased average value of Ca²⁺.

It should be noted that work by ?] showed that the purinergic G protein-coupled receptor P2Y was **not** expressed in cerebral endothelial cells but were expressed at the "glio-vascular interface" (not really sure what the authors meant by this or how the glio-vascular interface was defined). In addition from immunolabelling experiments by the same group showed that the connexin Cx43 was strongly expressed at the end feet of astrocytes.

1.3.2 Notes

Again as in version 0 the model is based on a compartment system with seven compartments as shown in 1.2. A BK channel was added to the Ostby model of the astrocyte providing a flux of K^+ into the perivascular space. This channel is formulated on the basis of the work by [32] with the Nernst potential of the channel a function of the ratio of internal to external K^+ along with the equilibrium of the open probability and characteristic time constant functions of the membrane potential v_k , which in contrast to [21] is independent of Ca^{2+} . It is assumed that the external $[K^+]_e$ is a constant. Importantly because the model does not include Ca^{2+} there is no sarcoplasmic reticulum. This will be included in version 1.1 (see section 1.3.3).

Luminal agonists acting on P2Y receptors on the endothelial cell surface provide a flux of IP_3 into the endothelial cytosol. This concentration of IP_3 is transported via gap junctions between endothelial and smooth muscle cells providing a source of sarcoplasmic derived Ca^{2+} in the smooth muscle cell. The model is able to relate a neuronal input signal to the corresponding vessel reaction. Results indicate that blood flow mediated IP_3 production via the agonist ATP has a substantial effect on the contraction/dilation dynamics of the SMC. The resulting variation in cytosolic Ca^{2+} can enhance and inhibit the flow of blood to the cortical tissue. IP_3 coupling between endothelial and smooth muscle cells seems to be important in the dynamics of the smooth muscle cell. The VOCC channels are, due to the hyperpolarisation from K^+ SMC efflux, almost entirely closed and do not seem to play a significant role during neuronal activity. The current model shows that astrocytic Ca^{2+} is not necessary for neurovascular coupling to occur in contrast to a number of experiments outlining the importance of astrocytic Ca^{2+} in NVC, however this Ca^{2+} pathway is not the only one mediating NVC. Importantly agonists in flowing blood have a significant influence on the endothelial and smooth muscle cell dynamics.

1.3.3 version 1.1:

Dormanns et al [14],[15] this is the **STABLE VERSION**

1.3.4 version 1.11:

version 1.1 + astrocytic Ca^{2+} + EET (mediation of BK channel) pathway

NOT YET IMPLEMENTED but is a topic branch

For this version the model contains the Ca^{2+} pathway originally developed by [21] in addition to the K^+ in the astrocyte. The astrocyte (AC) model contains different types of active and passive ion channels. These ion channels and pumps are captured in a set of differential equations to describe the conservation of mass for the corresponding species concentrations in the SC, the AC and the PVS. The ion channels for potassium (J_{KCC1} , J_{NKCC1} , J_K , J_{NaK} and J_{BK}), sodium (J_{NBC} , J_{NKCC1} , J_{NaK} and J_Na), chloride (J_{KCC1} , J_{NKCC1} and J_{Cl})

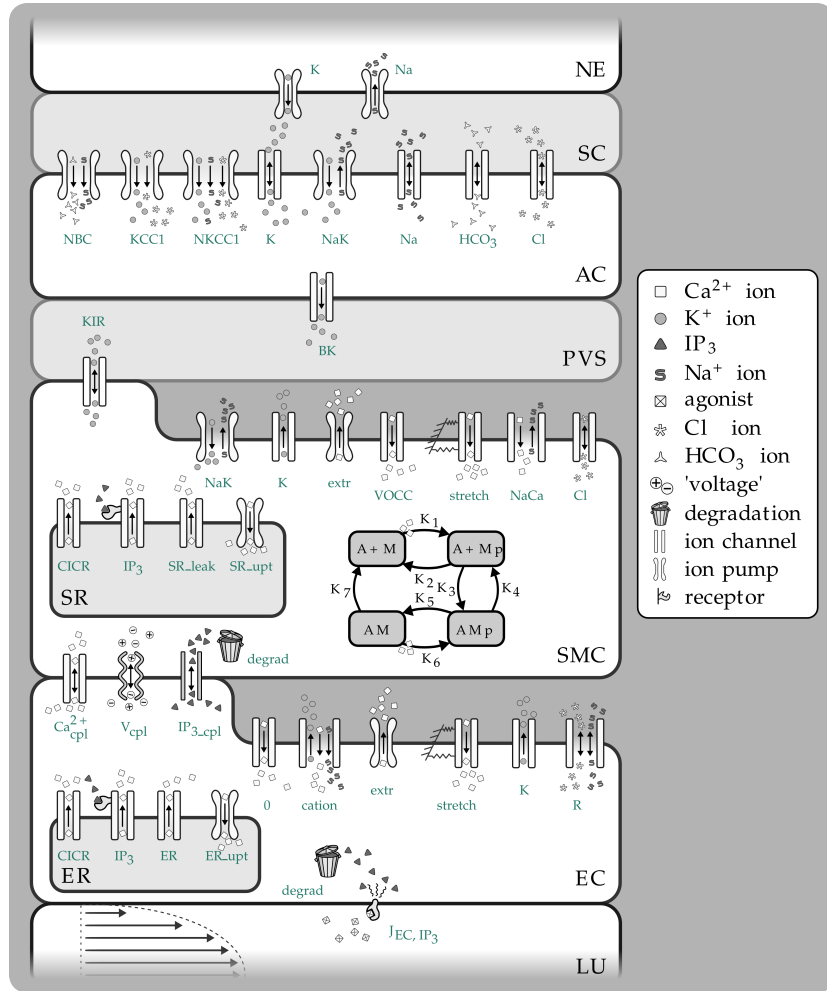


Figure 1.2: Overview of the complete NVC Model of version 1.0 including all subsystems. Abbreviations: NE - Neuron, SC - Synaptic cleft, AC - Astrocyte, PVS - Perivascular space, SMC - Smooth muscle cell, SR - Sarcoplasmatic reticulum, EC - Endothelial cell, ER - Endoplasmatic reticulum, LU - Lumen. NBC - Sodium bicarbonate pump, KCC1 - Potassium chloride cotransporter pump, NKCC1 - Sodium potassium chloride cotransporter pump, BK - Large conductance potassium channel, VOCC - Voltage-operated calcium channel, CICR - Calcium induced calcium release channel, R - Residual current regrouping channel, K₁ - K₇ - reaction rate constants, M - free nonphosphorylated cross bridges, Mp - free phosphorylated cross bridges, AMP - attached phosphorylated cross bridges, AM - attached dephosphorylated latch bridges.

and bicarbonate (J_{HCO_3}) are included. Note that the bicarbonate and chlorine fluxes are coupled with the Na⁺ and K⁺ fluxes to obtain a neutral in- or efflux

membrane voltage-wise.

The release of glutamate from the neuron in the synaptic cleft is simulated by creating a smooth pulse function ρ that describes the ratio of bound to total glutamate receptors on the synapse end of the astrocyte. This induces an IP_3 release into the cell, causing the release of Ca^{2+} from the ER into the cytosol, which then leads to the production of EET. The K^+ release into the PVS is controlled by the BK-channels. The opening of the BK-channels is regulated by the membrane voltage, as well as the EET and Ca^{2+} concentration. Figure 1.3 shows the whilst Figure 1.4 shows the full model.

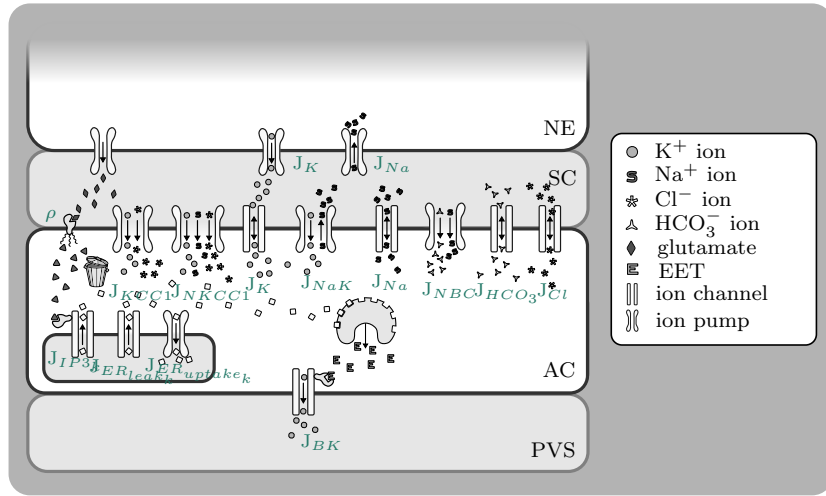


Figure 1.3: Overview of the Astrocyte ion channels showing additional Ca^{2+} and EET pathways which mediate the BK K^+ channel.

Results from this model indicate a similar profile to that found in version 1.0 however, when the neuronal pulse stops the flux through the BK potassium channel on the astrocyte is reduced compared to version 1.0 . The flux in the K_{IR} channel on the SMC is larger due to the increased K^+ in the PVS. This leads to a variation in the radius profile. Figure 1.5 shows the BK potassium channel flux, Figure 1.6 the flux in the K_{IR} and Figure 1.7 the radius profile. All Figures compare version 1.0 and 1.1 . In the original Farr and David model [21] the BK channel equation for the equilibrium open probability was given as

$$n_\infty = \frac{1}{2} [1 + \tanh(\frac{v + eet_{shift}[EET] - v_3}{v_4})] \quad (1.3.1)$$

$$v_3 = -\frac{v_5}{2} \tanh(\frac{[Ca] - Ca_3}{Ca_4}) + v_6 \quad (1.3.2)$$

Hence the BK channel is mediated by both EET and Ca^{2+} . In version 1.0 no Ca^{2+} was present hence the equilibrium value needed to be altered and this is

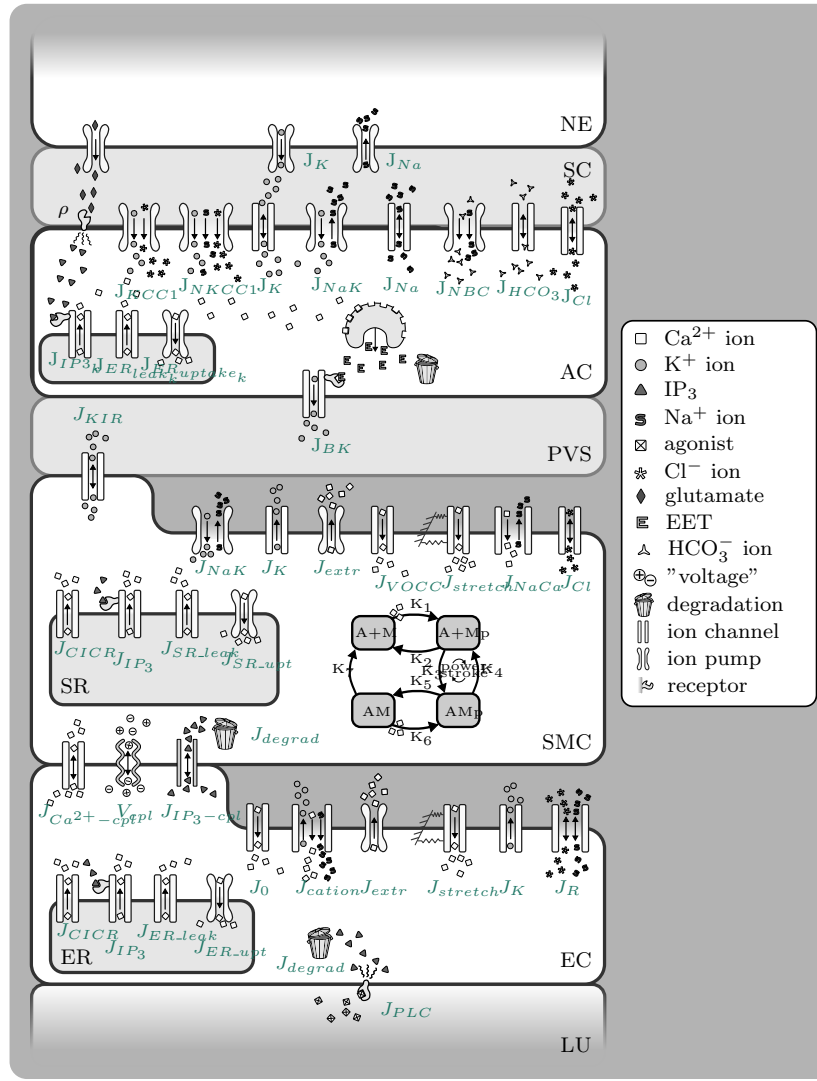


Figure 1.4: Overview of the version 1.1 model showing the glutamate influx into the SC.

given below.

$$n_\infty = \frac{1}{2} [1 + \tanh(\frac{v + v_6}{v_4})] \quad (1.3.3)$$

$$v_6 = 22mV \quad (1.3.4)$$

Results comparing the version 1.0 with version 1.1 shows that $v_3 \ll v_6$. The lower value therefore induces the BK channel to close earlier and leave an increased amount of potassium in the PVS. It should also be noted that the time

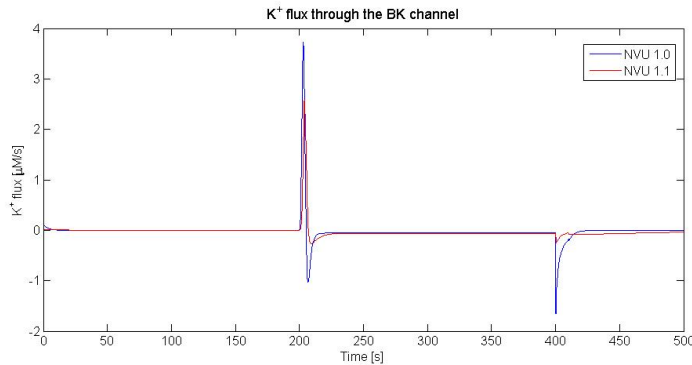


Figure 1.5: Comparison of versions 1.0 and 1.1 for the astrocyte BK channel

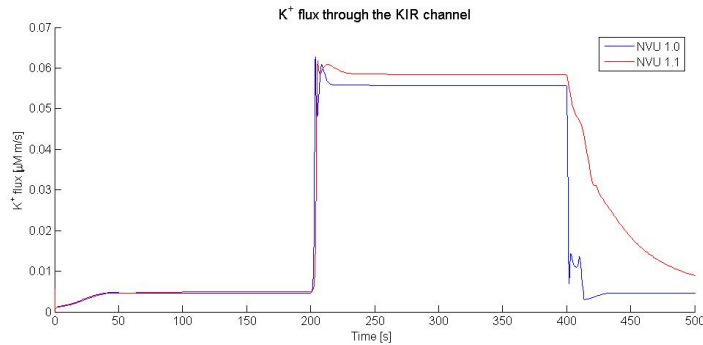


Figure 1.6: Comparison of versions 1.0 and 1.1 for the astrocyte K_{IR} channel

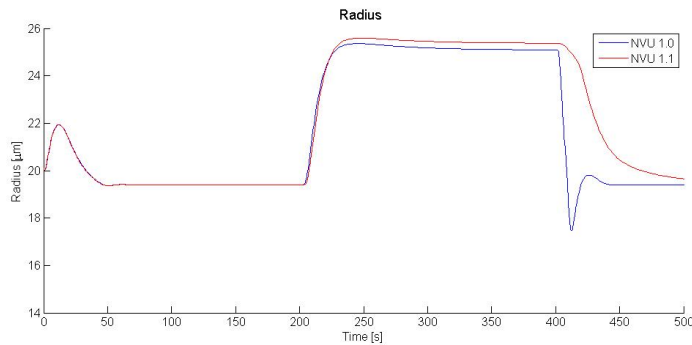


Figure 1.7: Comparison of versions 1.0 and 1.1 for the radius change during neuronal activation

constants for the channel opening/closing are different for the different models

since for version 1.0 (i.e.no astrocytic Ca^{2+}) we have

$$\phi_w = \cosh\left(\frac{v + v_6}{2v_4}\right) \quad (1.3.5)$$

with $v_6 = \text{constant}$, whereas for version 1.1 we have that

$$\phi_w = \cosh\left(\frac{v + v_3}{2v_4}\right) \quad (1.3.6)$$

with v_3 a function of Ca^{2+} . It is interesting to note that Ca^{2+} is not a necessary condition for neurovascular coupling as stated by Filosa [22] (see the work of Nizar et al. [56]), however their group did then indicate the importance of K^+ [23].

Lastly in this section work by Hadfield et al. [33] utilised the paper of Rzegalinski et al. [60] to model the role of arachidonic acid in the pathway towards the production of EET and 20-HETE from Ca^{2+} . Harder et al. [38] looked at (a review of) the role of cytochrome P450 enzymes as part of the pathway to EET and 20-HETE.

1.3.5 version 1.12:

version 1.11 + TRPV4 channel **NOT YET IMPLEMENTED** but is a topic branch

this work has been implemented by Jeorik de Ruijter as part of his internship in 2015

His report can be found in Appendix A Experiments by Dunn et al. [17] seemed to show that TRPV4 ion channels produced enhanced Ca^{2+} concentrations in the endfeet of astrocytes and in contrast to Tran et al. [65] amplifies the neurovascular coupling response. Furthermore, previous work by Girouard et al. [30] indicated that the K^+ ion BK channel was mediated by astrocytic "endfoot" Ca^{2+} and that increasing Ca^{2+} caused a reversal of dilation to constriction. it is unknown at present whether NVU version 1.1 can show this. Work by intern Joerik de Ruijter (during first half of 2015) has produced a model which models the constriction/dilation experimental results of [17]. At the moment this has yet to be integrated into NVU. We will use the newly developed NVS code to produce both Matlab and C for the integration of Joerik's work into NVU. This will be NVU version 1.2.

need to check if the VOCCs are modelled. If not then we need to do it

the results in the figures seem to be in contrast to the text. Joerik states that the constant nernst potential model is best for astrocytic Ca^{2+} and the figures show that the conductance of the TRPV4 channel is a sensitive parameter. However there are no results which indicate whether a reduction/increase in Ca^{2+} produces a corresponding dilation/constriction in the perfusing radius.

Interestingly increasing PVS K^+ as we know induced both dilation and constriction however the evidence from [30] indicated that when the K_{IR} channel

was blocked by Ba^{2+} it removed the dilation but not the constriction. **what was causing the constriction?**. It is suggested that the "switch" is based on both "endfoot" Ca^{2+} and PVS K^+ . Suppose a K^+ such that in normal circumstances it induces a dilation then blocking that particular BK channel changes a dilation to a constriction via the astrocytic "endfoot" Ca^{2+} . There is some experiemntal data in [30] (see Figure 3B) with which we can compare our own dilation/constriction (as a function of ECS K^+) see Figure 7 in [14].

ref needed here for the book chapter from which the model has been taken

equations required here

Myoendothelial feedback

Tran et al. [65] hypothesised the existence of feedback between the SMC contraction and the EC. The proposed feedback pathway on the activation of the SMC contraction is such that the depolarisation of the SMC induces IP_3 whihc crosses the myoendothelial gap junction and triggers Ca^{2+} release from IP_3Rs . The resulting Ca^{2+} activate Ca^{2+} -mediated $IK K^+$ channels resulting in hyperpolarisation and a reduction in the contraction.

This process seems to have a number of problems. Firstly it assumes that the SMC contraction is done without any EC influence, i.e. that the contraction is triggered by agonists in the ECS. How this comes about is unclear. Secondly the hyperpolarisation of the SMC is done via some form of voltage gap junction. Yet membrane voltage variations in space can only occur if there is ion movement from one cell to another. How or what ions move is unclear.

1.3.6 version 1.2:

version 1.12 plus nitric oxide model NOT YET IMPLEMENTED

A model of NO production from both neuron and endothelial cell is now available. Experimental work by Andrews et al [2] shows the importance of stress induced NO production and its dependence on ATP autocrine signaling and CCE. This work can provide some validation data. Figure 11 in the paper also provides a possible pathway that our model has yet to look at (although we may have already done this !). In addition the same group [1] has provided experimental data that our model needs to utilise. **this work has been submitted to the Journal of Theoretical Biology** basic method is set out below

1.3.7 Model Development

The potential of NO as an important vasodilating messenger molecule is assessed using a holistic mathematical model that includes the dynamics of NO in the NVU. With the help of this model the most crucial signalling pathways are

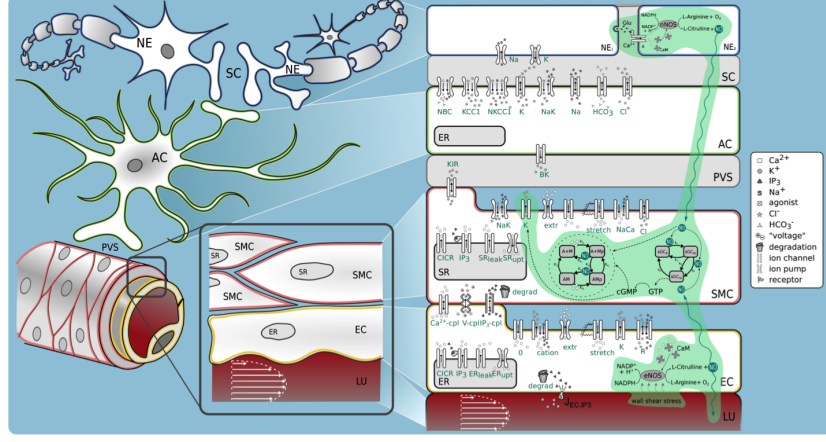


Figure 1.8: Overview of the complete NVC Model of version 1.0 with NO pathway.

analysed and the influence of NO in NVC investigated, including the localisation of the main contributing source.

Therefore, our previous foundation NVU model [21, 14] is extended by mathematical equations that represent production, diffusion and consumption of NO in different cell types, as well as the interaction of NO with other biochemical species and ion channel open probabilities.

As in the previous models of an NVU [21, 14] we divide the full model into seven compartments: the neuron (NE), the synaptic cleft (SC), the astrocyte (AC), the perivascular space (PVS), the smooth muscle (SMC) and endothelial (EC) compartments and the arteriolar lumen (LU). Connectivity is provided by inputs and outputs in form of values or time-dependent functions for ion fluxes, membrane potential and ion channel open probability of each of the compartments which act as a coupling between them.

Our NO model focusses on the NO production by the two constitutive isoforms of nitric oxide synthase, nNOS and eNOS [26]. Both enzymes' activation is mediated by intracellular Ca^{2+} in the NE and EC, respectively. In addition, eNOS gets activated by blood flow induced wall shear stress in the cerebral arterioles [42]. Due to its high diffusion coefficient NO diffuses rapidly into other compartments, shown in experiments [52] and in kinetic simulations [49, 48]. When NO reaches the SMC it interacts with intracellular enzyme activation and regulates SMC relaxation[69].

A schematic representation of the compartments and the NO signalling pathway in the NVU is given in Figure 1.9, reaching from its synthesis in the NE and the EC to the relaxation of the SMC.

The dynamics of NO in the involved compartments are mathematically described using mass balance formulations. Like this, the concentration of NO in each domain is determined by the production $P_{NO,m}$, subtracted with the

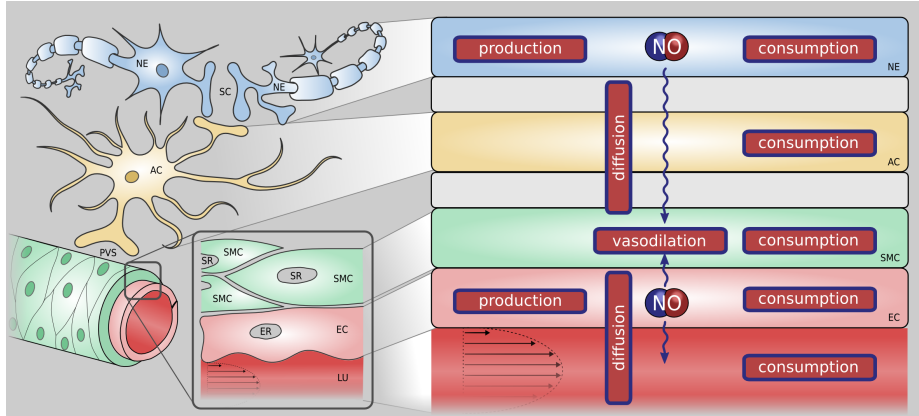


Figure 1.9: NO signalling pathway in NVC. NO is produced in the neuron (NE) and the endothelial cell (EC) and diffuses into other compartments, where it gets consumed by chemical reactions. In the smooth muscle cell (SMC) it leads to relaxation and therefore vasodilation. SC - Synaptic cleft, AC - Astrocyte, ER - Endoplasmic reticulum, PVS - Perivascular space, SR - Sarcoplasmic reticulum, LU - Lumen.

consumption $C_{NO,m}$ within the cell, i.e. the reaction with oxygen or other molecules, and the diffusion $D_{NO,m}$ from and into other compartments.

The NO concentration $[NO]_m$ is given by the solution of the following generic first-order non-linear differential equation:

$$\frac{d[NO]_m}{dt} = P_{NO,m} - C_{NO,m} + D_{NO,m}, \quad (1.3.7)$$

where $m \in \{n, k, i, j\}$ notates the cell indices for NE, AC, SMC and EC, respectively.

1.3.8 NO Production

The production rate of NO is dependent on the concentration of activated nitric oxide synthase. L-Arginine (L-Arg), oxygen (O_2) and nicotinamide adenine dinucleotide phosphate (NADPH) are the biochemical substrates needed for the NO production [9], where L-Arg is the requisite and sole nitrogen donor [28]. L-Arg is oxidized to L-Citrulline and the biochemical reaction leads to the production of $NADP^+$, water and NO. This five-electron oxidation reaction takes place in two steps, the overall stoichiometric chemical formula reads as follows:



For the reaction several biomolecule cofactors such as flavin mononucleotide (FMN), flavin adenine dinucleotide (FAD) and tetrahydrobiopterin (H_4B) are needed.

Constitutive NOS isoforms, nNOS, and eNOS, are thought to be the most influential NO producers and are critical for maintenance of homeostasis [26, 28]. On the basis of this we consider NEs and ECs as most influential producers of NO and assume no production in other cell types, therefore $P_{NO,k}$, $P_{NO,i} = 0$.

Neuronal NO Production

NO synthesis in the NE is catalysed by nNOS in response to glutamate-induced calcium influx into the post-synaptic neuron. An overview of the model detail is given in Figure 1.10.

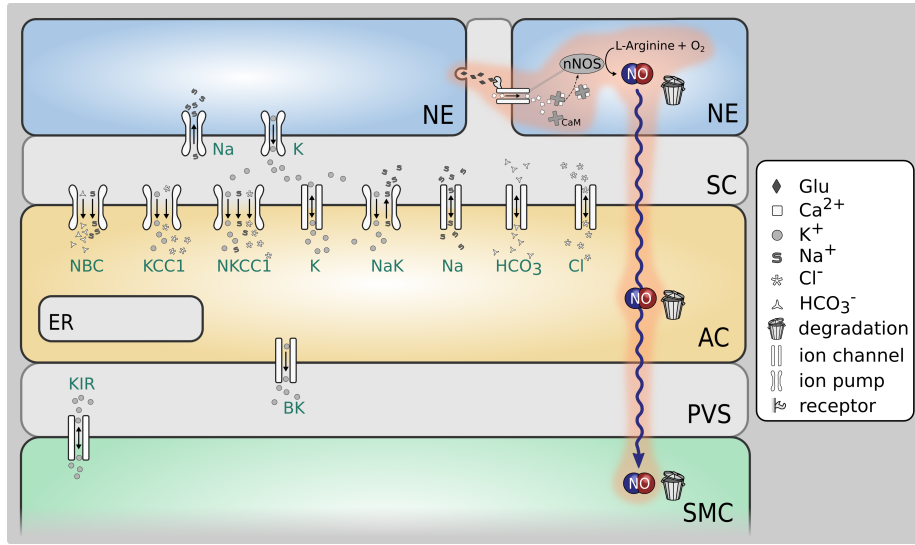


Figure 1.10: Graphical representation of the mathematical model, detail. The biochemical reaction that produces NO in the NE is catalysed by the enzyme nNOS and depends on the available concentration of L-Arg and O_2 . The model addition to our previous foundation model [14] is highlighted in orange. NE - Neuron, SC - Synaptic cleft, AC - Astrocyte, PVS.

The NO production in the NE depends on the amount of activated nNOS [$nNOS_{act}$] [27], whose catalytic activity is sensitive to the availability of the substances O_2 and L-Arg [9]. We express it mathematically as

$$P_{NO,n} = P_{max} \frac{[O_2]_n}{K_{m,n}^{O_2} + [O_2]_n} \frac{[L\text{-Arg}]_n}{K_{m,n}^{L\text{-Arg}} + [L\text{-Arg}]_n}, \quad (1.3.8)$$

where P_{max} is the maximum neuronal production rate and given by

$$P_{max} = V_{NO,n_{max}} [nNOS_{act}], \quad (1.3.9)$$

with the maximum nNOS catalytic rate $V_{NO,n_{max}}$ and the neuronal O_2 and L-Arg concentrations, $[O_2]_n$ and $[L\text{-Arg}]_n$, respectively. $K_{m,n}^{O_2}$ and $K_{m,n}^{L\text{-Arg}}$ are

the associated Michaelis constants [9, 10].

The nNOS activation in the NE is triggered by the chemical neurotransmitter glutamate (Glu) in response to neuronal activation. In a chemical synapse, when an action potential reaches the axon terminal of the presynaptic NE, it allows the release of Glu from vesicles into the synaptic cleft (SC) which then binds to Glu-sensitive receptors of the postsynaptic NE's dendrite and is subsequently removed from the synaptic cleft by diffusion and hydrolysis [45].

As a stimulation input to the model we give a Glu concentration of $[2] \times 10^{-6}$ mol/m³ in the SC during neuronal activation. Before and after stimulation we assume a zero value of $[\text{Glu}]_{sc}$. Neuronal NOS is often colocalised with ionotropic N-methyl-D-aspartate receptors (NMDA-Rs) [55, 27, 5], which are receptor complexes including transmembrane ion channels in the NE that are opened or closed in response to the binding of Glu [4]. These channels provide Ca²⁺ influx into the cytosol. The two subtypes of NMDA-Rs, NR2A and NR2B, show different opening probability kinetics and expressed values. We model the open probabilities w of NMDA-Rs with different subunits with dependency of neuronal Glu concentration using a Michaelis-Menten kinetics formulation to fit the experimental data from [63] (see Figure ??):

$$w_{NR2,i} = \frac{[\text{Glu}]_{sc}}{K_m^i + [\text{Glu}]_{sc}}, i \in \{A, B\}, \quad (1.3.10)$$

where K_m^A and K_m^B are fitted Michaelis constants.

At an open state NMSDA-Rs are highly permeable to calcium ions [41]. The equation for the neuronal inward calcium current I_{Ca} in femtoamps (fA) per open NMDA-R is given by [63]:

$$I_{Ca} = \frac{4v_n G_M (P_{Ca}/P_M)([\text{Ca}^{2+}]_{ex}/[M^+])}{1 + e^{(\alpha_v(v_n + \beta_v))}} \cdot \frac{e^{(2v_n F/(RT))}}{1 - e^{(2v_n F/(RT))}} \quad (1.3.11)$$

with the Faraday's constant F , the neuronal membrane potential v_n (assumed to be constant during activation, an average value of the neuronal spiking activity of multiple action potentials. This is a simplified mathematical description, but suitable for our purpose as the model is focusing on Glu-effected Ca²⁺ changes in the NE), the conductance G_M , the ratio of the NMDA-R permeabilities to Ca²⁺ and to monovalent ions, respectively, P_{Ca}/P_M , the external Ca²⁺ concentration $[\text{Ca}^{2+}]_{ex}$, the concentration of monovalent ions (intra- and extracellular $[M^+]$, translation factors α_v and β_v , the temperature T and the universal gas constant R .

Santucci and Raghavachari arrive at estimates of 0.63 NR2A- and 11 NR2B-NMSDA-Rs, on average, per synapse [63]. Therefore, the total calcium current $I_{Ca,tot}$ reads as follows:

$$I_{Ca,tot} = I_{Ca}(0.63w_{NR2,A} + 11w_{NR2,B}). \quad (1.3.12)$$

The rate of change in neuronal cytosolic Ca²⁺ concentration in $\mu\text{M s}^{-1}$ is given by [63]:

$$\frac{d[\text{Ca}^{2+}]_n}{dt} = \frac{(I_{Ca,tot}/(2FV_{spine})) - \kappa_{ex}([\text{Ca}^{2+}]_n - [\text{Ca}^{2+}_{rest}]_n)}{1 + A}. \quad (1.3.13)$$

here V_{spine} is the volume of the neuronal dendritic spine (used together with F to convert the electrical flux $I_{Ca,tot}$ (in fA) into a molar flux (in $\mu\text{M s}^{-1}$)), the decay rate constant of internal Ca^{2+} concentration κ_{ex} , the resting Ca^{2+} concentration $[\text{Ca}^{2+}_{rest}]_n$ and the buffer capacity A [63].

We formulate the concentration of activated neuronal NO synthase $[nNOS_{act}]_n$ in $\mu\text{M s}^{-1}$ as the solution of the following rate equation [39]:

$$\frac{d[nNOS_{act}]_n}{dt} = V_{maxNOS} \frac{[CaM]_n}{K_{actNOS} + [CaM]_n} - \mu_2[nNOS_{act}]_n , \quad (1.3.14)$$

where V_{maxNOS} is the maximal rate of nNOS activity, μ_2 is the deactivation rate [11], and K_{actNOS} is the corresponding Michaelis constant [39].

The concentration of calmodulin / calcium complexes is given by [13]:

$$[CaM] = \frac{[\text{Ca}^{2+}]_n}{m_c} \quad (1.3.15)$$

with m_c , the number of Ca^{2+} bound per calmodulin:

$$m_c = \frac{[\text{Ca}^{2+}]_n}{\phi_n} \frac{d\phi_n}{d[\text{Ca}^{2+}]_n} , \quad (1.3.16)$$

where ϕ_n , the sum of all states of bound Ca^{2+} with respect to free $[\text{Ca}^{2+}]_n$, is

$$\phi_n = 1 + Q_1[\text{Ca}^{2+}]_n + Q_1Q_2[\text{Ca}^{2+}]_n^2 + Q_1Q_2Q_3[\text{Ca}^{2+}]_n^3 + Q_1Q_2Q_3Q_4[\text{Ca}^{2+}]_n^4 \quad (1.3.17)$$

with the binding constants Q_1 to Q_4 [13].

Endothelial NO Production

NO production in the EC is catalysed by the constitutive enzyme isoform eNOS, whose catalytic activity is sensitive to the availability of the substances O_2 and L-Arg [9]. An overview of the model detail is given in Figure 1.11.

The endothelial NO production can be mathematically expressed by

$$P_{NO,j} = V_{NO,j_{max}}[\text{eNOS}_{act}] \frac{[\text{O}_2]_j}{K_{m,j}^{O_2} + [\text{O}_2]_j} \frac{[\text{L-Arg}]_j}{K_{m,j}^{L-Arg} + [\text{L-Arg}]_j} . \quad (1.3.18)$$

The maximal activity of eNOS $V_{NO,j_{max}}$ is controlled by the intracellular calcium concentration $[\text{Ca}^{2+}]_j$ [9] and additionally it depends on the wall shear stress (wss) which occurs due to the blood flow through the perfusing arteriole [11].

Fluid shear stress activates a pathway involving phosphatidylinositol 3-kinase (PI3K) and the serine/threonine-specific protein kinase enzyme, which phosphorylates eNOS [25].

[59] and [11] describe the elastic strain energy stored within the vessel membrane by adapting mathematical models of [67] and [53], who focus on quantifying exogenous Ca^{2+} -entry via shear stress-gated ion channels.

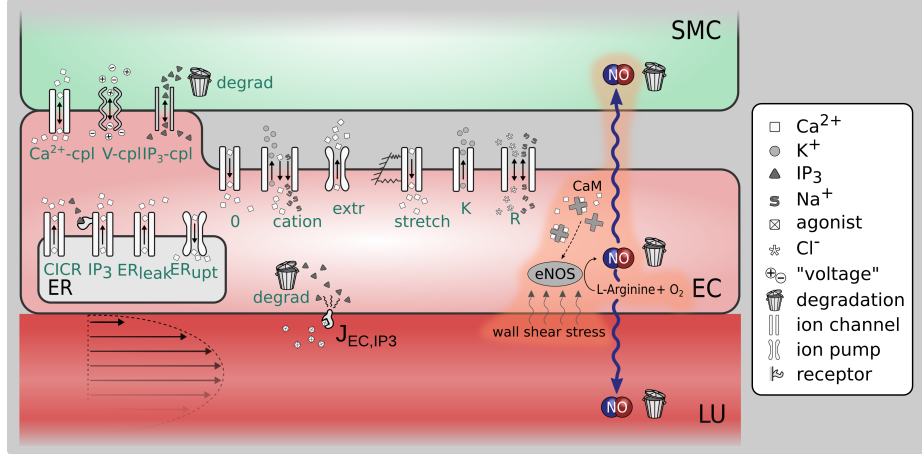


Figure 1.11: Graphical representation of the mathematical model, detail. The biochemical synthesis of NO in the EC is catalysed by the enzyme eNOS. It depends on the available concentration of the substances L-Arg and O₂ and is mediated by wall shear stress. The model addition to our previous foundation model [14] is highlighted in orange. SMC - Smooth muscle cell, EC - endothelial cell, LU - lumen.

The concentration of activated eNOS is given by the solution of the following differential equation [11]:

$$\frac{d[eNOS_{act}]}{dt} = \lambda \frac{K_{dis}[Ca^{2+}]_j}{K_{eNOS} + [Ca^{2+}]_j} + (1-\lambda)g_{max}F(\tau_\omega) - \mu_2[eNOS_{act}] . \quad (1.3.19)$$

The activation of eNOS by the cytosolic free calcium concentration in EC, $[Ca^{2+}]_j$, is given by the first term of the equation, where K_{dis} describes the eNOS-caveolin disassociation rate and K_{eNOS} is the Michaelis-Menten constant. g_{max} the maximal wss-induced eNOS activation rate, μ_2 denotes the deactivation rate [11].

The function $F(\tau_\omega)$ describing the elastic strain energy stored within the membrane is given by [67]:

$$F(\tau_\omega) = \frac{1}{1 + \alpha_j e^{-W(\tau_\omega)}} - \frac{1}{1 + \alpha_j} . \quad (1.3.20)$$

Here α_j is a zero shear open channel constant [11]. Note that we have added the term $\frac{1}{1 + \alpha_j}$ in order to deactivate the endothelial synthase of NO in the presence of no wss.

The strain energy density function $W(\tau_\omega)$ is taken from [67]:

$$W(\tau_\omega) = W_0 \frac{\left(\tau_\omega + \sqrt{16\delta_{WSS}^2 + \tau_\omega^2} - 4\delta_{WSS} \right)^2}{\tau_\omega + \sqrt{16\delta_{WSS}^2 + \tau_\omega^2}} \quad (1.3.21)$$

with W_0 , a shear gating constant and δ_{WSS} , the membrane shear modulus [11].

The wall shear stress τ_ω in the arteriolar wall depends on the regional cerebral blood flow (rCBF) Q . We assume Hagen-Poiseuille flow for cerebral arterioles:

$$Q = \frac{\Delta P \pi r^4}{8\eta L}, \quad (1.3.22)$$

where $\Delta P/L$ is the pressure drop over a given length of pipe (arteriole) and η is the dynamic viscosity of the fluid (blood). Both are assumed to be constant. The radius r of the arteriole is determined by the dynamics of the actin-myosin phosphorylation model by Hai and Murphy [34] used in our NVU model [14].

The wall shear stress, i.e. the frictional force per unit area, reads as follows:

$$\tau_\omega = \frac{4\mu Q}{\pi r^3}. \quad (1.3.23)$$

This creates a positive feedback mechanism, since increased wall shear stress will result in higher NO production from the EC, leading to vasodilation and further variation in wall shear stress.

look at paper by Andrews et al [2] and [1] for experimental evidence on endothelial NO production. These papers give some indication of the importance of ATP and capacitive calcium entry CCE mediated production of NO.

look at paper by Andrews et al [2] and [1] for experimental evidence on endothelial NO production.

1.3.9 Nitric Oxide Diffusion

The mathematical description of the NO diffusion is approached in many references [68, 50, 48]. It can be derived from Fick's second law describing a general diffusion of a substance over time in space. Steady-state conditions can be assumed, because diffusivity of NO is very high (diffusion coefficient $D_{c,NO} = 3300 \text{ } \mu\text{m}^2 \text{ s}^{-1}$) whereas the consumption of NO, represented by R_{NO} , is shown to be rather slow [66]. Instead of using complex partial differential equations, we simplify the diffusion formulation, using the Einstein-Smoluchowski equation to describe the characteristic time $\tau_{\Delta x}$ that is needed for NO to diffuse over a certain distance, Δx , from the centre of one cell to another, which reads as [48]:

$$\tau_{\Delta x} = \frac{\langle \Delta x \rangle^2}{2D_{c,NO}}. \quad (1.3.24)$$

The distance between the centre of the EC layer and the centre of the SMC layer, x_{ji} , is 3.75 μm [44] and the distance between the centre of the NE layer and the one of the SMC layer is estimated to be 50 μm with the astrocyte in the middle between them.

For the diffusion of NO from one compartment into another, we can write

$$D_{NO,m} = \frac{[NO]_{out} - [NO]_{in}}{\tau_{\Delta x}}; m \in \{n, k, i, j\}. \quad (1.3.25)$$

NO diffusivity is assumed to be constant even though Vaughn *et al.* propose that the value of $D_{c,NO}$ varies for different regions [66]. Furthermore, we do not consider concentration gradients within the cytosol (lumped parameter approach).

The compartment model above describes the diffusion between the different domains, but does not consider the amount of NO that is released in the lumen and is scavenged by reactions with haemoglobin. Butler *et al.* and Kavdia and Popel, who base their results on numerical simulations, find that the NO concentration in the lumen is zero after a distance of approximately half of the radius [6, 43]. Therefore, the diffusion flux J , i.e. the amount of ions leaving the EC per unit area and time, described by Fick's first law can be approximated as:

$$J = -D_{c,NO} \frac{\partial [NO]_j}{\partial x} \approx -D_{c,NO} \frac{\Delta [NO]_j}{\Delta x} \approx -D_{c,NO} \frac{[NO]_j}{r/2} \quad (1.3.26)$$

J is converted into a concentration leaving the region per unit time by multiplying with the arteriolar surface area and dividing by the volume. The arteriole is treated as a hollow cylinder with radius r and a given length δz :

$$D_{NO,j} = \frac{2\pi r \delta z}{\pi r^2 \delta z} \left(-D_{c,NO} \frac{[NO]_j}{r/2} \right) \approx \frac{-4D_{c,NO}[NO]_j}{r^2} \quad (1.3.27)$$

1.3.10 NO Consumption

As a free radical, NO reacts readily with biochemical species containing unpaired electrons, such as molecular oxygen, superoxide anions and metals [55]. NO gets scavenged in the cytosol of all cell types through which it diffuses. Mathematically, the scavenging term for all model compartments is given as (following [44]):

$$R_{NO} = k_m [NO]_m C_m; m \in \{n, k, i, j\}, \quad (1.3.28)$$

where C_m is the concentration of reactive species in the cell type and k_m represents the reaction rate constant.

1.3.11 NO in the SMC

NO diffuses through all cell types and clearly reaches the SMC, which forms the contractile core of the NVU model [14]. NO, via its second messenger cyclic guanosine monophosphate (cGMP), influences the SMC contraction mechanism and the open probability of the big potassium channel (BK), see Figure 1.12.

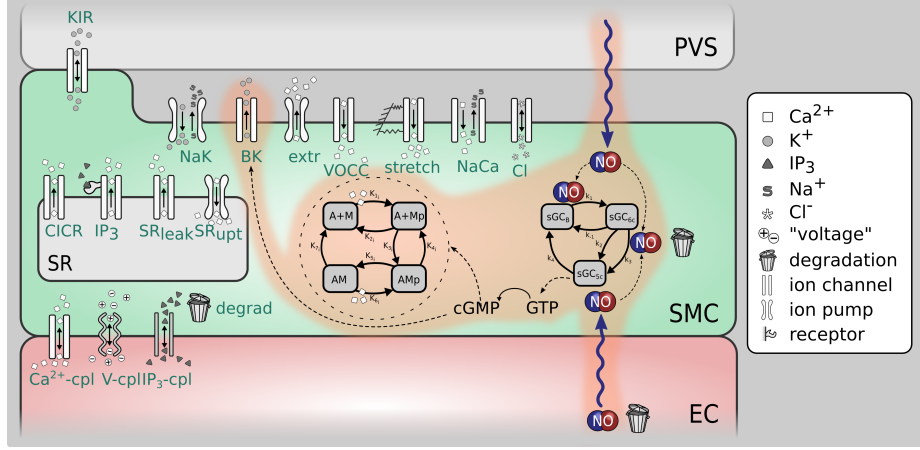


Figure 1.12: Graphical representation of the mathematical model, detail. NO in the smooth muscle cell (SMC) influences the contraction mechanism and the open probability of the big potassium channel (BK). The model addition to our previous foundation model [14] is highlighted in orange. PVS - Perivascular space, EC - endothelial cell.

The time rate of change of NO concentration in the SMC $[NO]_i$ is the sum of the diffused concentrations from the NE and the EC subtracted by the amount of NO that is scavenged by reactions with oxygen. This is written as:

$$\frac{d[NO]_i}{dt} = \frac{[NO]_n - [NO]_i}{\tau_{ni}} + \frac{[NO]_j - [NO]_i}{\tau_{ij}} - k_i[NO]_i , \quad (1.3.29)$$

where the NO consumption rate constant k_i reflects the activity of various NO scavengers [69].

In the SMC NO activates soluble guanylyl cyclase (sGC), an enzyme catalysing the formation of the second messenger cGMP. The kinetics of sGC and its complexes are described by Yang *et al.* with reaction rate constants from Condorelli and George [69, 12]. The sGC system with E_b , the fraction of sGC in the basal state, E_{6c} , the fraction of sGC in the intermediate form and E_{5c} , the fraction of sGC in the fully activated form, is described by the following set of equations [69]:

$$\begin{aligned} \frac{dE_b}{dt} &= (-k_1[NO]_i - k_{-1})E_b + (k_4 - k_{-1})E_{5c} + k_{-1} \\ \frac{dE_{5c}}{dt} &= (-k_3[NO]_i - k_2)E_b + (-k_3[NO]_i - k_2 - k_4)E_{5c} + k_3[NO]_i + k_2 \\ E_{6c} &= 1 - E_b - E_{5c} , \end{aligned} \quad (1.3.30)$$

where k_{-1} to k_4 are rate constants, of which k_4 depends on the cGMP concen-

tration:

$$k_4 = C_4[cGMP]^m . \quad (1.3.31)$$

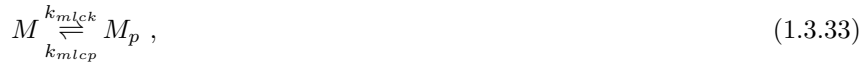
Here m reflects the strength of the cGMP feedback and C_4 is a rate constant [69]. The cGMP concentration is determined by

$$\frac{d[cGMP]}{dt} = V_{max,sGC}E_{5c} - \frac{k_{pde}[cGMP]^2}{K_{m,pde} + [cGMP]} , \quad (1.3.32)$$

where $V_{max,sGC}$ is the maximum cGMP production rate, $K_{m,pde}$ the Michaelis-Menten constant and k_{pde} the phosphodiesterase rate constant [69].

1.3.12 NO-mediated dilation

Yang *et al.* suggested two pathways as to how NO can lead to local vasodilation of arterioles in the brain [69]. Firstly, by indirectly influencing the SMC contractile system that is determined by the formation of cross bridges between the actin and myosin filaments and that was first described by Hai and Murphy [34]. There are four possible states for the formation of myosin: free nonphosphorylated cross bridges (M), free phosphorylated cross bridges (Mp), attached phosphorylated cross bridges (AMp) and attached dephosphorylated latch bridges (AM). The second messenger of NO, cGMP changes the rate constants K_2 and K_5 for the dephosphorylation of Mp to M and AMp to AM by myosin light-chain phosphatase (MLCP) [69]. In our previous fundamental NVU model [14] we used the rate constants based on the model of [46] where $K_2, K_5 = [0.5]/s$. [69] used the following reduced two-state model to describe the phosphorylation kinetics:



where

$$k_{mlcp} = k_{mlcp}^b + k_{mlcp}^c \frac{[cGMP]^{n_{H,mlcp}}}{[cGMP]^{n_{H,mlcp}}} \quad (1.3.34)$$

with an estimated Hill coefficient $n_{H,mlcp}$ of 2.

To adjust the reduced model to the [34] model used by [46], we scale the two factors k_{mlcp}^b and k_{mlcp}^c in order to achieve $K_2, K_5 = [0.5]/s$ for no NO production.

The second pathway concerns the open probability, w_i , of the BK channel in the SMC, which is a function of the membrane potential, v_i and is shifted to the left (in the membrane potential space) by cGMP, as shown in Figure 1.13 [64].

In the NVU model [14] the open probability of the BK channel in the SMC is described by the equation of [46]:

$$\frac{dw_i}{dt} = \lambda_i (K_{act_i} - w_i) , \quad (1.3.35)$$

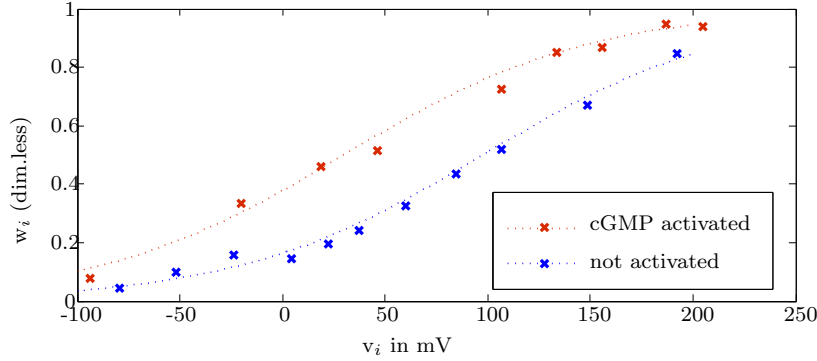


Figure 1.13: cGMP activation of the open probability of the BK channel in the SMC [64].

with the equilibrium state K_{act_i} given by

$$K_{act_i} = \frac{([Ca^{2+}]_i + c_{wi})^2}{([Ca^{2+}]_i + c_{wi})^2 + \beta_i \exp(-([v_i - v_{Ca3i}] / R_{Ki}))}. \quad (1.3.36)$$

Here the constants β , v_{Ca3i} and R_{Ki} describe the channel activation. We assume that in the v_i range of interest there is an approximately constant shift of w_i when activated by cGMP that can be modelled by making c_{wi} a function of cGMP, so that :

$$c_{wi} = \frac{1}{1 + \alpha_i \exp(\gamma_i [cGMP])} \quad (1.3.37)$$

with α_i and γ_i as translation factors that are chosen to give the desired shift of w_i upon cGMP stimulation as observed in experiments [64].

up to this point NVS versions exist beyond we will need to put code through NVS

Influence of the Blood fluid flow on Nitric Oxide production

Our current model does not provide a viable influence of the blood flow in the arterioles. We have shown through simple models that the flux of IP₃ has a substantial influence yet fluid shear stress and the transport mechanisms through the endothelial cell (essentially the blood brain barrier) are not modelled in a sufficient manner. Fadel et al. [20] produces a computational model of NO production and transport in a parallel plate flow chamber. The work looks at (using an FE model to solve the resulting pdes) NO concentration in both the fluid (simple Poiseuille flow) and the "tissue". In the case of integrating with NVU our main concern is the rate at which NO is produced in the EC. The production rate can come about through a shear mediated ion channel and the activation of the P2Y receptor by ATP. The spatial concentration of ATP in the

fluid boundary layer is a function of the wall shear stress. An analytical solution has been done by [?] which could help in determining the ATP concentration and hence NO in the EC. A review paper by ?] provides a substantial amount of data and Figure (1) indicates helpful possible pathways.

has the above been implemented in the nitric oxide model ?

We need to be mindful of the relationship between cGMP baseline and the SMC BK open probability . The reason for this is that if we change the radius of the perfusing arteriole then the shear stress changes and there is a consequential change in the baseline of cGMP due to variations in the activation of eNOS. We can therefore get a non-physiological negative concentration of cGMP for the resting baseline ! At present this issue is dealt with by never allowing the cGMP concentration to go below zero.

1.4 version 2.0:

Elshin/Chang model of neuron and extracellular space **NOT YET IMPLEMENTED**

check Elshin's model coupled with correct version 1.1

This model includes the work of Chang et al. [8] which was originally developed to investigate the propagation of large potassium waves in the cortex as a model for cortical spreading depression. The major difference between version 1.1 and 1.2 is that the neuron model of Ø stby et al. [57] has now been replaced by a neuron consisting of a soma (includes axon) and dendrite along with an extracellular space.

need to explain the difference between extracellular space and synaptic cleft

1.4.1 Model Development from work of Chang et al

An eight-compartment continuum mathematical model comprised of a soma, dendrite, extracellular space compartment, astrocyte, perivascular space, smooth muscle cell, endothelial cell, and lumen compartment will be compiled from different existing models. For simplicity reasons, the neurovascular unit is divided into two components namely a neuron component and a vascular component. The neuron component is comprised of the somatic, dendritic and extracellular space compartment. The vascular component is comprised of the astrocyte, perivascular space, smooth muscle cell, endothelial cell, and lumen compartment. Importantly the new model now includes the effects of oxygen on the metabolism.

1.4.2 Neuron Components, based on the model by Chang et al [8]

There are many different types of neurons, with differences in size, shape and physiological properties. In this project we have considered a generic neuron model with its basic features. The neuron component is a three compartment model consisting of a soma compartment, dendrite compartment and extracellular space compartment. The three major ions sodium, potassium, and chlorine and their associated channels are considered. Inter compartmental communications is enabled in the three compartments using a lumped parameter approach. Figure 1.14 shows the complete model.

we need to check that the dynamics of the astrocyte and the consequential dynamics of the SMC/EC and dilation/contraction model are the same for this model as they are for version 1.2

check dilation dynamics of ver 2.0 are the same compared to ver 1.2

Membrane potential and Cross-membrane currents

The total cross membrane currents is the sum of the voltage dependent sodium and potassium currents, sodium, potassium and chlorine leak currents, and the sodium-potassium exchange current. The membrane potentials of the neuronal components, $E_{m,*}$ (* is either s for somatic or d for dendritic), are governed by the coupled partial equations

$$C_m \frac{\partial E_{m,s}}{\partial t} = -I_{s,tot} + \frac{1}{2R_a\delta_d^2}(E_{m,d} - E_{m,s}) \quad (1.4.1)$$

$$C_m \frac{\partial E_{m,d}}{\partial t} = -I_{d,tot} + \frac{1}{2R_a\delta_d^2}(E_{m,s} - E_{m,d}) \quad (1.4.2)$$

where C_m is the membrane capacitance per unit surface area (μ farad/cm 2), R_a is the input resistance of the effective dendritic tree(ohms), δ_d is the half length of the effective dendritic tree(cm). $I_{s,tot}$ and $I_{d,tot}$ are the total cross-membrane ionic currents per unit surface area(mA/cm^2) for soma and dendrite and are given by

$$I_{s,tot} = I_{s,Na,tot} + I_{s,K,tot} + I_{s,Cl,tot} \quad (1.4.3)$$

$$I_{d,tot} = I_{d,Na,tot} + I_{d,K,tot} + I_{d,Cl,tot} \quad (1.4.4)$$

where $I_{s,Na,tot}$, $I_{s,K,tot}$, $I_{s,Cl,tot}$ are the total ionic currents of sodium ,potassium and chlorine ions of the soma respectively and $I_{d,Na,tot}$, $I_{d,K,tot}$, $I_{d,Cl,tot}$ are the total ionic currents of sodium ,potassium and chlorine ions of the dendrite respectively. These cross ionic currents simulate the diffusion of ions from

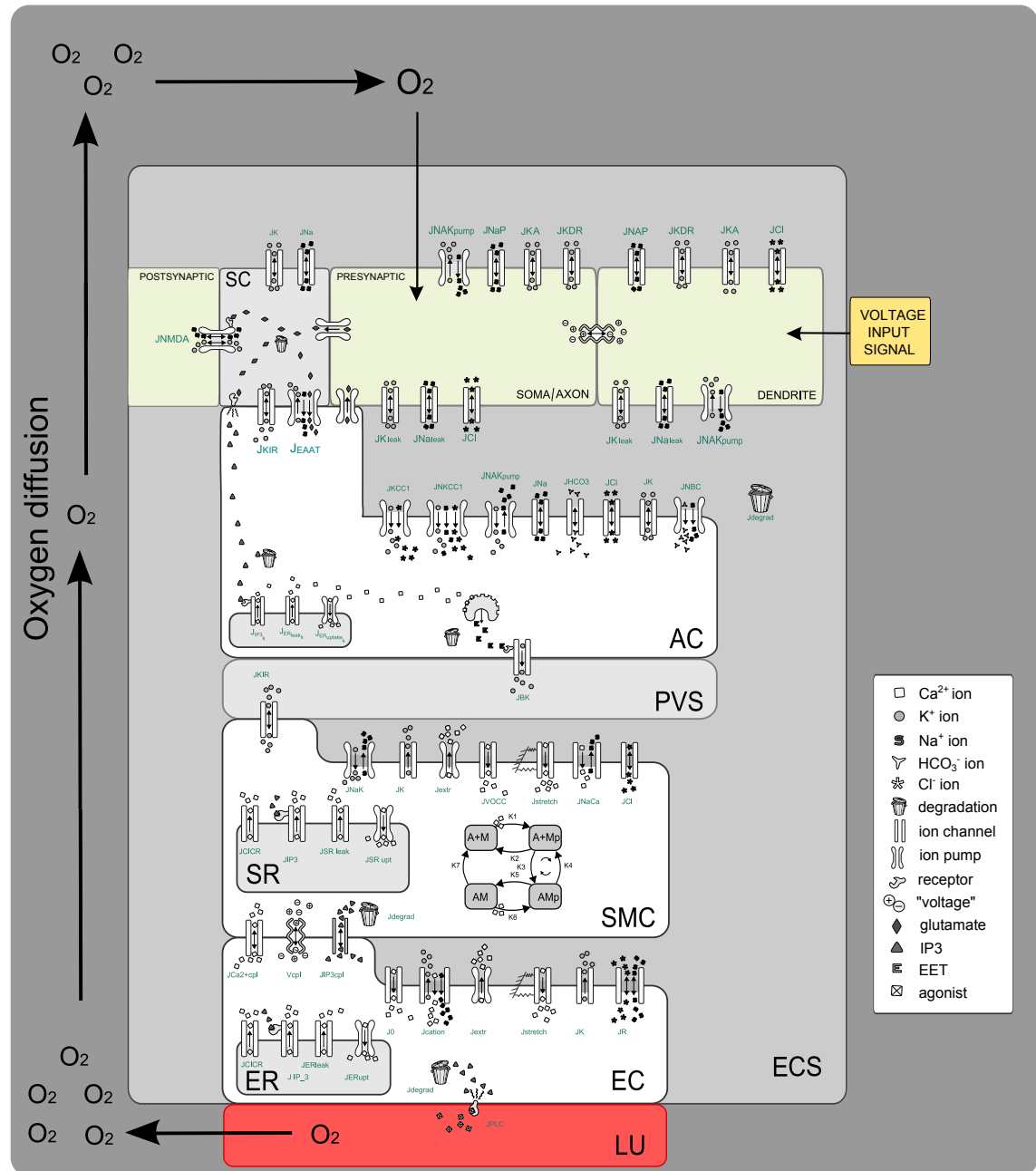


Figure 1.14: Overview of the complete neurovascular unit for version 2.0 using the new neuron/astrocyte model taken from [8]. NE-Neuron, SC-Synaptic cleft, AC-Astrocyte, PVS-Perivascular space, ECS- extracellular space, SMC-Smooth muscle cell, EC-Endothelial cell, LU-Lumen

the dendrite to the soma. Indeed in this particular model the "soma" is really the soma and the axon.

The somatic compartment total sodium current is given by $I_{s,Na,tot} = I_{s,Na,P} + I_{s,Na,leak} + I_{s,Na,pump}$ where $I_{s,Na,P}$ is the current through persistent-type sodium channels, $I_{s,Na,leak}$ is the current through sodium leak channels, $I_{s,Na,pump}$ is the sodium current through the sodium/potassium exchange pump. The dendritic compartment total potassium current is given by $I_{s,K,tot} = I_{s,K,DR} + I_{s,K,A} + I_{s,K,leak} + I_{s,K,pump}$ where $I_{s,K,DR}$ is the current through delayed rectifier type potassium channels, $I_{s,K,A}$ is the current through transient type potassium channels, $I_{s,K,leak}$ is the current through potassium leak channels, $I_{s,K,pump}$ is the potassium current through the sodium/potassium exchange pump. The dendritic compartment have all these channels in addition to NMDA(N-methyl-D-aspartate) channels which are permeable to sodium and potassium ions. There is evidence that glutamate is released from cells when extracellular potassium is elevated [?]; [?] and high extracellular potassium enhances NMDA receptor activation [?]. Hence, the glutamate-dependent depolarisation of the neuron is modelled as NMDA receptor activation. So, the NMDA channel current will be a function of both membrane potential and extracellular potassium.

The cross-membrane currents of the voltage dependent ion channels are modelled using the Goldman-Hodgkin-Katz(GHK)equation

$$I_{ion,GHK} = m^p h^q \frac{g_{ion,GHK} F E_m [[ion]_i - \exp(\frac{-E_m}{\phi}) [ion]_e]}{\phi [1 - \exp(\frac{-E_m}{\phi})]} \quad (1.4.5)$$

where $g_{ion,GHK}$ is the maximal conductance value and permeability is absorbed into this parameter. The factors in the parameter $\phi = RT/F$ are R, the universal gas constant, T, the absolute temperature, and F, the Faraday constant. The conductance and concentration of the ions are ion and compartment specific. The parameters m and h are the ion specific activation and inactivation gating variables. The sodium, potassium and chlorine leak currents are calculated by Hodgkin-Huxley(HH) model given by

$$I_{ion,HH} = g_{ion,HH} (E_m - E_{ion}) \quad (1.4.6)$$

where $g_{ion,HH}$ is the constant conductance for the specific ion and E_{ion} is the Nernst potential for the specific ion. The Nernst potential is given by

$$E_{ion} = \frac{RT}{ZF} \log \frac{[ion]_e}{[ion]_i} \quad (1.4.7)$$

where Z is the valence of the ionic species, $[ion]_e$ is the concentration of the ion in the extracellular space and $[ion]_i$ is the concentration of the ion in the intracellular space.

$$\frac{1}{2R_a \delta_d^2} (E_{m,d} - E_{m,s}) \quad (1.4.8)$$

is the current moving from the dendrite to the soma (and along the axon to the presynaptic cleft). This current is established by a voltage variation in the

dendrite as a way of simulating a synaptic action potential from one synapse to another. Neuronal activation is made apparent by a Gaussian voltage profile input into the dendrite voltage equation for a specified time. This induces a current in the dendrite which via equation 1.4.22 allows the soma membrane voltage to change and induce potassium and glutamate efflux into the synaptic cleft.

Voltage dependent ion channels

The electrically excitable property of the neuron is simulated using the classical Hodgkin and Huxley kinetic description, ?? reference. This description consisted of an identification of the ionic species that carry the current, the steady state activation and inactivation curves for the current, and a measure of channel kinetics. They used peak conductances from voltage clamp experiments to estimate steady-state curves and the exponential rise or fall of the conductance to estimate kinetic properties. The model assumes each channel to have one or more independent gates , each of which are either in a open or closed state. All of its gates must be in a open state for the channel to be open. The variable conductance value is given by $g = g_{max}m^p h$. In this expression g_{max} is the maximal conductance of the channel, m and h are the fraction of activation and inactivation gates in the open state respectively. The rate at which the activation and inactivation gates open and close in response to the membrane potential are according to the equations

$$\frac{dm}{dt} = \alpha_m(V)(1 - m) - \beta_m(V)m \quad (1.4.9)$$

$$\frac{dh}{dt} = \alpha_h(V)(1 - h) - \beta_h(V)h \quad (1.4.10)$$

These equations state that the closed activation gates, (1-m), open at rate $\alpha_m(V)$, while the open activation gates, m, close at a rate $\beta_m(V)$. It is similar for the inactivation gates. The rate functions, $\alpha_m(V)$ and $\beta_m(V)$, are functions that depend on the voltage across the membrane. The forms of the functions α and β are usually determined through a mix of theoretical and empirical considerations and they are of the form

$$\alpha(V) = a_0 \exp\left(\frac{-\delta V}{s}\right) \quad (1.4.11)$$

$$\beta(V) = b_0 \exp\left(\frac{(1 - \delta)V}{s}\right) \quad (1.4.12)$$

where a_0 , b_0 , and δ are positive constants, with $0 \leq \delta < 1$. A gate that tends to open on depolarisation will have $s < 0$, while a gate that tends to open on hyperpolarisation will have $s > 0$. These exponential forms are modified to fit

the experimental data. The equation of the rate of change of activation gates may be rewritten as

$$\frac{dm}{dt} = \frac{m_\infty(V) - m}{\tau_m(V)} \quad (1.4.13)$$

where

$$m_\infty(V) = \frac{\alpha_m(V)}{\alpha_m(V) + \beta_m(V)} \quad (1.4.14)$$

and

$$\tau_m(V) = \frac{1}{\alpha_m + \beta_m(V)} \quad (1.4.15)$$

These expressions can be similarly written for inactivation gates. The functions $m_\infty(V)$ and $h_\infty(V)$ are called the steady-state activation and steady-state inactivation curves respectively. The values of m and h will get asymptotically close to the steady state if voltage is held constant for a sufficient length of time. The functions τ_m and τ_h are called the time constant curves of the activation and inactivation gates respectively and it describes the variation of the time constant with the membrane potential. Thus the varying response of different channels to membrane potential is modelled with the experimental data containing maximal conductances and rate functions of the activation and inactivation gates of the individual channels. The expressions used in the neuron model that describe the voltage-dependent rate functions are based on a model of hippocampal pyramidal cells described by Traub et al (?]).

Ionic concentrations change in the neuronal components

The rates of change of ionic concentration in the soma and dendrite are due to the membrane currents and the exchange between soma and dendrites . The exchange between the somatic and dendritic compartments is modelled by a flux proportional to the difference between their ion concentrations. The equation describing the rate of change of ions in the soma is

$$\frac{\partial [ion]_{i,s}}{\partial t} = -\frac{A_s}{FV_s} I_{s,ion,tot} + \frac{D_{ion}(V_d + V_s)}{2\delta_d^2 V_s} ([ion]_{i,d} - [ion]_{i,s}) \quad (1.4.16)$$

The notation, D_{ion} , is the ion diffusion coefficient in aqueous solution taking into account tortuosity and volume fraction (?]) and F is the Faraday constant. The quantities A_s and A_d are the surface areas of the soma and dendrite respectively in the total fixed volume given by the sum of the fixed somatic volume V_s , dendritic volume V_d , and extracellular volume, V_e . The equation describing the rate of change of ions in the dendrite is

$$\frac{\partial [ion]_{i,d}}{\partial t} = -\frac{A_d}{FV_d} I_{d,ion,tot} + \frac{D_{ion}(V_s + V_d)}{2\delta_d^2 V_d} ([ion]_{i,s} - [ion]_{i,d}) \quad (1.4.17)$$

The local rates of change of the extracellular space ions are due to the membrane currents and the buffering of potassium ions by glial cells. To ensure electro neutrality, the initial extracellular concentration of the anion Cl^- is chosen to be equal to the sum of the concentration of cations Na^+ and K^+ in the extracellular space. Also, the initial intracellular concentration of chloride is chosen in such a way that its Nernst potentials matched the resting membrane potential of -70 mV. The existence of immobile anions has been assumed in the soma and dendrites to achieve intracellular electro neutrality. Astrocyte, a type of glial cell, plays important roles in neurovascular coupling mechanism (Attwell et al. [3]). One of the important roles of the astrocytes is the clearance of extracellular potassium ([?]). It is achieved through a variety of inward rectifying potassium channels. The buffering is also bolstered by the extreme polarity of the astrocyte cell membranes with membrane potential near the Nernst potential for potassium.

what is the nernst potential at this stage for potassium?

The equations describing the rate of change of ions in the extracellular compartment with the Chang model [8] is given by

need Chang reference

$$\frac{\partial [ion]_e}{\partial t} = \frac{1}{f_e F} \left(\frac{A_s I_s, [ion], tot}{V_s} + \frac{A_d I_d, [ion], tot}{V_d} \right) + V_{buffer}(x, t) \quad (1.4.18)$$

The extracellular space volume was defined as 15% of the intracellular space volume based on published data ([?]); ([?]). The differential equation governing the potassium buffering flux is given by

$$V_{buffer}(x, t) = -\frac{\partial B(x, t)}{\partial t} = \mu_+[K^+]_e B(x, t) \exp\left(\frac{[K^+]_e - 5.5}{-1.09}\right) - \mu_-(B_0 - B(x, t)) \quad (1.4.19)$$

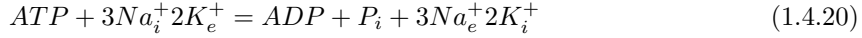
where $B(mM)$ is the free buffer concentration, the rate constants $\mu_+ = \mu_- = 8.0 \times 10^{-6} ms^{-1}$ determine the speed at which potassium is buffered, and $B_0 = 200 mM$ is the effective total buffer concentration. The equation describes strong buffering of extracellular potassium for concentrations above 5.5 mM. The initial value of the free buffer concentration is set to maintain steady state when the extracellular potassium is at its resting value (3.5 mM). Here the extracellular space volume fraction is given by $f_e = V_e/(V_s + V_d)$.

However the buffer term $V_{buffer}(x, t)$ was introduced to model the influx of potassium by astrocytic mechanisms. The Chang model did not have an astrocyte compartment. With the new model an astrocyte is included and thus the buffering term is no longer needed.

need to define a proper link for the $[ion]_e$ conservation equation now that the buffer term is not needed

1.4.3 Sodium-Potassium Exchange pump and their oxygen dependency

When an action potential is elicited, the sodium ions enter the cell, and potassium ions leave the cell. The primary role of Na+/K+ ATPase exchange pump in the neuronal membrane is to restore ionic concentrations to their homoeostatic state. The Na+/K+ ATPase pump is a transmembrane protein with two extracellular binding sites for potassium, three intracellular binding sites for sodium, and a single intracellular binding site for ATP. The pump moves out three intracellular sodium ions and two extracellular potassium ions against their electrochemical gradients and hence the need for energy. The pumps are fuelled by dephosphorylation of ATP (Adenosine triphosphate) in the cell and are given by



ATP is replenished by the reattachment of a phosphate ion to ADP(Adenosine diphosphate).The biochemical pathways through which ATP is generated is powered by cellular respiration through both aerobic and anaerobic processes. Only about 5% of ATP production is independent of oxygen (?]). Since the energy in the form of ATP is highly dependent on tissue oxygen concentration, the Na+/K+ ATPase exchange pump in the neuronal membrane is modelled as a variable dependent on the availability of oxygen. The potassium and sodium currents in the soma and dendrite are given by $I_{*,K,pump} = -2I_{*,pump}$ and $I_{*,Na,pump} = 3I_{*,pump}$, respectively. The total currents due to the sodium/potassium exchange pump in the soma and dendrite is given by

$$I_{*,pump} = I_{max} \gamma_{*,pump,1} \gamma_{*,pump,2} \quad (1.4.21)$$

where

$$\gamma_{*,pump,1}([K^+]_e, [Na^+]_i, *) = \left(1 + \frac{[K^+]_{e,0}}{[K^+]_e}\right)^{-2} \left(1 + \frac{[Na^+]_{i,0}}{[Na^+]_{i,*}}\right)^{-3} \quad (1.4.22)$$

Simulation of the BOLD response

Elshin's work uses the model of Chang et al [8] and links it with NVU version 1.0 (and probably version 1.1). The output from this model allows for analysis of the time-dependent behaviour of both CBF (cerebral blood flow) and $CMRO_2$ the metabolic rate of oxygen consumption. Buxton et al [?] have developed a simple model for BOLD response based on assumed functional forms for CBF and $CMRO_2$. They utilise a "balloon" model which evaluates the CBV (cerebral blood volume) $v(t)$ and the mass conservation of deoxygenated blood $q(t)$ such that

$$\frac{dq}{dt} = \frac{1}{\tau_{MTT}} \left[f(t) \frac{E(t)}{E_0} - \frac{q(t)}{v(t)} f_{out}(v, t) \right] \quad (1.4.23)$$

$$\frac{dv}{dt} = \frac{1}{\tau_{MTT}} [f(t) - f_{out}(v, t)] \quad (1.4.24)$$

here τ_{MTT} is the characteristic mean transit time through the balloon at rest, $f(t)$ is the CBF, $E(t)$ the oxygen extraction fraction with E_0 the resting value for extraction fraction, F_{out} is the outflow from the balloon and is given by

$$f_{out} = v^{\frac{1}{\alpha}} + \tau \frac{dv}{dt} \quad (1.4.25)$$

Hence the output from Elshin's model can replicate the time-dependent behaviour of both q and v and in doing so simulate the BOLD signal given by Buxton et al [?] as

$$\frac{\delta S}{S_0} = A (1 - f^{\alpha-\beta} m^\beta) \quad (1.4.26)$$

with $m = \frac{E}{E_0} f$, the normalised metabolic rate of oxygen consumption.

1.4.4 version 2.1

version 2.0 + neuron Ca^{2+} This model is that funded by the CMRF. Astrocytic and neuronal Ca^{2+} can be validated by work from Owen Jones at Otago Univ.

1.4.5 version 2.2:

version 2.1 + version 1.2 whic is essentially the introduction of nitric oxide pathway

NOT YET IMPLEMENTED

1.4.6 Integration with the model of Cloutier [?]

Equation 1.4.22 describes the action of the pump dependent on the initial concentration of extracellular potassium and intracellular sodium concentrations. The second pump represents the oxygen dependent production of ATP by the mitochondria [?] and it takes the form

$$\gamma_{*,pump,2}([O_2]) = 2 \left(1 + \frac{[O_2]_0}{(1-\alpha)[O_2] + \alpha[O_2]_0} \right)^{-1} \quad (1.4.27)$$

where $[O_2]$ is the tissue oxygen concentration and $[O_2]_0$ is the initial equilibrium value of oxygen concentration. This expression indicates that the pumping rate will be reduced whenever there is a decrease of the oxygen level in the tissue.

proper oxygen model that fits with Cloutier is crucial see section 2.2.1 and section 1.4

1.4.7 Mitochondrial modelling

It is clear that with the Cloutier model [?] the mitochondrial function is modelled relatively simply by an input of oxygen, $[\text{ADP}]$ and a resulting rate

of change of [NADH] to produce [ATP]. A more complex model developed by Beard [?] suggests that we might be able to combine Cloutier and Beard together. **HOWEVER** this would increase the complexity, number of o.d.e.s and resulting parameters to a large, probably unsustainable number. Hence we will need to look closely at Beard [?] to develop a *black-box* approach which fits nicely with Cloutier.

Note that there is a correction to [?] that being [?]. Here the table of parameters has a number of important changes to values.

Or conversely look at Cloutier as a *black-box* and introduce Beard as the main model.

black-box Beard and link to Cloutier or black-box Cloutier and link to Beard

. Although not a modelling paper [62] provide some good background on mitochondrial membrane potential during reactive oxygen species generation. This paper should be read in conjunction with [?]. An excellent review paper on Mitochondria, endothelial cell function and vascular diseases is given by Tang et al [?]. Research indicates that with Alzheimer's disease there exists reduced activity of α -ketoglutarate dehydrogenase complex (KGDHC). Work by Berndt et al [?] through a complex model simulates the relationship between reduced KGDHC and mitochondrial ATP production, redox state, transmembrane potential, and generation of ROS by the respiratory chain. **The simulation of ROS has particular importance.**

email sasha.bulik@charite.de for the code

look at integrating mitochondrial models into a single model linked with NVU

1.4.8 integration of Cloutier model into version 2.1?

Work has been ongoing into developing a more physiological neuron and astrocyte model. This has been based on the work by Cloutier et al [?]. Figure 1.15 shows the pathways that will become part of the full model. Why do we need to do develop the model to this level of complexity and can we ever validate it ? The answer to the second question is that we validate each module then assume the full model is also validated. The first question requires some explanation. From a mathematical perspective we would wish to make the model as simple as possible to mathematically and numerically analyse the dynamics etc. However the majority of funding for such research does not come from the mathematical community but from the biological and clinical funding bodies. It is therefore crucial that the model shows physiological correctness and that experiments in the numerical domain can explain those experiments in the "in vivo" and "in vitro" domains.

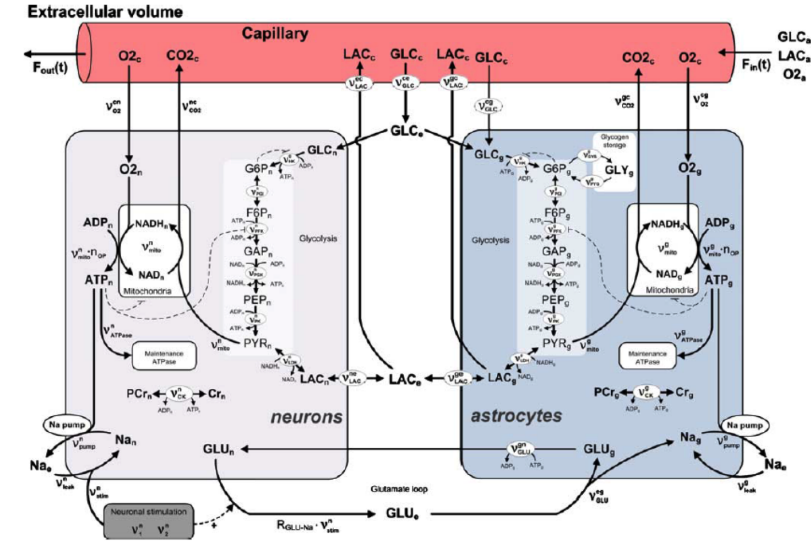


Figure 1.15: Overview of the complete Model due to Cloutier et al [?].

1.5 Neuro-vascular Simulator

In order to develop NVU simulation code that works both in a Matlab environment and parBRAIN the group had considerable problems with bugs that came about with trying to rewrite Matlab code in C. The group (led by Kathi and Kon) devised a python code which took .ini files as input and provided exact copies of functional code in both Matlab and C thereby alleviating the problem with porting bugs. A description of the NVS (as it is known) is given below.

Chapter 2

Parallel Implementation of NVU: parBRAIN

2.1 parBrain (version 0)

This section provides details and future trends for the parallelisation of NVU where the neurovascular coupling model is integrated into a tissue slice decomposed into tissue blocks. Each block contains an adaptive perfusing arteriole that is regulated by the NVU model.

2.1.1 parallel NVU code and Non-dimensionalisation

The NVU model (version 1.0 and soon to be version 1.1) has been integrated into an H-tree environment which allows for scalable parallel simulations of a large number of tissue blocks. This software is termed **parBrain**. An H-tree is a space filling tree such that in the case of simulating cortical perfusion each leaf of the tree models a penetrating arteriole into the cortex. Each leaf is dynamic since its time-dependent state is governed by the NVU output as shown above. Figure 2.1 shows the basic make-up of the environment.

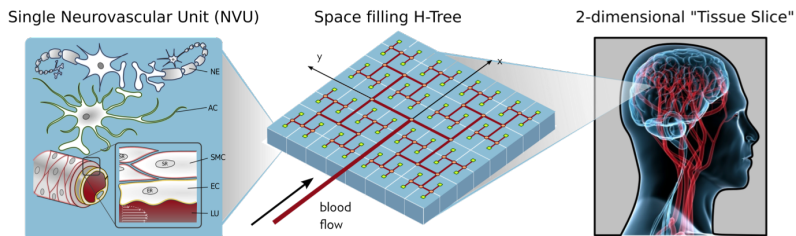


Figure 2.1: Overview of the H-tree integrated with NVU units.

2.1.2 scaling results for the parallel H-tree

These results have been evaluated using version 1.0 of the envy-you code. It is noted that the wall clock time is substantial to simulate 200 physiological seconds compared to a non-parallel Matlab version that simulates just a single NVU. For the parallel version to scale properly then the time taken to simulate a single NVU should be roughly the same for n cores to simulate n NVUs. As can be seen in the Figures that this is in fact the case. However, the time for each simulation is excessive, the reason for this is the use of a home-grown implicit Euler solver. Even though, using Newton iteration, the time step sizes should be relatively large it still takes extremely small steps. This may be due to the number of reasons, possibly the differing time-scales of the ion channels or the "stiffness" of the resulting equations. Non-dimensionalisation will certainly allow us to examine the relative sizes of components of the equations. However great care must be taken since Sneyd et al

need to find this reference

have shown that even small elements which one would normally ignore (due to their relative size) can dramatically alter the dynamics of the full system.

Work will continue on developing the parallel code (by Richard Brown at

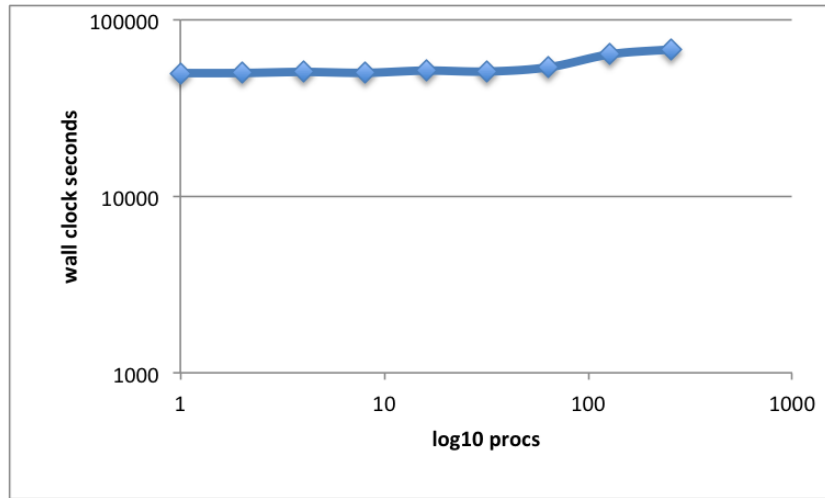


Figure 2.2: parBrain Weak Scaling.

Massey, who wrote the original parallel implementation) for new ode solvers that can adapt to the varying timescales. In addition the **parBrain** model will be continually updated by new versions of the NVU model. Initially the group will look to non-dimensionalise the envy-you version 1.0 that is used in **parBrain**.

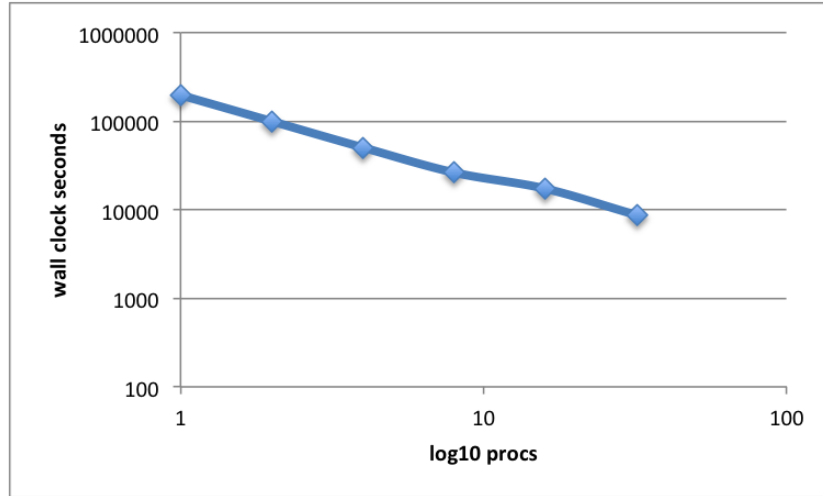


Figure 2.3: parBrain strong scaling.

2.1.3 Diffusion across tissue blocks

At present the tissue blocks are independent even though they represent a "continuous" tissue. Hence the parallel model has to simulate the diffusion of ions through the tissue. This is not a trivial exercise since it will require a considerable increase in communication between processor cores. However due to the way in which the tissue slice is decomposed the communication will be "local". **diffusion has been successfully implemented** What do we need to diffuse, in terms of ions and messenger molecules, across the tissue block boundaries? Extracellular K^+ is certainly important due to its crucial part played in cortical spreading depression, whilst Ca^{2+} in the SR/ER would clearly not diffuse. Na^+ will need to be diffused as this has an effect on the K^+Na^+ ATPase pump on the neuron membrane. Ions and glutamate effluxed into the synaptic space would not be diffused as it is assumed that the synaptic space is not part of the extracellular space.

Paper by [?] provides an insight into the diffusion and advection in complex networks. They impose a capillary network composed of axially aligned capillary segments joined in a random fashion. A hexagonal grid is used to find steady state concentration profiles within the tissue. Fickian diffusion (Laplacian operator) is modelled with an approximation on the hexagonal grid. Significant under-relaxation is needed for convergence. However the paper does give important insights into how the parBrain code can be developed for diffusion across tissue boundaries.

[?] model gap junctions in astrocytic networks simulating Ca^{2+} waves from cell to cell and this will have consequence when we come to look at how ions diffuse across tissue boundaries in the parallel code.

2.1.4 Capillary models and their integration with NVU

At present the NVU model terminates with a perfusing arteriole. It is assumed that the oxygen flow into a tissue block is distributed instantaneously and homogeneously into the cerebral tissue. This is clearly not the case. Work on capillary perfusion has been done by a variety of research groups and the group at Canterbury has published a relatively state-of-the-art model [61]. It is unclear how this model can be integrated into either envy-you version 1.1 or parBrain. However the input to the Safaeian model is a simple flow inlet which could be the perfusing arteriole. **is this level of detail necessary? Does it help in determining the cerebral function? can it provide additional information for integration into the NTS system?** Also see the work (noted above) in section 2.2.1.

”To Pericyte or not to Pericyte”? , that is the question

Are pericytes important in determining neurovascular coupling? Papers seem to contradict each other. The first by Hamilton et al. [37] and further exemplified by the same group [?] promotes the idea that pericytes modulate capillary diameter in response to neural activity (glutamate release produces messengers that relax pericytes) and infer that neurovascular regulation at the capillary level is pericyte dominant. In addition they state that capillaries dilate before perfusing arterioles hence producing over 80 % of blood flow increase. On the other hand [?] provides evidence for the opposite.

The paper by Hill et al [?] clearly indicates that pericytes do NOT have contractile properties. We there do not need to integrate pericytes into the model.

2.2 Integration of NVU with the (IBM) Neural Tissue Simulator

the relationship with IBM has gone very silent. We do not expect this to be rejuvenated any time soon.

Recently the brain group has been in negotiation with IBM to integrate the NVU model with the Neural Tissue Simulator (NTS), under the leadership of James Kozloski [?], [?] and an internal IBM document [?]. This software tool extends requirements and constraints of previous neuronal and neural circuit simulation methods, creating a tissue coordinate system. They have developed a novel tissue volume decomposition, and a hybrid branched cable equation solver. The decomposition divides the simulation into regular tissue blocks and distributes them on a parallel multithreaded machine (in this case a Blue Gene/P). The solver computes activation and functionality of neurons that have been divided arbitrarily across blocks. They demonstrate thread, strong, and weak scaling of the approach on a machine with more than 4000 nodes and up to four threads per node. Scaling synapses to physiological numbers had little

effect on performance, since the decomposition approach generates synapses that are almost always computed locally. The largest simulation included in the scaling results comprised 1 million neurons, 1 billion compartments, and 10 billion conductance-based synapses and gap junctions. [?][?] discusses the implications of the ultrascalable Neural Tissue Simulator, and with their results estimate requirements for a simulation at the scale of a human brain.

2.2.1 Transport across the BBB

[?] provide a substantially complex model of transport (gas exchange) across the blood-tissue barrier. The model utilises four regions (RBC, plasma, interstitial fluid and parenchymal cell).

Spatial profiles are given for a number of variables as a function of blood flow including pH, O_2 consumption and CO_2 production. The spatial independent variable was chosen to represent a 0.1 cm component of a capillary. Radial diffusion is treated an instantaneous given the small distance travelled from lumen across the tissue boundary. Axial diffusion is simulated. Boundary conditions for concentrations at $x = 0$ are assumed constant. However for our purposes we do not need axial profiles in a capillary but a spatially averaged value that allows us to estimate the concentrations of O_2 etc in the tissue. This would probably help with the work

can we use this, by implementing a spatially averaged value of concentrations in the NVU model?

2.2.2 Draft NVU model for parBRAIN

We show below in Figure 2.4 a draft sketch of how the NVU may be used in parBRAIN by linking (nearest neighbour) NVUs. Notice that we need to make clear as to whether we have two or just a single extracellular space (ECS). There are ten compartments

1. synaptic cleft
2. Astrocyte
3. Dendrite
4. Soma/Axon
5. Extracellular Space i)
6. Extracellular Space ii)
7. perivascular space PVS
8. smooth muscle cell SMC
9. endothelial cell EC

Basic Unit for parBRAIN.jpg

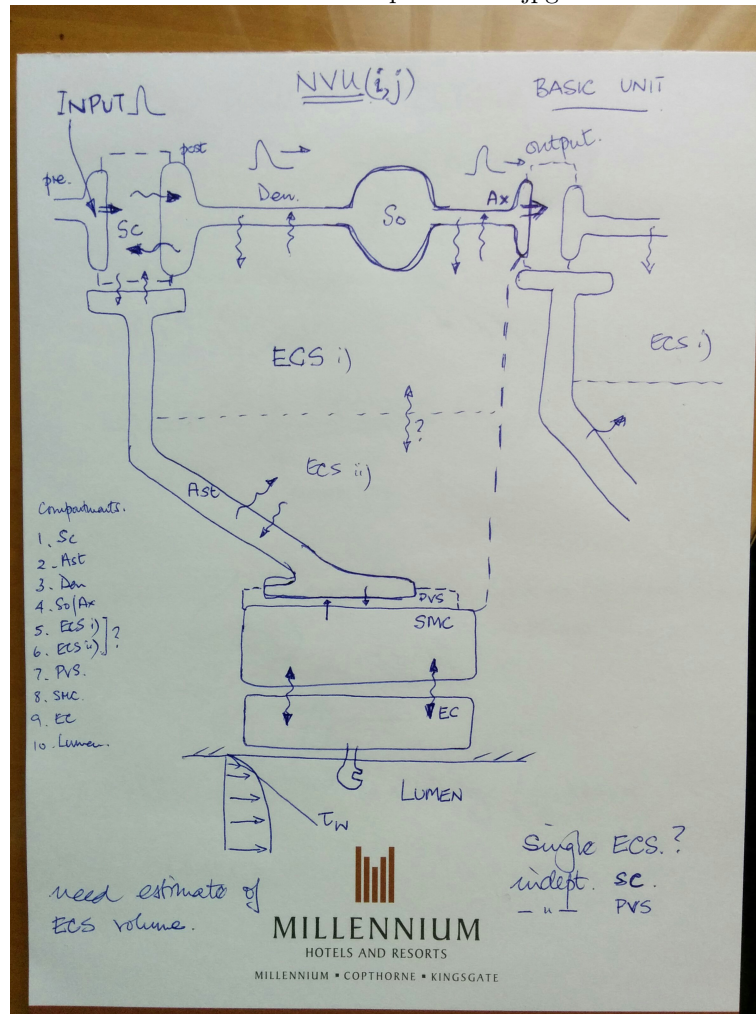


Figure 2.4: draft sketch of basic NVU with possible use in parBRAIN

10. Lumen (blood flow)

Figure 2.5 indicates a possible variation to the parBRAIN model. For this case in contrast to the diffusion where nearest neighbour connection is utilised to simulate diffusion we can introduce a more complex connectivity, not for ion transport, but for connecting outputs from the axon to the input (post synaptic dendrite) of each NVU model. **What does this simulate ?** This might simulate connections of certain types of neurons to those which are geographically distant yet over the length scale of the vasculature is not necessarily distant. **Maybe the basal ganglia connectivity?.**

2.3 Some clinical models

The main question here is : Is the present model capable of investigating certain clinical phenomena?

2.3.1 Modelling the long-term disease states: Alzheimer's, Brain injury etc.

Although neurovascular coupling is a useful model to simulate the contraction/dilation of perfusing arterioles and thence oxygenation of the cerebral tissue and the integration of reactive species with the resulting consequence of mitochondrial dysfunction it **does not** enable the simulation of the long-term effects felt in Alzheimer's disease. The work of [?] may provide a viable method for modelling long-term effects. They use singular perturbation theory to encompass the two time scales "allowing conditions under which the diseased state can maintain the slow movement toward diseased state equilibrium".

can we use the method of [?] to model slow disease states such as plaque growth and Alzheimer's?

What is the fast variable in Alzheimer's?

2.3.2 Cortical Spreading Depression (CSD), Subarachnoid hemorrhage (SAH) and traumatic brain injury (TBI)

We look at the condition of subarachnoid hemorrhage since it seems that ECS K^+ has a particularly important role to play in determining the continued perfusion of ischaemic cerebral tissue this is exemplified by the perspective editorial in Nature Medicine by Lo [?]. Dreier [16] reviews the role of spreading depression and ischaemia in neurological diseases. The review puts forward a number of interesting phenomena which our model may well be able to simulate. In a substantial number of cases cortical spreading depression (CSD) occurs which can support several important physiological states. Shin et al [?] present data showing anoxic depolarisation cause vasoconstriction and reduce CBF in the ischaemic cortex strengthening the argument for modelling.

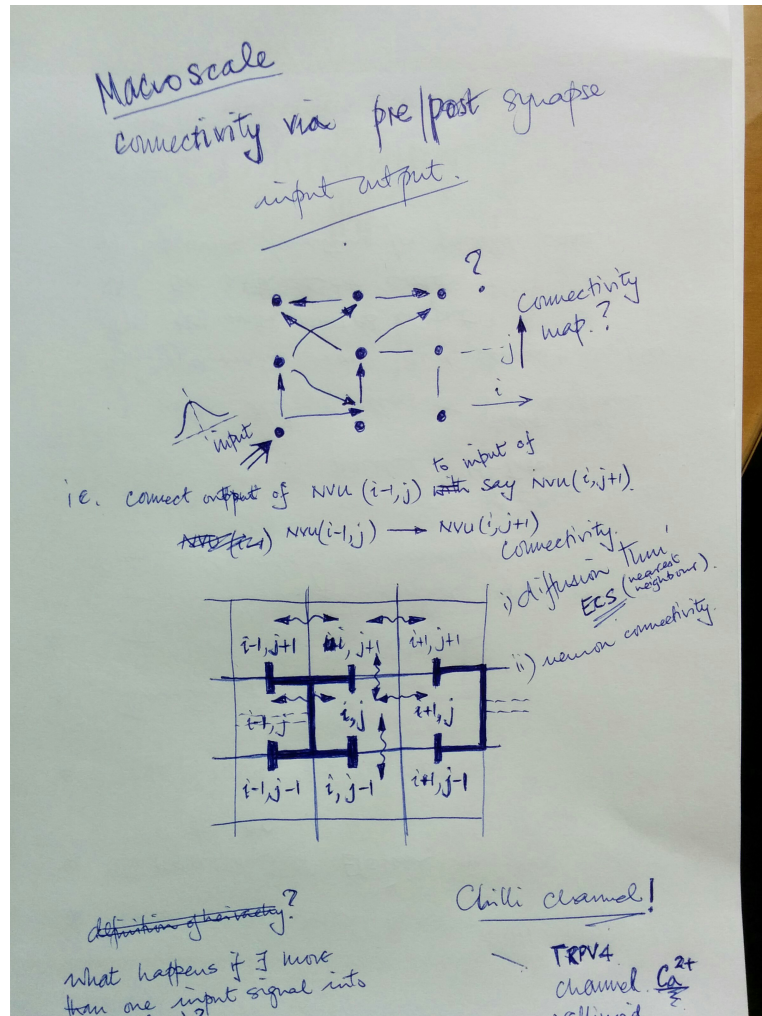


Figure 2.5: draft sketch of basic NVU with possible use in parBRAIN

1. During CSD neurotransmitters such as GABA, glutamate are released in high concentrations whereby sustained cation influx occurs enhancing depolarisation. These high concentrations of glutamate signal vascular smooth muscle through a variety of pathways including arachidonic acid.
2. metabolism and energy demand are increased
3. CSD induces a rise in regional CBF (spreading hyperaemia) however despite this pockets of ischaemic tissue can occur. the increased rate of metabolism is not fully matched by the increase in rCBF.
4. tissue ATP falls, glucose concentration increases substantially along with the release of lactate and ECS pH falls.
5. basal K⁺ increases during SAH with a consequential shift from spreading hyperaemia to spreading ischaemia
6. basal NO decreases since it is scavenged by the increased haemoglobin due to the haemorrhage and possibly the uncoupling of eNOS along with rho kinase.
7. see Figure 4 in [16]
8. **Lisa's work with the [?] model is now important along with Elshin's new neuron model**
9. Michelle should work on mitochondrial models see [?]

[?] indicates that ischaemia (such as stroke) open gap junctions between neurons, the P_{x1} channel. This channel opening may result in an efflux of ATP and glucose resulting in a decrease in the recovery rate from the ischaemic insult. [?] reviews the current state of effects of SAH on NVC. With the increase of K⁺ and extravascular haemoglobin (causing reduced NO) dilation (see [?] for experimental evidence) is shifted to constriction which reduces blood flow and causes further ischaemia to an already deprived cerebral area. The authors state that increased K⁺ causes a switch between dilation to constriction and of course we can already model this. They suggest that inversion of neurovascular coupling after SAH is due to increased basal BK channel activity and increased K⁺ in the PVS. There is also experimental evidence given in [?] noting especially Figures 5 and 7.

[?] provides experimental evidence for the role of glial KIR channels and Na⁺/K_{ATPase}-pump in regulating ECS K⁺ (in the rat hippocampus). They state that K⁺ dynamics are independent of the neuronal membrane potential but are a function of the "balance" between extruded K⁺ by those neurons which are firing and the K⁺ buffered by the glial mechanism. This is important in determining the correct ECS K⁺ crucial for modelling SAH etc. A good explanation of uncontrolled depolarisation of neurons following stroke or brain ischaemia is given in [?].

The work of [?] gives evidence concerning the increase in oxygen consumption (by approx 71 %) and surprisingly an increase of CBF by approx 238 % which they state impaired NVC after CSD. In the following 2 hours the authors suggested impaired NVC by looking at the local field potential (LFP) versus CBF. Early work by [?] provides evidence of pH changes during CSD and cerebral ischaemia caused they hypothesise by hyperpolarisation. As cited above [?] by modelling astrocytic networks simulate the consequence of CSD-triggered Ca^{2+} .

2.4 Experimental Validation

- we have started a collaboration with Jason Berwick in Sheffield (UK).
put in details of Berwick lab
- we should look more closely at the work of Bai et al with respect to the TRPV4 channel and its relationship with Alzheimers. [?], [?]
- there is a small but important piece of validation with the work by Mauban et al [54]. The paper provides a relationship between calcium concentration in the SMC with variation in diameter of the perfusing arteriole (see Figure 4 in [54]).
- investigate the published work of the Hillman lab at Columbia see http://orion.bme.columbia.edu/~hillman/brain_imaging.html.
- investigate work of Edith Hamel see <https://www.mcgill.ca/neuro/research/researchers/hamel>
- work with KC Brennan : *in vivo* cortical spreading depression (Salt Lake, Utah)
- look at paper by Andrews et al [2] and [1] for experimental evidence on endothelial NO production.

Chapter 3

Literature review notes

Amiri et al [?] using a Morris Lecar model of a neuron investigate neural synchronisation along with the functional contribution of astrocytes in neuronal synchrony using computer simulations and field potential recordings. The structure is based on the CA1 hippocampal area. Models show that astrocytes are able to change the threshold value of transition from synchrony to asynchronous behaviour. The model consists of both pyramidal and inhibitory interneurons. Astrocytes are connected to both pyramidal and interneurons. This particular paper may have some important information when looking at the role of ATP production from astrocytes and how this affects the LTP and LTD of neurons.

Lecrux and Hamel [51] review neurovascular coupling in brain function and disease. They suggest that the main pathway is via COX-1 and the association of GABA interneurons along with astrocytes form the relationship with glutamatergic pyramidal neurons. They state that NO is NOT a primary mediator of the CBF response to neuronal stimulation but rather a permissive factor required for vasodilation by other pathways. In addition there seems to be clear evidence of the role of EETs in functional hyperaemia (this is via the arachidonic acid pathway) and that EETs may also act in a paracrine fashion by enhancing astrocytic Ca^{2+} leading to the opening of Ca^{2+} sensitive K^+ channels. Finally they state that increases in perivascular K^+ can induce vasodilation which supports our current model. It is therefore clear that we should look at the COX-1 pathway as well as K^+ . Lecrux and Hamel also write about the possible relationship between neurovascular coupling and Alzheimers; indeed they mention that some authors consider AD to be a vascular disease [70].

look at GABA interneurons and the glutamatergic pyramidal neurons forming a COX-1 type pathway via AA and EETs. In contrast to the K^+ pathway that we currently support.

[36] shows further evidence of the relationship between internuerons via GABA and functional hyperaemia.

The abstract states

Brain perfusion is tightly coupled to neuronal activity, is commonly used to monitor normal or pathological brain function, and is a direct reflection of the interactions that occur between neuronal signals and blood vessels. Cerebral blood vessels at the surface and within the brain are surrounded by nerve fibers that originate, respectively, from peripheral nerve ganglia and intrinsic brain neurons. Although of different origin and targeting distinct vascular beds, these "perivascular nerves" fulfill similar roles related to cerebrovascular functions, a major one being to regulate their tone and, therein, brain perfusion. This utmost function, which underlies the signals used in functional neuroimaging techniques and which can be jeopardized in pathologies such as Alzheimer's disease, stroke, and migraine headache, is thus regulated at several levels. Recently, new insights into our understanding of how neural input regulate cerebrovascular tone resulted in the rediscovery of the functional "neurovascular unit." These remarkable advances suggest that neuron-driven changes in vascular tone result from interactions that involve all components of the neurovascular unit, transducing neuronal signals into vasoconstrictor responses not only through direct interaction between neurons and vessels but also indirectly via the perivascular astrocytes. Neurovascular coupling is thus determined by chemical signals released from activated perivascular nerves and astrocytes that alter vascular tone to locally adjust perfusion to the spatial and temporal changes in brain activity.

in addition they state

Recently, in cortical and hippocampal brain slices, it was evidenced that application of norepinephrine triggers increases in intracellular Ca²⁺ concentrations ($[Ca^{2+}]_i$) in astrocytes and perivascular astrocytic end-feet and that this response elicited constriction of the microarterioles on which the end-feet abutted [?]. Furthermore, the authors were able to show that the contraction was mediated by 20-HETE, a cytochrome P450A derivative of arachidonic acid. However, other studies in cortical brain slices showed that a rise in astrocytic $[Ca^{2+}]_i$ after increased neuronal activity by electrical stimulation [22] or synaptically released glutamate [71] induced dilatations of cortical arterioles. In the latter study, the vasoactive signaling molecule corresponded to a cyclooxygenase product of arachidonic acid, likely PGE2, but could not be unequivocally demonstrated. Furthermore, it was suggested by Filosa and colleagues [22] that suppression of $[Ca^{2+}]_i$ oscillations and accompanying vasomotion in microarterioles, possibly due to smooth muscle hyperpolarization, was involved in coupling local perfusion to increased neuronal activity. Despite apparent discrepancies between findings of microvascular contraction and dilatation mediated by changes in astrocytic Ca²⁺, likely because of different experimental paradigms and the use or not of preconstricted vessels

in the slices, these studies emphasize the importance of further assessing this newly identified intermediary role of astrocytes in transducing neuronal signals into vasomotor responses [?] [?] and whether or not the endothelium is required for their vasomotor effects [?]. Furthermore, as can be appreciated, several recent studies have used brain slices to investigate the role of astrocytes or neurons (see LOCAL INTERNEURONS) in the regulation of micro- vascular tone. Although limited by the fact that brain slices are maintained in artificial conditions in which vessels are not pressurized and do not have intraluminal flow, it is unarguable that such preparations, in which neuronal glial vascular interactions are preserved and can be assessed in a controlled manner, offer an additional means to isolated microvessels and whole animal experiments for investigating the microcirculation.

?] proposes that hypoxia facilitates Alzheimer's pathology by upregulating BACE1 gene expression. Figure 3.1 shows the basic hypothesis which was the kernel of an (unsuccessful) HRC grant in 2013. **This particular area of work is a high priority for our group.**

Rejuvinate the BACE1/hypoxic hypothesis for another HRC grant application

?] provides a model of brain circulation and importantly energy metabolism. Their model was used to investigate and compare with NIRS signals (oxyhemoglobin concentrations). The model for functional hyperaemia is relatively simple compared to our model. However the energy consumption model is worth looking at. Equations for the Banaji model can be found at [?]

investigate energy model of mitochondrial oxygen consumption of [?] perhaps we should compare with the model of ?]

?] shows through experimentation that hypoxia induces an intracellular Ca^{2+} rise and that ROS is the key indicator of hypoxic vasoconstriction. The Ca^{2+} rise is mediated by a reduction in the FK506 binding protein (an inhibitor of RyR). The experiments are done on pulmonary arteries and it is yet to be shown as to whether this particular phenomenon occurs in cerebral arteries. Again this could be linked to the work on the BACE1 expression.

Ostergaard et al. [58] provides experimental evidence of neurovascular coupling during cortical spreading depression. The group defines a capillary transit time heterogeneity (CTH) which looks at the variation in transit times for RBCs passing through the capillary bed. They state that CTH reduces oxygen extraction efficacy. It is expected (according to their

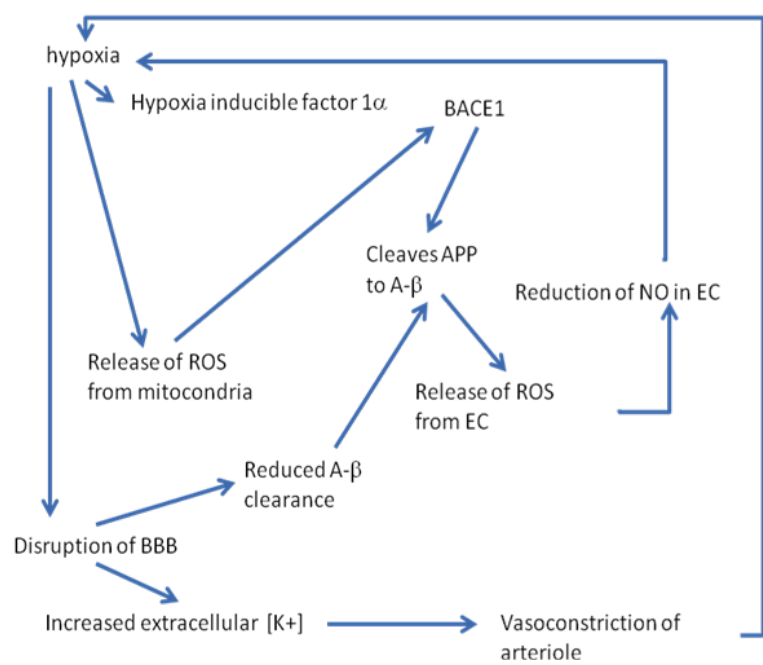


Figure 3.1: Sketch of hypothesis for hypoxic mediated production of ROS etc.

hypothesis) that reduction in CTH would increase oxygen efficient extraction during functional hyperaemia. They state that the recent study by [] indicates control of CBF and CTH is done via pericytes. However a more recent publication by [] indicates that pericytes have no contractile ability and do not participate in functional hyperaemia. Althought this paper by Ostergaard provides experimental evidence it does not in any way support the physiological phenomena that clearly occurs during metabolic activation and subsequent increase in CBF.

The clinical group of Ostergaard from Aarhus seem to attribute all phenomena (including BOLD signals which they refer to another group) to CTH. In reality this is a somewhat "blinkered" view to say the least.

LaFerla [47] provides an excellent review of calcium dyshomeostasis (a perturbation way from the cellular ionic equilibrium) and intracellular signalling in Alzheimer's disease.

Chapter 4

New projects

4.1 ATP/Astrocyte messaging from dendrite to dendrite: An intercellular model of heterosynaptic metaplasticity

This is the start of notes for a new project involving the Owen Jones/Cliff Abraham's lab.

There is substantial evidence of non-transporter mediated neuron-astrocyte communication. Early reports showed glutamate or GABA-mediated currents in cultured astrocytes (Bowman and Kimelberg, 1984; Hsli, Andrs, and Hsli, 1979; Kettenmann, Backus, and Schachner, 1984). Functional neurotransmitter receptors have since been found on astrocytes; among them are AMPARs (Seifert and Steinhauer, 1995), NMDARs (A. Serrano, Robitaille, and Lacaille, 2008), mGluRs (Nicoletti, et al., 1990), mAChRs (Ulas, 1988), ARs (Porter and McCarthy, 1995) and P2Rs (Neary and Zhu, 1994). However, receptor expression varies with astrocyte subtype (Matthias, et al., 2003; A. Serrano, et al., 2008) and development (Cai, Schools, and Kimelberg, 2000; Seifert, Zhou, and Steinhauser, 1997; Sun, et al., 2013).

Astrocytes respond to iGluR and mGluR activation with, respectively, rapid influx and intracellular release of Ca²⁺ (Cornell-Bell, Finkbeiner, Cooper, and Smith, 1990; Glaum, Holzwarth, and Miller, 1990). Cytosolic Ca²⁺ signals spread within and between astrocytes as Ca²⁺ waves, allowing long-range communication within cell networks. These waves require the formation of IP₃ (Leybaert, Paemeleire, Strahonja, and Sanderson, 1998), and are also triggered by acetylcholine (Araque, Martn, Perea, Arellano, and Buo, 2002), adenosine and ATP (Porter and McCarthy, 1996), GABA (Fraser, et al., 1995) and mechanical stimulation (Charles, Merrill, Dirksen, and Sanderson, 1991). They may also appear spontaneously

(Nett, Oloff, and McCarthy, 2002; Parri and Crunelli, 2001). Evoked astrocytic Ca^{2+} signals are highly plastic. They are augmented or depressed by varying patterns of synaptic stimulation (Perea and Araque, 2005), and display lasting increases in frequency with repeated generation (Pasti, Pozzan, and Carmignoto, 1995; Pasti, Volterra, Pozzan, and Carmignoto, 1997). Further, astrocytic A2BRs trigger widespread and sustained generation of asynchronous Ca^{2+} events lasting ≤ 20 min (Kawamura and Kawamura, 2011).

The nature of astrocyte-astrocyte Ca^{2+} signaling has been heavily debated. These signals were first thought to spread via GJNs (Enkvist and McCarthy, 1992). Astrocytes are extensively coupled via GJNs comprised of opposed connexin43 (Cx43) hemichannels (Giaume, et al., 1991; Yamamoto, Ochalski, Hertzberg, and Nagy, 1990), which allow passage of small molecules such as Ca^{2+} and IP₃ (Saez, Connor, Spray, and Bennett, 1989). Inter-astrocytic signaling via GJNs is enhanced in an activity-dependent manner (Enkvist and McCarthy, 1994; Rouach, Glowinski, and Giaume, 2000), and is bidirectionally regulated via channel phosphorylation by serine-threonine kinases (Kwak, et al., 1995; Sez, Martinez, Braes, and Gonzalez, 1998; Shah, Martinez, and Fletcher, 2002). However, cultured astrocytes display intercellular Ca^{2+} waves even when not coupled by GJNs (Hassinger, Guthrie, Atkinson, Bennett, and Kater, 1996). The extent of Ca^{2+} wave propagation is also independent of GJN coupling (Blomstrand, Berg, Eriksson, Hansson, and Rnnbck, 1999). Further, these waves are visible in Cx43-KO mutant mice (Suadicani, Brosnan, and Scemes, 2006).

An extracellular mode of communication between astrocytes has been identified. Ca^{2+} signaling between astrocytes is inhibited by blockers of purinergic receptors or by ectonucleotidases (Cotrina, Lin, and Nedergaard, 1998; Guthrie, et al., 1999). Previous reports of gap-junctional contribution to this process may be due to the inhibitory actions of GJN antagonists on P2X7Rs or connexin hemichannels, a trigger (Suadicani, et al., 2006) or source (Cotrina, Lin, Alves-Rodrigues, et al., 1998) of astrocytic ATP release, respectively. Importantly, ATP triggers further ATP release from neighbouring astrocytes (C. M. Anderson, Bergher, and Swanson, 2004). ATP can therefore trigger regenerative Ca^{2+} signals within the astrocytic network. As a caveat, GJNs may still be sufficient, if not essential, for mediating Ca^{2+} waves, as purine and GJN mediated Ca^{2+} waves can operate in tandem in culture (Paemeleire, et al., 2000).

Taken together, the results of the experiments in this thesis can be combined into a plausible explanation of how neurons and astrocytes generate temporally and spatially widespread metaplasticity in CA1 (Fig 4.1). The results implicate M1-AChRs as a likely trigger of the signalling cascade culminating in metaplasticity, whether via Gq-coupled Ca^{2+} release or by facilitated firing. It is also likely that M1-AChRs are responsible through either of these mechanisms for recruitment of astrocytes in SO. A

parsimonious explanation of purinergic involvement is that astrocytes respond to activation by releasing ATP, which triggers widespread signalling within the astrocytic network. This signalling could be accomplished via GJNs, but given the limited evidence for purely GJN-mediated communication between astrocytes, it is more likely that connexins, in the form of hemichannels, in fact serve as the source of released ATP. From here, ATP is hydrolysed extracellularly to adenosine which acts on A2BRs. Given the canonical actions of A2BR-mediated neuronal signalling, it is probable that the relevant receptors are on astrocytes. Further, given that BAY 60-6583 could prime SR synapses even when ejected into SO, it is plausible that A2BRs are the trigger of widespread intercellular communication, perhaps via the same mechanism described by Kawamura and Kawamura. The consequences of activating astrocytic A2BRs (namely, cytokine release) also provide a candidate mechanism for ultimately inhibiting LTP. Several components of this model are yet to be validated; however they provide testable hypotheses for further experimentation. Thus, a complete mechanistic explanation of heterosynaptic metaplasticity in CA1 is obtainable from the model.

In Figure 4.1 we have the following definitions.

- SO = stratum Oriens (contains the basal dendrites)
- SP = stratum Pyramidale (contains the cell bodies of pyramidal cells)
- SR = stratum Radiatum (contains the apical dendrites)
- SLM = stratum Lacunosum Moleculare (contains the tuft dendrites)

At some point in the cortical tissue an A_2B receptor is activated by ATP. This mediates an increase in cytosolic Ca^{2+} , this in turn increases ATP production from the cell and ATP then diffuses to the neighbouring tissue. The pathway now has two possibilities.

1. ATP acts on a purinergic receptor P2Y and releases Ca^{2+} which continues the path
2. ATP acts on an A_2B receptor and the path is continued

We intend to utilise version 2.* with parBRAIN to simulate this effect. A sketch is given in Figure 4.2. Our reason for using version 2.* is because we will need to diffuse ATP through the ECS (which all versions 1.* do not have). The version 2.*/parBRAIN code will need to have the ability to connect any variable within a subdomain with any other subdomain. At present parBRAIN can diffuse through the PVS (which is not physiologically realistic).

Figure 4.3 is taken from ?] and shows a schematic of the purinergic autocrine/paracrine regulation of Ca^{2+} dynamics. However the authors seem to concentrate on the perceived increase in (what look like from the data) random oscillations and frequencies. There is a large increase in (what

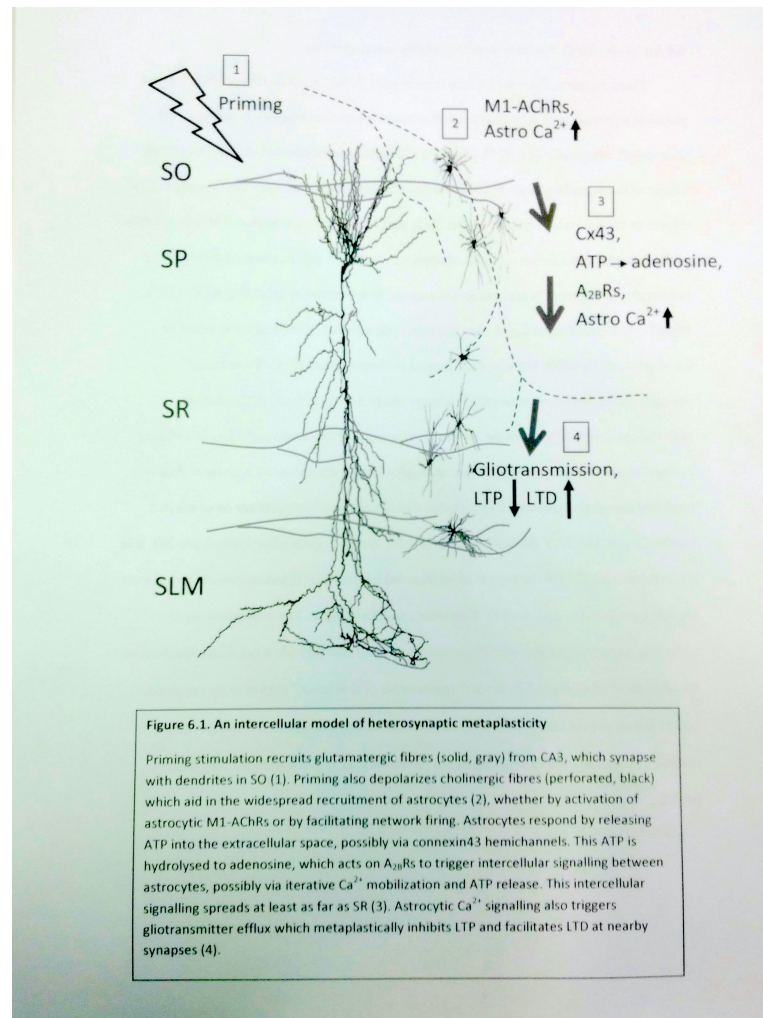


Figure 4.1: Sketch of heterosynaptic metaplasticity

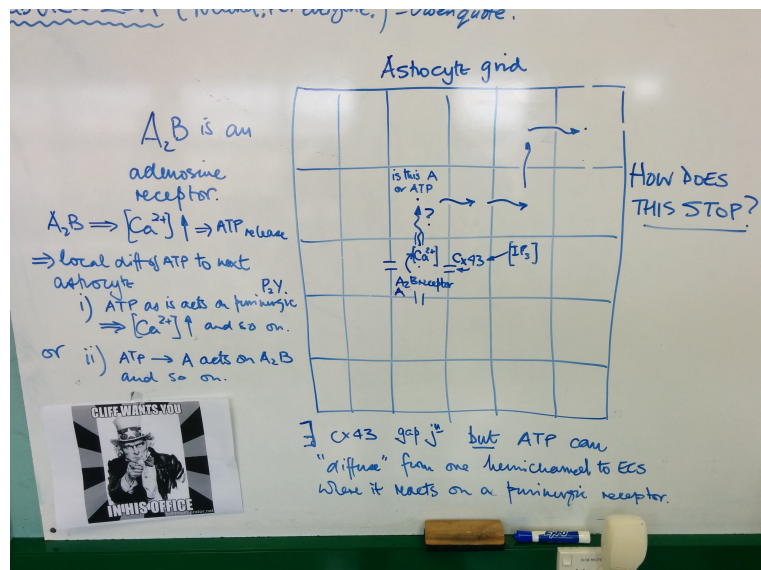


Figure 4.2: Sketch of possible communication of

they call) transient Ca^{2+} following ATP injection onto the brain slice. The so called oscillations do seem to be random and may possibly be just Ca^{2+} "puffs" released from the ER stores. But the main point to be taken from this is that on injection of ATP the Ca^{2+} increases and subsequently releases more ATP from the cell via CBX (carbenoxolone)-sensitive gap junction hemichannels. Mediated by the increase in ecto-ATPase via PKC activation the ATP is dephosphorylated to adenosine which then diffuses to an adenosine receptor (AdoR) on a different astrocyte which repeats the process and so on. carbenoxolone is an effective blocker of gap junctions.

One of the issues here is that we do not have as much data as we would like to provide the parameter values for the pathway suggested in Figure 4.3. We will need to dig deep into the paper of ?] and ask questions of Owen and Cliff.

We do have a possible problem here since the neuron compartment model of ELshin uses the entire neuron in the compartment ; meaning that there are parameters for the the resistance and half-length of the dendritic tree. So if we wish to use the compartments as sub-domains that cover a single pyramidal neuron then we will need to look carefully at the neuron model in each sub-domain. Rather than one neuron in a single sub-domain as is the case at present we will need to "split" the neuron" across the entire domain.

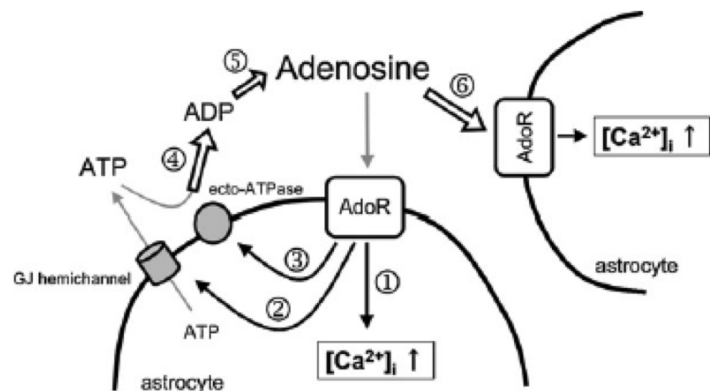


Figure 4.3: schematic of the purinergic autocrine/paracrine regulation of Ca^{2+} dynamics

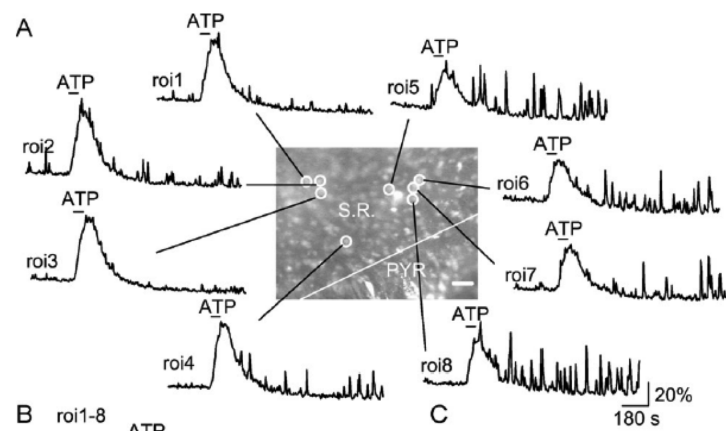


Figure 4.4: time dependent profiles for 8 rois of Ca^{2+} dynamics taken from [?]

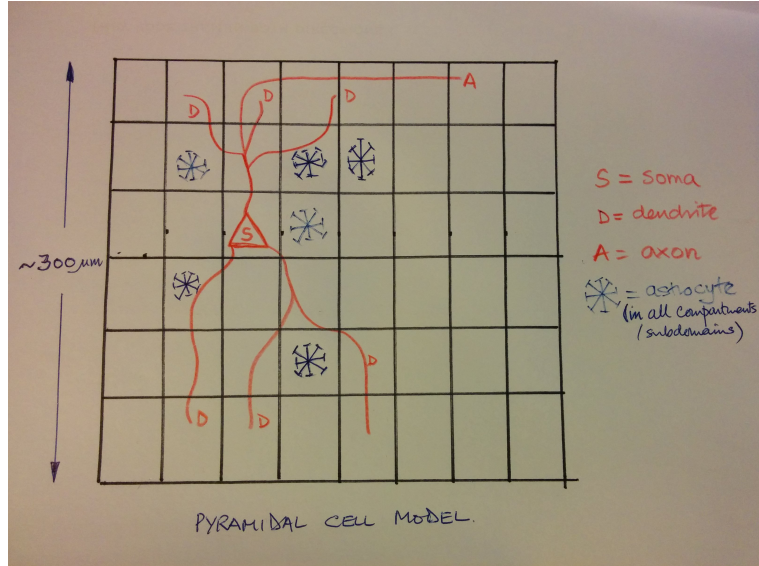


Figure 4.5: schematic of a pyramidal cell mapped onto a tissue slice with associated astrocytes

4.1.1 Algorithm development

In order to simulate the diffusion of adenosine in the cerebral tissue the neuron dendrites and soma need to be mapped across the subdomains of the computational tissue slice. So each subdomain holds a section of the dendrite or axon. Then a discrete version of the neuron model equations is needed. As we shall see we can utilise this discrete methodology to our advantage. We need to solve for the membrane potential E_m governed by the partial equation which is similar to 1.4.1 and 1.4.2 but has the full diffusion format rather than a linear gradient approximation

$$C_m \frac{\partial E_m}{\partial t} = -I_{s,tot} + \frac{1}{2R_a} \frac{\partial E_m}{\partial x^2} \quad (4.1.1)$$

and the ion concentration along the dendrite and axon/soma projections

$$\frac{\partial [ion]_{cyto,i}}{\partial t} = -\frac{A_s}{FV_s} I_{s,i,tot} + \frac{D_{ion}(V_d + V_s)}{2V_s} \frac{\partial [ion]_{cyto,i}}{\partial x^2} \quad (4.1.2)$$

for each ion species i. We discretise the equations in a number of ways depending on the form of the ionic currents. For linear Hodgkin Huxley forms then we use a similar manner to that found in the book by Gabbiani and Cox (Mathematics for Neuroscientists, Academic Press, 2010). When this works we will then use the more robust but more complex algorithm of Wagner and Kozloski [?]. Finally we will utilise the Gold-

man/Hodgkin/Katz ionic current equations (which are inherently non-linear). As noted in section 1.4.2 we also need to solve for the ion concentrations and the associated activation variables m and h . Their equations are given below as

$$\frac{dm}{dt} = \alpha_m(V)(1 - m) - \beta_m(V)m \quad (4.1.3)$$

$$\frac{dh}{dt} = \alpha_h(V)(1 - h) - \beta_h(V)h \quad (4.1.4)$$

These equations state that the closed activation gates, $(1-m)$, open at rate $\alpha_m(V)$, while the open activation gates, m , close at a rate $\beta_m(V)$. It is similar for the inactivation gates. The rate functions, $\alpha_m(V)$ and $\beta_m(V)$, are functions that depend on the voltage across the membrane. The forms of the functions α and β are usually determined through a mix of theoretical and empirical considerations and they are of the form

$$\alpha(V) = a_0 \exp\left(\frac{-\delta V}{s}\right) \quad (4.1.5)$$

$$\beta(V) = b_0 \exp\left(\frac{(1-\delta)V}{s}\right) \quad (4.1.6)$$

where a_0 , b_0 , and δ are positive constants, with $0 \leq \delta \leq 1$. A gate that tends to open on depolarisation will have $s < 0$, while a gate that tends to open on hyperpolarisation will have $s > 0$. These exponential forms are modified to fit the experimental data. The equation of the rate of change of activation gates may be rewritten as

$$\frac{dm}{dt} = \frac{m_\infty(V) - m}{\tau_m(V)} \quad (4.1.7)$$

where

$$m_\infty(V) = \frac{\alpha_m(V)}{\alpha_m(V) + \beta_m(V)} \quad (4.1.8)$$

and

$$\tau_m(V) = \frac{1}{\alpha_m + \beta_m(V)} \quad (4.1.9)$$

We should also define the appropriate boundary conditions at the ends of the axon/dendrite such that

$$\frac{\partial E_m}{\partial x} = (0, t) = \frac{\partial E_m}{\partial x}(L, t) \quad (4.1.10)$$

and that things begin at rest so that

$$E_m(x, 0) = E_{m,r}, \quad m(x, 0) = m_{inf}(E_{m,r}), \quad h(x, 0) = H_{inf}(E_{m,r}), \quad n(x, 0) = n_{inf}(E_{m,r}). \quad (4.1.11)$$

Suppose that the entire length of the neuron is of length, L. Then we choose $N_x = \frac{L}{dx}$ compartments and a specific timestep dt. Variables are evaluated on the associated space-time grid such that

$$E_{m,i}^j \approx E_m((i - 1/2)dx, (j - 1)dt) \quad (4.1.12)$$

$$m_i^j \approx m((i - 1/2)dx, (j - 1)dt) \quad (4.1.13)$$

$$ion_i^j \approx ion((i - 1/2)dx, (j - 1)dt) \quad (4.1.14)$$

$$i = 1, \dots, N_x, \quad j = 1, \dots, N_t \quad (4.1.15)$$

We now need to discretise the gate variables m and h. This is achieved with a trapezoidal approximation so that equations ?? and ?? can be written as

$$m_i^j - m_i^{j-1} = \alpha_m(E_m^{j-1})dt - (\alpha_m(E_m^{j-1}) + \beta_m(E_m^{j-1}))(m_i^j + m_i^{j-1})dt/2 \quad (4.1.16)$$

and simplified as

$$m_i^j = \frac{(1/dt - (\alpha_m(E_m^{j-1}) + \beta_m(E_m^{j-1}))/2)m_i^{j-1} + \alpha_m(E_m^{j-1})}{1/dt + (\alpha_m(E_m^{j-1}) + \beta_m(E_m^{j-1}))/2} \quad (4.1.17)$$

this is repeated for the gating variable h.

There is a simpler notation where we use the format of

$$\frac{dm_i}{dt} = \frac{m_{i,inf}(E_m(t)) - m_i(t)}{\tau_m(E_m(t))} \quad (4.1.18)$$

so that the discretised equation for m becomes

$$m_i^j = \frac{(2\tau_m(E_m^{j-1}) - dt)m_i^{j-1} + 2m_{i,inf}(E_m^{j-1})dt}{2\tau_m(E_m^{j-1} + dt)} \quad (4.1.19)$$

with a similar equation for h. We now discretise the equations for membrane potential E_m 4.1.1 and the various ion concentrations 4.1.2. We collect the compartmental terms into vectors such that

$$\mathbf{E}_m = (E_{m,1}^j, E_{m,2}^j, \dots, E_{m,N_x}^j)^T \quad (4.1.20)$$

$$\mathbf{ion}_k^j = (ion_{k,1}^j, ion_{k,2}^j, \dots, ion_{k,N_x}^j)^T \quad (4.1.21)$$

Following the form given in by Gabbiani and Cox (Mathematics for Neuroscientists, Academic Press, 2010, pages 120, 121) then

$$C_m \frac{\mathbf{E}_m^{j-1/2} - \mathbf{E}_m^{j-1}}{dt/2} = G_a \mathbf{S} \cdot \mathbf{E}_m^{j-1/2} - I_{total}(\mathbf{E}_m^{j-1/2}) + I_{stim} \quad (4.1.22)$$

$$\frac{\mathbf{ion}_k^{j-1/2} - \mathbf{ion}_k^{j-1}}{dt/2} = D \mathbf{S} \cdot \mathbf{ion}_k^{j-1/2} - \frac{2}{Fa} I_{total}(\mathbf{E}_m^{j-1/2}) \quad (4.1.23)$$

where a is the area of the dendrite/axon and \mathbf{S} is the standard difference matrix for diffusion. We can write this as a linear system for $\mathbf{E}_m^{j-1/2}$ and $\mathbf{ion}_k^{j-1/2}$.

$$(diag((\mathbf{d}_{E_m}^j + 2C_m/dt) + G_a \mathbf{S}) \mathbf{E}_m^{j-1/2} = (2C_m/dt) \mathbf{E}_m^{j-1} + \mathbf{f}_{E_m}^j \quad (4.1.24)$$

$$(diag((\mathbf{d}_{ion}^j + 2/dt) + D \cdot \mathbf{S}) \mathbf{ion}^{j-1/2} = (2/dt) \mathbf{ion}^{j-1} + \mathbf{f}_{ion}^j \quad (4.1.25)$$

where the elements of $\mathbf{d}_{E_m}^j$ and \mathbf{d}_{ion}^j are functions of $E_m^{j-1/2}$ and those of $\mathbf{f}_{E_m}^j$ and \mathbf{f}_{ion}^j are constant functions.

Finally we update both \mathbf{E}_m and \mathbf{ion} using

$$\mathbf{E}_m^j = 2\mathbf{E}_m^{j-1/2} - \mathbf{E}_m^{j-1} \quad (4.1.26)$$

$$\mathbf{ion}^j = 2\mathbf{ion}^{j-1/2} - \mathbf{ion}^{j-1} \quad (4.1.27)$$

We should note that equation 4.1.24 is non-linear since the active ion currents are non-linear and are functions of the unknown $E_m^{j-1/2}$. Due to the active form of the Goldman/Hodgkin/Katz ion current given by

$$I_{GHK} = m^p h^q \frac{g_{ion} F E_m [ion]_{cyto} - e^{(\frac{-E_m}{\phi})} [ion]_{ext}}{\phi [1 - e^{(\frac{-E_m}{\phi})}]} \quad (4.1.28)$$

Hence they would therefore require an iterative scheme. However the equation is of parabolic form and can be solved using an iterative scheme. The passive leak currents are in the linear form of Hodgkin-Huxley given by $I_{k,HH} = g_{HH}(E_m - E_k)$ for the ion species k . We show the method of solution from discretising the equations 4.1.24 in the following format

$$E_{m,i}^{j-1/1} \left[1 + \frac{2\delta t G_a}{C_m (\delta x)^2} \right] - \frac{G_a \delta t}{C_m (\delta x)^2} \left[E_{m,i+1}^{j-1/2} + E_{m,i-1}^{j-1/2} \right] - \frac{\delta t}{C_m} I_l(E_{m,i}^{j-1/2}) = \frac{\delta t}{C_m} \left[I_n(E_{m,i}^j) \right] + E_{m,i}^j \quad i = 1, \dots, N_x \quad (4.1.29)$$

and for each ion species k ,

$$ion_{k,i}^{j-1/2} \left[1 + \frac{2\delta t D}{(\delta x)^2} \right] - \frac{D \delta t}{(\delta x)^2} \left[ion_{k,i+1}^{j-1/2} + ion_{k,i-1}^{j-1/2} \right] - \delta t I_l(ion_{k,i}^{j-1/2}) = \delta t \left[I_n(ion_{k,i}^j) \right] + ion_{k,i}^j \quad i = 1, \dots, N_x$$

(4.1.30)

Here I_l and I_n are the linear and non-linear parts of the ion current respectively. To solve this matrix system we iterate at each time step due to the non-linear currents. For this case we choose a starting membrane potential E_{m_0} and set of ionic species \mathbf{ion}_0 . These are then used in the non-linear current $I_n(E_{m_0}, \mathbf{ion}_0^j)$. We then solve for $E_{m,i}^{j-1/2}$ and $ion_{k,i}^{j-1/2}$. We use this value in the non-linear part of the discretised equations and again solve for $ion_{k,i}^{j-1/2}$ etc until there is no change in either $ion_{k,i}^{j-1/2}$ or $E_{m,i}^{j-1/2}$. To complete the full Crank-Nicolson step we then update as follows

$$\mathbf{E}_m^j = 2\mathbf{E}_m^{j-1/2} - \mathbf{E}_m^{j-1} \quad (4.1.31)$$

$$\mathbf{ion}_k^j = 2\mathbf{ion}_k^{j-1/2} - \mathbf{ion}_k^{j-1} \quad (4.1.32)$$

Finally we need to specify an equation for the ionic concentration in the extracellular space.

$$\frac{\partial \mathbf{ion}_{k,e}}{\partial t} = D_e \frac{\partial^2 \mathbf{ion}_{k,e}}{\partial x^2} + \frac{2}{F f_e} I_{total}(\mathbf{E}_m) \quad (4.1.33)$$

f_e is the volume fraction of the extracellular space (approximately 15%). The discretised equation becomes

$$\frac{\mathbf{ion}_{k,e}^{j-1/2} - \mathbf{ion}_{k,e}^{j-1}}{dt/2} = D_e \mathbf{S} \cdot \mathbf{ion}_{k,e}^{j-1/2} + \frac{2}{F} I_{total}(\mathbf{E}_m^{j-1/2}) \quad (4.1.34)$$

The time step is then incremented and the inner iteration is started anew. The neuron model developed above now needs to be embedded into a slice of tissue in a similar manner to that used in parBRAIN see Chapter 2. How do we do this?

neuron in tissue slice

As a first attempt we simplify the geometry of the neuron such that it has a linear form, i.e. that it is a simple active uniform cable. This is shown in Figure ???. We will extend this to the full dendritic tree at a later stage.

The normal size of the tissue slice when implementing an NVU coupled problem is of the order of millimeters. However a pyramidal neuron for instance is of the order of length 300-500 μm . In addition the discretised uniform cable would normally have approximately hundreds of compartments. This means that the neuron would only cross a few tissue slice subdomains. In fact on the basis of modelling dimensions from [?] a

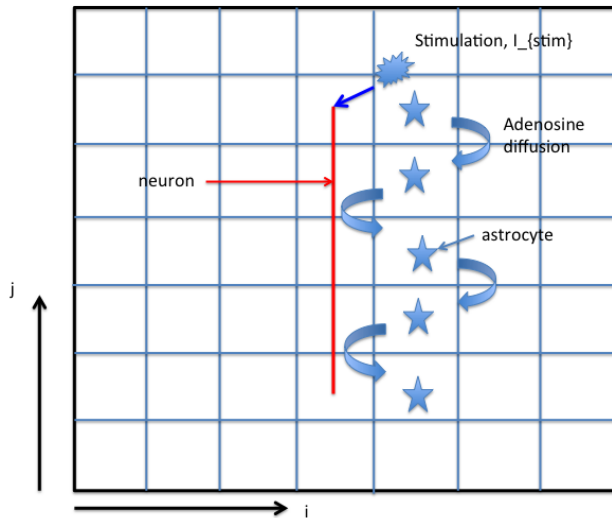


Figure 4.6: sketch of the simple neuron embedded into the tissue slice , showing the anticipated diffusion of adenosine from astrocyte to astrocyte

tissue slice that has 64 subdomains per side and the length of the tissue slice is 25.6 mm, then each subdomain is only $400 \mu\text{m}$ wide. Enough for a single neuron. Astrocytes, although have small cell bodies have a long extensions (pseudo-pods) so it is difficult to estimate their exact size. However I suspect that they can reach from one end of a neuron to another.

For the moment we treat the astrocytes as being small enough to have one in each subdomain and each subdomain has a characteristic length of the order of δx (the discretised length for the neuron model). We go back to the Figure ?? and investigate the best way to utilise the parBRAIN parallel code to solve the neuron model along with diffusion of adenosine/ATP from astrocyte to astrocyte.

Chapter 5

Priorities

5.1 Priority List

1. first item
2. second item etc.

Bibliography

- [1] Allison M. Andrews, Dov Jaron, Donald G. Buerk, Patrick L. Kirby, and Kenneth a. Barbee. Direct, real-time measurement of shear stress-induced nitric oxide produced from endothelial cells in vitro. *Nitric Oxide - Biology and Chemistry*, 23(4):335–342, 2010. ISSN 10898603. doi: 10.1016/j.niox.2010.08.003. URL <http://dx.doi.org/10.1016/j.niox.2010.08.003>.
- [2] Allison M Andrews, Dov Jaron, Donald G Buerk, and Kenneth a Barbee. Shear stress-induced NO production is dependent on ATP autocrine signaling and capacitative calcium entry. *Cellular and molecular bioengineering*, 7(4):510–520, December 2014. ISSN 1865-5025. doi: 10.1007/s12195-014-0351-x. URL <http://www.ncbi.nlm.nih.gov/pubmed/25386222>.
- [3] David Attwell, Alastair M Buchan, Serge Charpak, Martin Lauritzen, Brian A MacVicar, and Eric A Newman. Glial and neuronal control of brain blood flow. *Nature*, 468(7321):232–243, November 2010. ISSN 1476-4687. doi: 10.1038/nature09613. URL <http://www.pubmedcentral.nih.gov/articlerender.fcgi?artid=3206737&tool=pmcentrez&rendertype=abstract>.
- [4] Eduardo E Benarroch. *Basic neurosciences with clinical applications*. Butterworth-Heinemann, 2006.
- [5] D. S. Bredt. Nitric oxide signaling specificity – the heart of the problem. *Journal of Cell Science*, 116(1):9–15, January 2003. ISSN 00219533. doi: 10.1242/jcs.00183. URL <http://jcs.biologists.org/cgi/doi/10.1242/jcs.00183>.
- [6] Anthony R Butler, Ian L Megson, and Patrick G Wright. Diffusion of nitric oxide and scavenging by blood in the vasculature. 1425:168–176, 1998.
- [7] G Carmignoto, L Pasti, and T Pozzan. On the role of voltage-dependent calcium channels in calcium signaling of astrocytes in situ. *Jour.Neurosci*, 18(12):46374645, 1998.
- [8] Joshua C Chang, Kevin C Brennan, Dongdong He, Huaxiong Huang, Robert M Miura, Phillip L Wilson, and Jonathan J

Wylie. A mathematical model of the metabolic and perfusion effects on cortical spreading depression. *PloS one*, 8(8):e70469, January 2013. ISSN 1932-6203. doi: 10.1371/journal.pone.0070469. URL <http://www.ncbi.nlm.nih.gov/articlerender.fcgi?artid=3743836&tool=pmcentrez&rendertype=abstract>.

- [9] Kejing Chen and Aleksander S Popel. Theoretical analysis of biochemical pathways of nitric oxide release from vascular endothelial cells. *Free radical biology & medicine*, 41(4):668–80, August 2006. ISSN 0891-5849. doi: 10.1016/j.freeradbiomed.2006.05.009. URL <http://www.ncbi.nlm.nih.gov/pubmed/16864000>.
- [10] Kejing Chen and Aleksander S Popel. Vascular and perivascular nitric oxide release and transport: Biochemical pathways of neuronal nitric oxide synthase (NOS1) and endothelial nitric oxide synthase (NOS3). 42:811–822, 2007. doi: 10.1016/j.freeradbiomed.2006.12.007.
- [11] A Comerford and T David. and Calcium Production in Arterial Geometries : An Integrated Fluid Mechanics / Cell Model. 130(February):1–13, 2008. doi: 10.1115/1.2838026.
- [12] Peter Condorelli and Steven C George. In vivo control of soluble guanylate cyclase activation by nitric oxide: a kinetic analysis. *Biophysical journal*, 80(5):2110–2119, 2001.
- [13] Thomas H Crouch and Claude B Klee. Positive cooperative binding of calcium to bovine brain calmodulin. *Biochemistry*, 19(16):3692–3698, 1980.
- [14] K Dormanns, E M J van Disseldorp, R G Brown, and T David. Neurovascular coupling and the influence of luminal agonists via the endothelium. *Journal of theoretical biology*, 364C:49–70, August 2014. ISSN 1095-8541. doi: 10.1016/j.jtbi.2014.08.029. URL <http://www.ncbi.nlm.nih.gov/pubmed/25167790>.
- [15] K Dormanns, E von Disseldorp, R Brown, and T David. Neurovascular Coupling and the Influence of Luminal Agonists via the Endothelium. *Journal of Theoretical Biology*, 364:49–70, 2015.
- [16] Jens P Dreier. The role of spreading depression, spreading depolarization and spreading ischemia in neurological disease. *Nature medicine*, 17(4):439–447, April 2011. ISSN 1546-170X. doi: 10.1038/nm.2333. URL <http://www.ncbi.nlm.nih.gov/pubmed/21475241>.
- [17] Kathryn M Dunn, David C Hill-Eubanks, Wolfgang B Liedtke, and Mark T Nelson. TRPV4 channels stimulate Ca²⁺-induced Ca²⁺ release in astrocytic endfeet and amplify neurovascular coupling responses. *Proceedings of the National Academy of Sciences*, 110(15):6157–6162, 2013.

- [18] F R Edwards, G D S Hirst, and G D Silverberg. Inward Rectification in Rat Cerebral Arterioles; Involvement of Potassium Ions in Autoregulation. *Journal of Physiology*, 404(1):455–466, 1988.
- [19] Michelle a Erickson and William a Banks. Blood-brain barrier dysfunction as a cause and consequence of Alzheimer’s disease. *Journal of cerebral blood flow and metabolism : official journal of the International Society of Cerebral Blood Flow and Metabolism*, 33(10):1500–1513, October 2013. ISSN 1559-7016. doi: 10.1038/jcbfm.2013.135. URL <http://www.ncbi.nlm.nih.gov/pubmed/23921899>.
- [20] a a Fadel, K a Barbee, and D Jaron. A computational model of nitric oxide production and transport in a parallel plate flow chamber. *Annals of biomedical engineering*, 37(5):943–54, May 2009. ISSN 1573-9686. doi: 10.1007/s10439-009-9658-5. URL <http://www.ncbi.nlm.nih.gov/pubmed/19242805>.
- [21] Hannah Farr and Tim David. Models of neurovascular coupling via potassium and EET signalling. *Journal of theoretical biology*, 286(1):13–23, October 2011. ISSN 1095-8541. doi: 10.1016/j.jtbi.2011.07.006. URL <http://www.ncbi.nlm.nih.gov/pubmed/21781976>.
- [22] Jessica A Filosa, Adrian D Bonev, and Mark T Nelson. Calcium dynamics in cortical astrocytes and arterioles during neurovascular coupling. *Circulation research*, 95(10):e73–81, November 2004. ISSN 1524-4571. doi: 10.1161/01.RES.0000148636.60732.2e. URL <http://www.ncbi.nlm.nih.gov/pubmed/15499024>.
- [23] Jessica a Filosa, Adrian D Bonev, Stephen V Straub, Andrea L Meredith, M Keith Wilkerson, Richard W Aldrich, and Mark T Nelson. Local potassium signaling couples neuronal activity to vasodilation in the brain. *Nature neuroscience*, 9(11):1397–1403, November 2006. ISSN 1097-6256. doi: 10.1038/nn1779. URL <http://www.ncbi.nlm.nih.gov/pubmed/17013381>.
- [24] V M Filosa J.A. Blanco. Neurovascular coupling in the mammalian brain. *Exp Physiol*, 92(4):641–646, 2007.
- [25] B Fisslthaler, S Dimmeler, C Hermann, R Busse, and I Fleming. Phosphorylation and activation of the endothelial nitric oxide synthase by fluid shear stress. *Acta physiologica Scandinavica*, 168(1):81–88, January 2000. ISSN 0001-6772. URL <http://www.ncbi.nlm.nih.gov/pubmed/10691783>.
- [26] Ingrid Fleming and Rudi Busse. Endothelial Dysfunction: a Novel Therapeutic Target; NO: the Primary EDRF. 14:5–14, 1999.
- [27] U Förstermann, J P Boissel, and H Kleinert. Expressional control of the ‘constitutive’ isoforms of nitric oxide synthase (NOS I and NOS III). *The FASEB journal : official publication of the Federation of American Societies for Experimental Biology*, 12:773–790, 1998. ISSN 0892-6638.

- [28] Paul Forsythe, Mark Gilchrist, Marianne Kulka, and A Dean Befus. Mast cells and nitric oxide : control of production , mechanisms of response. 2001.
- [29] Helene Girouard and Costantino Iadecola. Neurovascular coupling in the normal brain and in hypertension, stroke, and Alzheimer disease. *Journal of Applied Physiology*, 100(1):328–335, January 2006. ISSN 8750-7587. doi: 10.1152/japplphysiol.00966.2005. URL <http://www.ncbi.nlm.nih.gov/pubmed/16357086>.
- [30] Hélène Girouard, Adrian D Bonev, Rachael M Hannah, Andrea Meredith, Richard W Aldrich, and Mark T Nelson. Astrocytic endfoot Ca²⁺ and BK channels determine both arteriolar dilation and constriction. *Proceedings of the National Academy of Sciences of the United States of America*, 107(8):3811–6, March 2010. ISSN 1091-6490. doi: 10.1073/pnas.0914722107. URL <http://www.pubmedcentral.nih.gov/articlerender.fcgi?artid=2840528&tool=pmcentrez&rendertype=abstract>.
- [31] Albert Goldbeter, Geneviève Dupont, and Michael J Berridge. Minimal model for signal-induced Ca²⁺ oscillations and for their frequency encoding through protein phosphorylation. *Proceedings of the National Academy of Sciences*, 87(4):1461–1465, 1990.
- [32] B. Gonzalez-Fernandez, J.M. Ermentrout. On the Origin and Dynamics of the Vasomotion of Small Arteries. *Mathematical Biosciences*, 167(2): 127–167, 1994.
- [33] James Hadfield, Michael J Plank, and Tim David. Modeling secondary messenger pathways in neurovascular coupling. *Bulletin of mathematical biology*, 75(3):428–443, March 2013. ISSN 1522-9602. doi: 10.1007/s11538-013-9813-x. URL <http://www.ncbi.nlm.nih.gov/pubmed/23358799>.
- [34] C M Hai and R A Murphy. Cross-bridge phosphorylation and regulation of latch state in smooth muscle Cross-bridge phosphorylation and regulation of latch state in smooth muscle. *American Journal of Cell Physiology*, 254: C99—C106, 1988.
- [35] Chi-ming Hai and Richard A Murphy. Ca²⁺ Crossbridge Phosphorylation, and Contraction. *Annual review of physiology*, 51(1):285–298, 1989.
- [36] Edith Hamel. Perivascular nerves and the regulation of cerebrovascular tone. *Journal of applied physiology (Bethesda, Md. : 1985)*, 100(3):1059–1064, March 2006. ISSN 8750-7587. doi: 10.1152/japplphysiol.00954.2005. URL <http://www.ncbi.nlm.nih.gov/pubmed/16467392>.
- [37] Nicola B Hamilton, David Attwell, and Catherine N Hall. Pericyte-mediated regulation of capillary diameter: a component of neurovascular coupling in health and disease. *Frontiers in neuroenergetics*, 2

(May):1–14, January 2010. ISSN 1662-6427. doi: 10.3389/fnene.2010.00005. URL <http://www.ncbi.nlm.nih.gov/pmc/articles/PMC2912025/>&tool=pmcentrez&rendertype=abstract.

- [38] D R Harder, R J Roman, and D Gebremedhin. Molecular mechanisms controlling nutritive blood flow: role of cytochrome P450 enzymes. *Acta physiologica scandinavica*, 168(4):543–549, 2000.
- [39] Yuji Hayashi, Masahiro Nishio, Yasuhito Naito, Hisayuki Yokokura, Yuji Nimura, Hiroyoshi Hidaka, Yasuo Watanabe, I I Cam-k II, Cam IV, Cam-k IV, and Ser. Regulation of Neuronal Nitric-oxide Synthase by Calmodulin Kinases *. 274(29):20597–20602, 1999.
- [40] Costantino Iadecola and Maiken Nedergaard. Glial regulation of the cerebral microvasculature. *Nature neuroscience*, 10(11):1369–1376, November 2007. ISSN 1097-6256. doi: 10.1038/nn2003. URL <http://www.ncbi.nlm.nih.gov/pubmed/17965657>.
- [41] Craig E Jahr and Charles F Stevenst. Calcium permeability of the N-methyl-D-aspartate receptor channel in hippocampal neurons in culture. 90(December):11573–11577, 1993.
- [42] R. Joannides, W. E. Haefeli, L. Linder, V. Richard, E. H. Bakkali, C. Thuillez, and T. F. Luscher. Nitric Oxide Is Responsible for Flow-Dependent Dilatation of Human Peripheral Conduit Arteries In Vivo. *Circulation*, 91(5):1314–1319, March 1995. ISSN 0009-7322. doi: 10.1161/01.CIR.91.5.1314. URL <http://circ.ahajournals.org/cgi/content/long/91/5/1314>.
- [43] Mahendra Kavdia and Aleksander S Popel. Wall shear stress differentially affects NO level in arterioles for volume expanders and Hb-based O₂ carriers. *Microvascular Research*, 66(1):49–58, July 2003. ISSN 00262862. doi: 10.1016/S0026-2862(03)00008-6. URL <http://linkinghub.elsevier.com/retrieve/pii/S0026286203000086>.
- [44] Mahendra Kavdia, Nikolaos M Tsoukias, and Aleksander S Popel. Model of nitric oxide diffusion in an arteriole: impact of hemoglobin-based blood substitutes. *American journal of physiology. Heart and circulatory physiology*, 282(6):H2245—53, June 2002. ISSN 0363-6135. doi: 10.1152/ajpheart.00972.2001. URL <http://www.ncbi.nlm.nih.gov/pubmed/12003834>.
- [45] James Keener and James Sneyd. *Mathematical Physiology: I: Cellular Physiology*. Springer, 2008. URL <http://books.google.co.nz/books?hl=en&lr=&id=HIkZ3QHbpTQC&oi=fnd&pg=PR7&dq=keener+sneyd+mathematical+physiology&ots=k6zeoVPXAQ&sig=aRIBo592DCPC5PrSn1lkaUG-E6M#v=onepage&q=keenersneydmathematicalphysiology&f=false>.

- [46] Michèle Koenigsberger, Roger Sauser, Jean-Louis JL Bény, and JJ Jean-Jacques Meister. Effects of arterial wall stress on vaso-motion. *Biophysical journal*, 91(September):1663–1674, September 2006. ISSN 0006-3495. doi: 10.1529/biophysj.106.083311. URL <http://www.ncbi.nlm.nih.gov/entrez/query.fcgi?artid=1544282&tool=pmcentrez&rendertype=abstract&http://www.sciencedirect.com/science/article/pii/S000634950671880X>.
- [47] Frank M LaFerla. Calcium dyshomeostasis and intracellular signalling in Alzheimer’s disease. *Nature reviews. Neuroscience*, 3(November):862–872, 2002. ISSN 1471003X. doi: 10.1038/nrn960.
- [48] J R Lancaster. BRIEF REVIEW A Tutorial on the Diffusibility and Reactivity of Free Nitric Oxide. 1(1):18–30, 1997.
- [49] Jack R Lancaster. Simulation of the diffusion and reaction of endogenously produced nitric oxide. *Proceedings of the National Academy of Sciences of the United States of America*, 91(17):8137–41, August 1994. ISSN 0027-8424. URL <http://www.ncbi.nlm.nih.gov/entrez/query.fcgi?artid=44560&tool=pmcentrez&rendertype=abstract>.
- [50] Michel Laurent, Michel Lepoivre, and Jean-pierre Tenu. Kinetic modelling of the nitric oxide gradient generated in vitro by adherent cells expressing inducible nitric oxide synthase. 113:109–113, 1996.
- [51] C LeCrux and E Hamel. Review: The neurovascular unit in brain function and disease. *Acta Physiologica*, 203:47–59, 2011.
- [52] T Malinski, Z Taha, S Grunfeld, S Patton, M Kapturczak, and P Tomboulian. Diffusion of Nitric Oxide in the Aorta Wall Monitored in Situ by Porphyrinic Microsensors. *Biochemical and Biophysical Research Communications*, 193(3):1076–1082, 1993. ISSN 0006-291X. doi: <http://dx.doi.org/10.1006/bbrc.1993.1735>. URL <http://www.sciencedirect.com/science/article/pii/S0006291X83717353>.
- [53] George A Mashour and Robert J Boock. Effects of shear stress on nitric oxide levels of human cerebral endothelial cells cultured in an artificial capillary system. pages 233–238, 1999.
- [54] Joseph R H Mauban, Seth T Fairfax, Mark a Rizzo, Jin Zhang, and Withrow Gil Wier. A method for noninvasive longitudinal measurements of $[Ca^{2+}]$ in arterioles of hypertensive optical biosensor mice. *American journal of physiology. Heart and circulatory physiology*, 307:H173–81, 2014. ISSN 1522-1539. doi: 10.1152/ajpheart.00182.2014. URL <http://www.ncbi.nlm.nih.gov/pubmed/24858846>.
- [55] Bernd Mayer and Benjamin Hernmens. Biosynthesis and action of nitric oxide in m malian cells. 0004(December), 1997.

- [56] Krystal Nizar, Hana Uhlirova, Peifang Tian, Payam A Saisan, Qun Cheng, Lidia Reznichenko, Kimberly L Weldy, Tyler C Steed, Vishnu B Sridhar, Christopher L MacDonald, and Others. In vivo Stimulus-Induced Vasodilation Occurs without IP₃ Receptor Activation and May Precede Astrocytic Calcium Increase. *The Journal of Neuroscience*, 33(19):8411–8422, 2013.
- [57] Ivar Ø stby, Leiv Ø yehaug, Gaute T Einevoll, Erlend A Nagelhus, Erik Plahte, Thomas Zeuthen, Catherine M Lloyd, Ole P Ottersen, and Stig W Omholt. Astrocytic Mechanisms Explaining Neural-Activity-Induced Shrinkage of Extraneuronal Space. *PLoS Computational Biology*, 5(1):1–12, 2009.
- [58] L. Ostergaard, J. P. Dreier, N. Hadjikhani, S. N. Jespersen, U. Dirnagl, and T. Dalkara. Neurovascular Coupling During Cortical Spreading Depolarization and -Depression. *Stroke*, pages 1–10, 2015. ISSN 0039-2499. doi: 10.1161/STROKEAHA.114.008077. URL <http://stroke.ahajournals.org/cgi/doi/10.1161/STROKEAHA.114.008077>.
- [59] M J Plank, D Wall, and T David. Atherosclerosis and calcium signalling in endothelial cells. *Progress in Biophysics and Molecular Biology*, 91:287–313, 2006.
- [60] Beverly A Rzigalinski, Peter F Blackmore, and Miriam D Rosenthal. Arachidonate mobilization is coupled to depletion of intracellular calcium stores and influx of extracellular calcium in differentiated U937 cells. *Biochimica et Biophysica Acta (BBA)-Lipids and Lipid Metabolism*, 1299(3):342–352, 1996.
- [61] Navid Safaeian and Tim David. A computational model of oxygen transport in the cerebrocapillary levels for normal and pathologic brain function. *Journal of cerebral blood flow and metabolism : official journal of the International Society of Cerebral Blood Flow and Metabolism*, 33(10):1633–1641, October 2013. ISSN 1559-7016. doi: 10.1038/jcbfm.2013.119. URL <http://www.ncbi.nlm.nih.gov/pubmed/23921901>.
- [62] Thomas H Sanderson, Christian a Reynolds, Rita Kumar, Karin Przyklenk, and Maik Hüttemann. Molecular mechanisms of ischemia-reperfusion injury in brain: pivotal role of the mitochondrial membrane potential in reactive oxygen species generation. *Molecular neurobiology*, 47(1):9–23, February 2013. ISSN 1559-1182. doi: 10.1007/s12035-012-8344-z. URL <http://www.pubmedcentral.nih.gov/articlerender.fcgi?artid=3725766&tool=pmcentrez&rendertype=abstract>.
- [63] David M Santucci and Sridhar Raghavachari. The Effects of NR2 Subunit-Dependent NMDA Receptor Kinetics on Synaptic Transmission and CaMKII Activation. 4(10), 2008. doi: 10.1371/journal.pcbi.1000208.
- [64] J. D. Stockand and S. C. Sansom. Mechanism of activation by cGMP-dependent protein kinase of large Ca²⁺-activated K⁺ channels in mesangial cells, 1996.

- [65] Cam Ha T Tran, Mark S Taylor, Frances Plane, Sridevi Nagaraja, Niko-laois M Tsoukias, Viktoriya Solodushko, Edward J Vigmond, Tobias Furstenhaupt, Mathew Brigdan, and Donald G Welsh. Endothelial Ca²⁺ wavelets and the induction of myoendothelial feedback. *American Journal of Physiology-Cell Physiology*, 302(8):C1226—C1242, 2012.
- [66] M W Vaughn, L Kuo, and J C Liao. Estimation of nitric oxide production and reactionrates in tissue by use of a mathematical model. *American Journal of Physiology-Heart and Circulatory Physiology*, 274(6):H2163—H2176, 1998.
- [67] T F Wiesner, B C Berk, R M Nerem, and R Obert M N Erem. A mathematical model of the cytosolic-free calcium response in endothelial cells to fluid shear stress. *Proceedings of the National Academy of Sciences*, 94(8):3726–3731, 1997.
- [68] J Wood and J Garthwaite. Models of the diffusional spread of nitric oxide: implications for neural nitric oxide signalling and its pharmacological properties. *Neuropharmacology*, 33(1):1235–1244, 1994. URL <http://www.sciencedirect.com/science/article/pii/0028390894900221>.
- [69] Jin Yang, John W Clark, Robert M Bryan, Claudia S Robertson, and S Claudia. Mathematical modeling of the nitric oxide/cGMP pathway in the vascular smooth muscle cell. *American Journal of Physiology-Heart and Circulatory Physiology*, 289(2):H886—H897, 2005. doi: 10.1152/ajpheart.00216.2004.
- [70] Berislav V Zlokovic. Neurovascular mechanisms of Alzheimer’s neurodegeneration. *Trends in neurosciences*, 28(4):202–208, April 2005. ISSN 0166-2236. doi: 10.1016/j.tins.2005.02.001. URL <http://www.ncbi.nlm.nih.gov/pubmed/15808355>.
- [71] M Zonta, M C Angulo, S Gobbo, B Rosengarten, K-A. Hossman, T Pozzan, and G Carmignoto. Neuron-to-Astrocyte signaling is central to the dynamic control of brain microcirculation. *Nature Neuroscience*, 6(1), 2003.

Appendices

.1 Appendix A: TRPV4 Channel work by de Ruijter

Addition of a stretch activated channel at the Astrocyte

Joerik de Ruijter ¹

Author

K. Dormanns ²

T. David ²

Supervisors

August 17, 2015

¹Department of Biomedical Engineering, Eindhoven University of Technology, The Netherlands

²Bluefern Supercomputing Unit, University of Canterbury, New Zealand

Contents

1	Introduction	2
1.1	Calcium signalling is critical for astrocyte function, TRPV4 is important in NVC.	2
1.1.1	Experimental results by Dunn et al. (2013)	3
1.1.2	Proposed model for calcium in astrocytic endfoot.	4
2	NVU model	6
2.1	NVU model	6
2.1.1	Neuron/Astrocyte	6
2.1.2	Smooth muscle cell and endothelial cell	9
2.1.3	Contraction model and wall mechanics	9
2.2	Results NVU model.	10
2.2.1	Influence of astrocytic calcium in NVU.	11
3	Methods	14
3.1	Sensitivity BK channel	14
3.1.1	Experimental results by Girouard et al. (2010) vs NVU model	14
3.1.2	Adaptations in the BK channel	15
3.1.3	Change the calcium dependency of the BK channel.	16
3.2	Bidirectional model, TRPV4 channel.	18
3.2.1	Bidirectional model.	18
3.3	TRPV implementation in NVU	20
4	Results	24
4.1	BK channel	24
4.2	TRPV4	26
5	Discussion	30
5.1	BK channel	30
5.2	TRPV4 channel	31
	Bibliography	32

Chapter 1

Introduction

A numerical model of neurovascular coupling (NVC) is presented by Dormanns et al. (2015). Neurovascular coupling refers to the process between neural activity and local changes in cerebral blood flow. The human/mammalian brain regulates the diameter of the vessel to control the local cerebral blood flow and thereby the oxygen and glucose supply. This process is also known as functional hyperaemia, where the blood flow increases when tissue is active. From literature it is known that disordered functional hyperaemia is associated with several pathologies such as Alzheimer's disease, cortical spreading depression, atherosclerosis and strokes (Dormanns et al., 2015). The pathways that lead to functional hyperaemia are still not fully understood, therefore more experimental and numerical research in this area is necessary. In several papers a neurovascular unit (NVU) is used to describe functional hyperaemia. A single NVU consists of a neuron, an astrocyte (a star-shaped glial cell), a smooth muscle cell and an endothelial cell. Multiple single NVU's may be coupled to create a model for NVC in the cerebral vascular tree. In this research a single NVU is considered. In this research we will have a closer look at role of calcium in the astrocyte, what is the effect of the calcium dependent BK channel in the NVU model? Also the addition of a stretch activated calcium channel at the astrocytic endfoot will be analysed. The motivation for this research are experimental results by Dunn et al. (2013), they show that calcium signalling is critical for astrocyte function and that TRPV4 channels are an important factor in NVC. The next section provides a summary of their work.

1.1 Calcium signalling is critical for astrocyte function, TRPV4 is important in NVC.

The work of Dunn et al. (2013) provides insights into how TRPV4 channels are involved in neurovascular coupling (NVC). They did several experiments where they looked at the influence of the TRPV4 channel on astrocytic endfoot Ca^{2+} signalling, the role of IP_3 -Mediated Ca^{2+} release induced by the TRPV4 channel and if EETs are involved in TRPV4 activation in NVC.

1.1.1 Experimental results by Dunn et al. (2013)

In this section the results presented by Dunn et al. (2013) are summarized. Before they did their experiments they provide some statements from literature, Dunn et al. (2013) used these statements as motivation to do their experiments.

- Calcium signalling is critical for astrocyte function.
- IP_3 -dependent Ca^{2+} signalling in astrocytes is also critical for NVC. Perisynaptic processes initiate IP_3 -dependent Ca^{2+} waves propagating to the astrocytic endfeet. So as a result the Ca^{2+} concentration in the astrocytic endfeet increases ($[Ca^{2+}]_i$). This increase in Ca^{2+} activates Ca^{2+} sensitive pathways, which cause dilation in the adjacent arteriole.
- Moderate $[Ca^{2+}]_i$ results in dilatation, high $[Ca^{2+}]_i$ results in constriction. This bidirectional vascular responds implies that $[Ca^{2+}]_i$ must be finely regulated.
- TRPV4 channels are present in the astrocytic endfeet. TRPV4 channels are thermosensitive, osmosensitive and mechanosensitive, they sense and respond to environmental signals.
- Epoxyeicosatrienoic acids (EETs) activates TRPV4 channels and are involved in NVC.
- TRPV4 channels are activated by moderate levels of $[Ca^{2+}]_i$ and inhibited by high levels of $[Ca^{2+}]_i$

Therefore it is likely that the TRPV4 channel is an important factor in astrocytic sensory and vasoregulatory functions. To provide evidence for TRPV4 channels in the perivascular astrocytic endfeet and demonstrate a dynamic synergy between TRPV4-mediated Ca^{2+} entry and ER Ca^{2+} release through IP_3Rs , Dunn et al. (2013) have set up different experiments on coronal brain slices from an adult mice. Here follows a summary of their experimental results:

- **TRPV4 channel activation increases endfoot Ca^{2+} signalling.** Exposure to the TRPV4 agonist GSK induced an increase of Ca^{2+} -oscillation frequency by $417\% \pm 113\%$ and an increase in the maximum amplitude of the oscillations by $77\% \pm 19\%$. Also, 11,12-EET induced an increase in the maximum amplitude of the oscillations by $52\% \pm 13\%$. EET did not have a significant effect on the frequency.
- **Ca^{2+} entry through TRPV4 channels stimulates IP_3R -mediated Ca^{2+} release in astrocytic endfeet.**
- **Astrocytic endfoot TRPV4 channels are engaged in NVC.** Applying the TRPV4 agonist GSK results in an average increase in endfoot $[Ca^{2+}]_i$ of 154 ± 23 nM, with vasodilation of the arteriole by $11\% \pm 3\%$. There was only one case where vasoconstriction (2%) was observed. So TRPV4 activation results dilation, the signalling terminates before reaching endfoot $[Ca^{2+}]_i$ levels that produces vasoconstriction.

- **Astrocytic endfoot TRPV4 channels augment the endfoot Ca^{2+} response to neural activation.** Consider the case where NVC is simulated by depolarizing neurons by EFS. When TRPV4 channels are inhibited there is a decrease of $45\% \pm 8\%$ rise in endfoot $[Ca^{2+}]_i$ compared to brain slices where TRPV4 channels are active.
- **Engagement of astrocytic endfoot TRPV4 channels in NVC is not mediated through activation by EETs.**

1.1.2 Proposed model for calcium in astrocytic endfoot.

In their discussion Dunn et al. (2013) propose the following model:

1. Direct activation of TRPV4 channels and activation of IP_3Rs by neuronal activity stimulates opening of the other channel through activation by Ca^{2+} .
2. Neural stimulation leads to elevation of astrocytic IP3, which leads to elevation of endfoot $[Ca^{2+}]_i$ that activates TRPV4. When a TRPV4 channel is activated, Ca^{2+} entry activates IP_3Rs , amplifying local Ca^{2+} signals and producing Ca^{2+} waves.
3. The Ca^{2+} signals ultimately terminate through Ca^{2+} -dependent channel inhibition.

How can these findings be used in the NVU model? IP_3Rs is already present in the NVU model, the amount of calcium released by this channel depends amongst other things on $[Ca^{2+}]_i$ and astrocytic IP3. A numerical model for a TRPV4 channel is proposed by Witthoft and Karniadakis (2012). This TRPV4 channel depends on $[Ca^{2+}]_i$, $[Ca^{2+}]_e$, stretch of the arteriole and the membrane voltage of the astrocyte. It would be interesting to implement a similar channel in the NVU model. According to Dunn et al. (2013) the calcium concentration in astrocyte has a significant role in NVC. Therefore it is important to have a closer look at the relation between $[Ca^{2+}]_i$ and the vessel radius in the NVU model. In the NVU model, neural stimulation leads to potassium release into the perivascular space through the BK-channel. This will open a KIR-channel at the smooth muscle cell (SMC), the efflux of potassium will hyperpolarise the membrane potential of the SMC. Calcium channels at the SMC will close and the calcium concentration in the SMC will decrease. This results in vessel dilatation. The potassium flux through the BK channel is dependent on [EET], $[Ca^{2+}]_i$ and the membrane potential of the astrocyte. To see if the current NVU model match with results of experiments the following question need to be answered: How sensitive is the BK channel for $[Ca^{2+}]_i$? Does moderate $[Ca^{2+}]_i$ result in dilatation and high $[Ca^{2+}]_i$ result in constriction? Experiments of Girouard et al. (2010) shows that the level of astrocytic endfoot Ca^{2+} determines dilation and constriction in NVC. Moderate elevations in astrocytic $[Ca^{2+}]_i$ (300-400 nM) induce dilation and higher elevations (>700 nM) induce constriction. It is known from Dormanns et al. (2015) that a high concentration of potassium in the perivascular space result in constriction and a moderate concentration gives dilation. A higher open probability of the BK-channel induced by a moderate calcium concentration in the astrocyte, should result in a moderate level of potassium in the perivascular space. An even higher open probability

induced by high calcium concentration in the astrocyte should result in a high level of potassium in the perivascular space. So the NVU model already contain some mechanics described by Dunn et al. (2013), but the extent to which they respond needs to be examined and a TRPV4 channel needs to be added.

Chapter 2

NVU model

2.1 NVU model

Dormanns et al. (2015) developed a NVU model which consists of several compartments: the neuron (NE), the synaptic cleft (SC), the astrocyte (AC), the perivascular space (PVS), the smooth muscle cell (SMC), the endothelial cell (EC) and the arterial lumen (LU). All the compartments are modelled as different subdomains, which allow interaction between the different subdomains (intercellular interactions). In each subdomain spatial difference are considered negligible, so the subdomains form a lumped model. The model used in this research is the NVU model by Dormanns et al. (2015) extended by glutamate induced astrocytic calcium release, described in the work of Farr and David (2011). In this section the compartments are described in more detail, an overview is given in figure 2.1.

2.1.1 Neuron/Astrocyte

To model the neuron/astrocyte an extended version of the model by Østby et al. (2009) is used. A large conductance potassium channel in the astrocyte is added, this channel provides a K^+ flux from the astrocyte into the PVS. The equations for this channel, also known as a BK channel, are based on the work of Gonzalez-Fernandez and Ermentrout (1994). For this research, a glutamate induced calcium pathway in the astrocyte is included. The equations were adapted from Farr and David (2011), their equations are based on Bennett et al. (2008) and Gonzalez-Fernandez and Ermentrout (1994). In this section the additional equations are described, the other equations can be found in the original paper for the NVU model by Dormanns et al. (2015).

Additional equations The K^+ flux through the BK channel (times the AC volume-area ratio R_k ; in $\mu M ms^{-1}$):

$$J_{BK_k} = \frac{g_{BK_k}}{F} w_k (v_k - E_{BK_k}) C_{correction} \quad (2.1)$$

with g_{BK_k} the conductance, v_k the membrane potential of the astrocyte and E_{BK_k} the nernst potential. The open probability of the BK channel (w_k) is

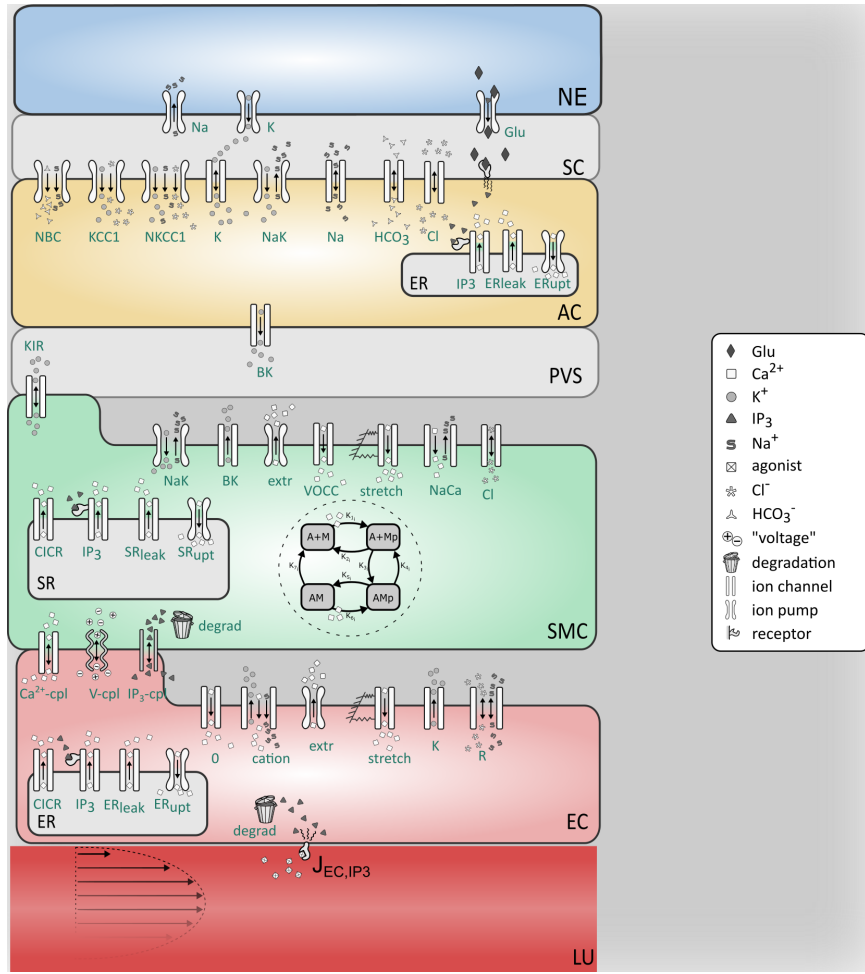


Figure 2.1: Overview of the complete NVU model presented by Dormanns et al. (2015). This overview includes glutamate induced calcium release in the astrocyte, described in the work of Farr and David (2011). The compartments are explained in more detail in section 2.1.

given by an ODE:

$$\frac{dw_k}{dt} = \phi_w (w_\infty - w_k) \quad (2.2)$$

Equilibrium state BK-channel (-):

$$w_\infty = 0.5 \left(1 + \tanh \left(\frac{v_k + (eet_{\text{shift}} eet_k) - v_3}{v_4} \right) \right) \quad (2.3)$$

eet_k is the EET concentration in the astrocyte. The time constant associated with the opening of BK channels:

$$\phi_w = \psi_w \cosh \left(\frac{v_k - v_3}{2v_4} \right) \quad (2.4)$$

Ca^{2+} dependent shift of the opening of the BK-channels:

$$v_3 = \frac{v_5}{2} \tanh \left(\frac{c_k - Ca_3}{Ca_4} \right) + v_6 \quad (2.5)$$

Here is c_k the calcium concentration in the astrocyte. So the open probability of the BK channel w_k is a function of c_k , eet_k and v_k . The Nernst potential E_{BK_k} is given by equation 2.6.

$$E_{BK} = \frac{R_g T}{z_{K^+} F} \ln \left(\frac{[Ca^{2+}]_p}{[Ca^{2+}]_k} \right) \quad (2.6)$$

With $[Ca^{2+}]_p$ the calcium concentration in the PVS. Ca^{2+} concentration in the astrocytic cytosol:

$$\frac{dc_k}{dt} = B_{\text{cyt}} (J_{IP_3} - J_{\text{pump}} + J_{ER_{\text{leak}}}) \quad (2.7)$$

B_{cyt} is a buffering function for calcium, J_{IP_3} is the Ca^{2+} flux from the ER to the cytosol in the astrocyte through IP_3 receptors by IP_3 :

$$J_{IP_3} = J_{\max} \left[\left(\frac{i_k}{i_k + K_i} \right) \left(\frac{c_k}{c_k + K_{\text{act}}} \right) h_k \right]^3 \times \left[1 - \frac{c_k}{s_k} \right] \quad (2.8)$$

$J_{ER_{\text{leak}}}$ is the Ca^{2+} leakage flux from the ER to the cytosol.

$$J_{ER_{\text{leak}}} = P_L \left(1 - \frac{c_k}{s_k} \right) \quad (2.9)$$

J_{pump} is ATP dependent Ca^{2+} pump flux from cytoplasm to the ER in the astrocyte:

$$J_{\text{pump}} = V_{\max} \frac{c_k^2}{c_k^2 + k_p u_{\text{pump}}^2} \quad (2.10)$$

The Ca^{2+} concentration in the astrocytic ER is given by:

$$\frac{ds_k}{dt} = \frac{1}{VR_{ER_{\text{cyt}}}} \left(\frac{dc_k}{dt} \right) \quad (2.11)$$

$VR_{ER_{\text{cyt}}}$ is the volume ratio between ER and the cytosol in the astrocyte. The inactivation variable for IP_3 :

$$\frac{dh_k}{dt} = k_{\text{on}} [K_{\text{inh}} - (c_k + K_{\text{inh}}) h_k] \quad (2.12)$$

The IP_3 concentration:

$$\frac{di_k}{dt} = r_h G - k_{deg} i_k \quad (2.13)$$

The EET concentration:

$$\frac{deetk_k}{dt} = V_{eet}(c_k - c_{k,min}) - k_{eet} eet_k \quad (2.14)$$

The NVU model mainly simulates two pathways in the astrocyte: A potassium related pathway where a neural signal releases potassium in the synaptic cleft, potassium channels at the astrocyte will open and there will be a potassium influx into the astrocyte. This depolarizes the astrocytic membrane and the BK channel at the endfoot of the astrocyte will open. This result in an efflux of potassium into the perivascular space. And there is a glutamate induced calcium pathway. During the neural signal, glutamate is released in the synaptic cleft and binds on glutamate receptors. This increases the IP_3 production in the astrocyte and there is a IP_3 induced Ca^{2+} release from the ER. The increase in Ca^{2+} results in Ca^{2+} -dependent EET production. Both EET and Ca^{2+} increase the open probability of the BK channel, see equation 2.5 and 2.3.

2.1.2 Smooth muscle cell and endothelial cell

The smooth muscle cell (SMC) is connected to the perivascular space and the endothelial cell (EC). The model is based on the work of Koenigsberger et al. (2006). The communication from the astrocyte to the SMC is accomplished by a KIR channel, an inward-rectifier potassium ion channel. Neural activity will increase the potassium concentration in the PVS ($[K^+]_p$), this will activate the KIR channel and there will be an outflux of potassium into the PVS. This hyperpolarizes the membrane of the SMC and the voltage operated calcium channel (VOCC) will close and thereby further influx of Ca^{2+} into the SMC. The change in the calcium concentration in the SMC ($[Ca^{2+}]_i$) will influence the radius of the vessel (see section 2.1.3). The biochemical behaviour of the KIR channel is modelled according to experimental data from Filosa et al. (2006). The SMC is coupled to the endothelial cell by three coupling functions: $J_{Ca_{cpl}^{2+}}$, $J_{V_{cpl}}$ and $J_{IP_3_{cpl}}$. The endothelial cell is connected to the lumen by IP_3 generation due to activation of membrane receptors by agonists flowing in the arteriolar lumen. IP_3 allows Ca^{2+} release from the reticulum, in both the SMC and EC. The production of IP_3 in the EC is given by $J_{EC_{IP_3}}$, this parameter can be treated as a constant over time. Changing $J_{EC_{IP_3}}$ to different values (from $0.18 \mu M s^{-1}$ to $0.40 \mu M s^{-1}$) can induce vasomotion. During vasomotion the radius and the Ca^{2+} concentration show harmonic oscillations. Figure 2.1.2 gives an overview of the channels in the SMC and EC.

2.1.3 Contraction model and wall mechanics

The arterial contraction model is based on the work of Hai and Murphy (1989). Actin and myosin filaments in the SMC will form cross bridges mediated by Ca^{2+} . There are four possible states for the formation of myosin: free non-phosphorylated cross bridges (M), free phosphorylated cross bridges (Mp), attached phosphorylated cross bridges (AMp) and attached dephosphorylated

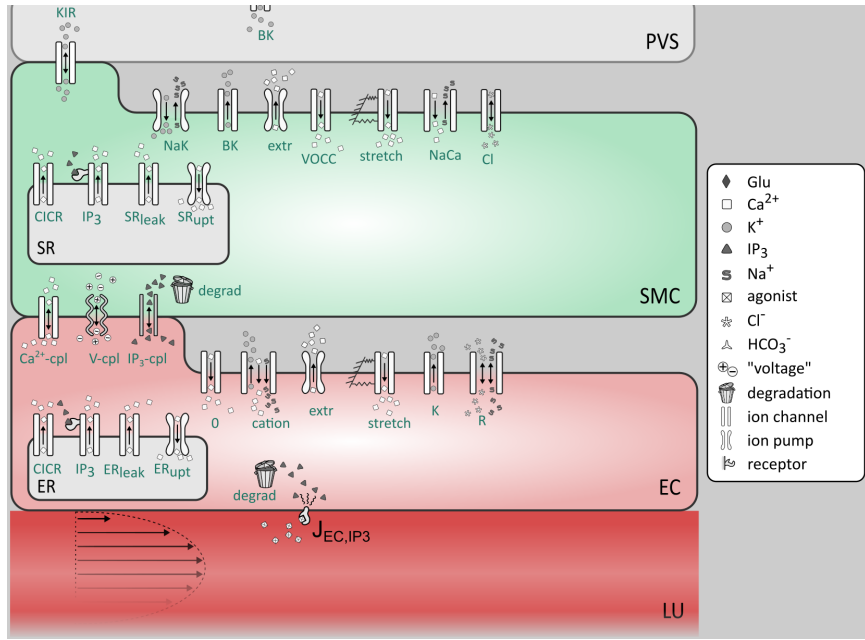


Figure 2.2: Overview of the smooth muscle cell (SMC) and endothelial cell (EC) subcompartments of the NVU model by Dormanns et al. (2015).

latch bridges (AM). The rate constants K_n ($n = 1, \dots, 7$) determine cross bridge formation, K_1 and K_6 are dependent on $[Ca^{2+}]_i$. An overview is given in figure 2.1.3. The fraction of attached myosin cross bridges, F_r , is used as input for the mechanical wall subsystem. F_r is related to the circumferential stress in the arterial wall and so to the radius of the vessel. So a decrease in $[Ca^{2+}]_i$ will result in dilation and an increase in $[Ca^{2+}]_i$ will result in constriction. The equations can be found in the appendix.

2.2 Results NVU model.

In this section the results of the NVU model, as discussed in section 2.1, are presented. Figure 2.4 shows neural stimulation for 250 seconds, where glutamate and potassium are released in the synaptic cleft. The neural stimulation is given from 100 to 350 seconds. There is an influx of potassium into the AC, this depolarizes the membrane of the AC (B). The glutamate activates IP_3 release in the AC (C), this results in Ca^{2+} release from the ER and production of EET (G). The depolarization of the membrane, the increased astrocytic concentrations of Ca^{2+} and EET result in an outflux of potassium through the BK channel into the PVS. The KIR channel at the SMC is activated by the higher level of potassium in the PVS (D) and the KIR channel will also release K^+ into the PVS. This hyperpolarises the membrane of the SMC and the calcium channels will close. This results in a lower calcium concentration in the SMC (F) and the radius will increase (H).

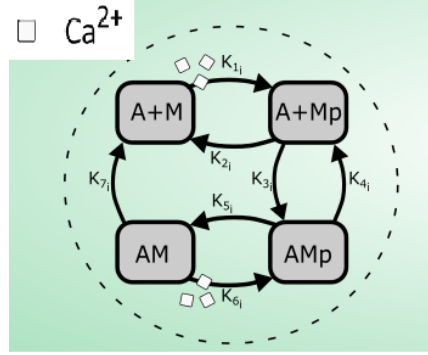


Figure 2.3: Overview of the contraction model by Hai and Murphy (1989)

2.2.1 Influence of astrocytic calcium in NVU.

The papers of Dunn et al. (2013) and Girouard et al. (2010) show that Ca²⁺ is an important factor in NVC. Moderate elevations in astrocytic [Ca²⁺]_i (300-400 nM) should induce dilation and higher elevations (>700 nM) induce constriction. J_{max} determines the Ca²⁺ release from the ER into the astrocyte. The factor α is introduced to vary J_{max} , see equation 2.15. To simulate moderate and high Ca²⁺ in the AC, α is set to different values to release more Ca²⁺ from the ER into the astrocytic cytosol.

$$J_{max} = \alpha \cdot J_{max} \quad (2.15)$$

Figure 2.5 shows the results for different values of α , the same neural input is applied as in section 2.2. For $\alpha = 1$ moderate calcium concentration is modelled, $\alpha = 9$ gives high levels of calcium. When α is increased, the Ca²⁺ and EET concentrations increase, this gives a higher open probability for the BK channel w_k . For different values of J_{max} , K_p and the radius change with a maximum of 4 %, although the open probability w_k is increased a 10-fold. So for high concentrations of Ca²⁺ in the astrocyte (induced by high values of J_{max}) we observe dilation instead of constriction, this is in contradiction with the experimental results by Girouard et al. (2010).

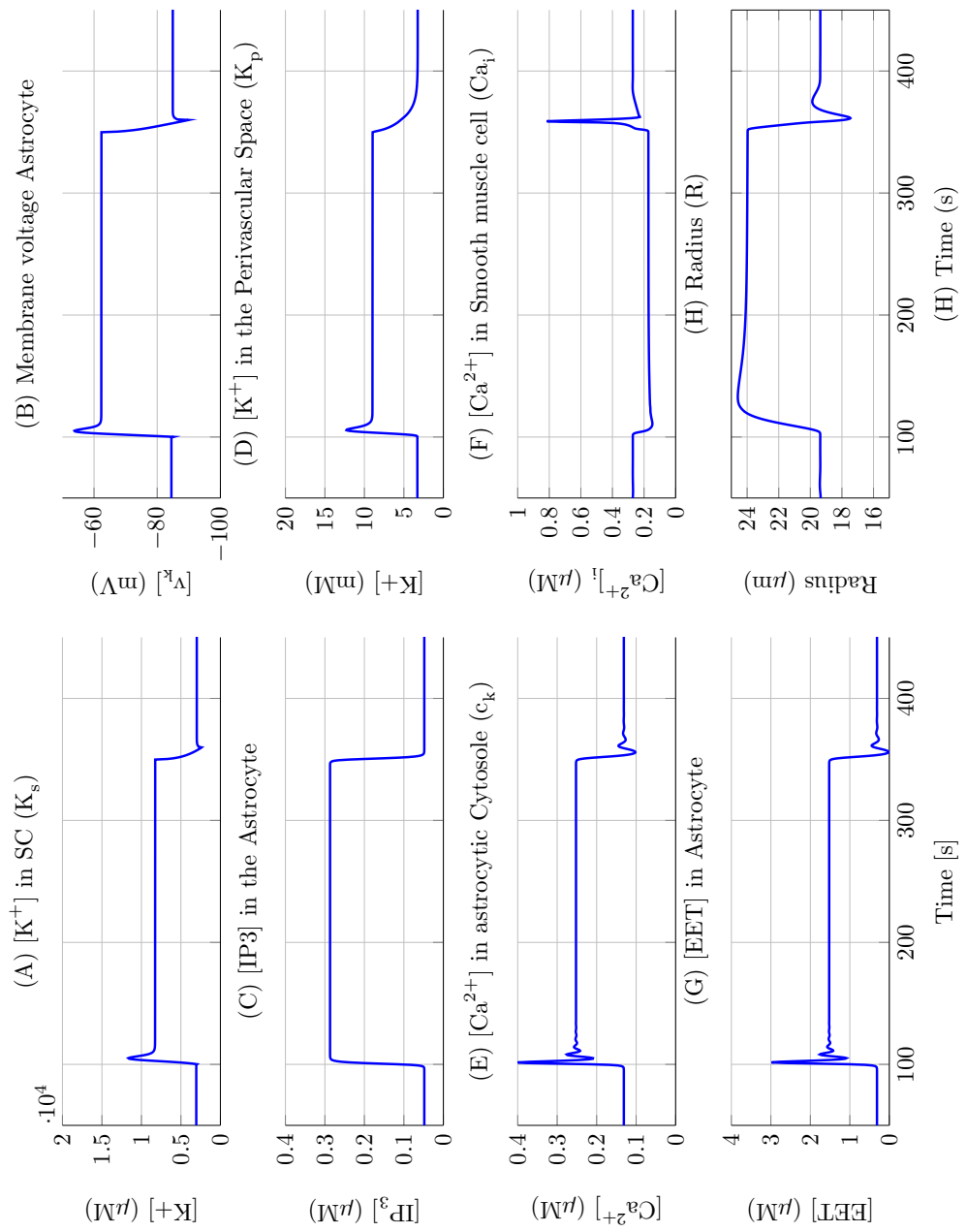


Figure 2.4: standard NVU simulation

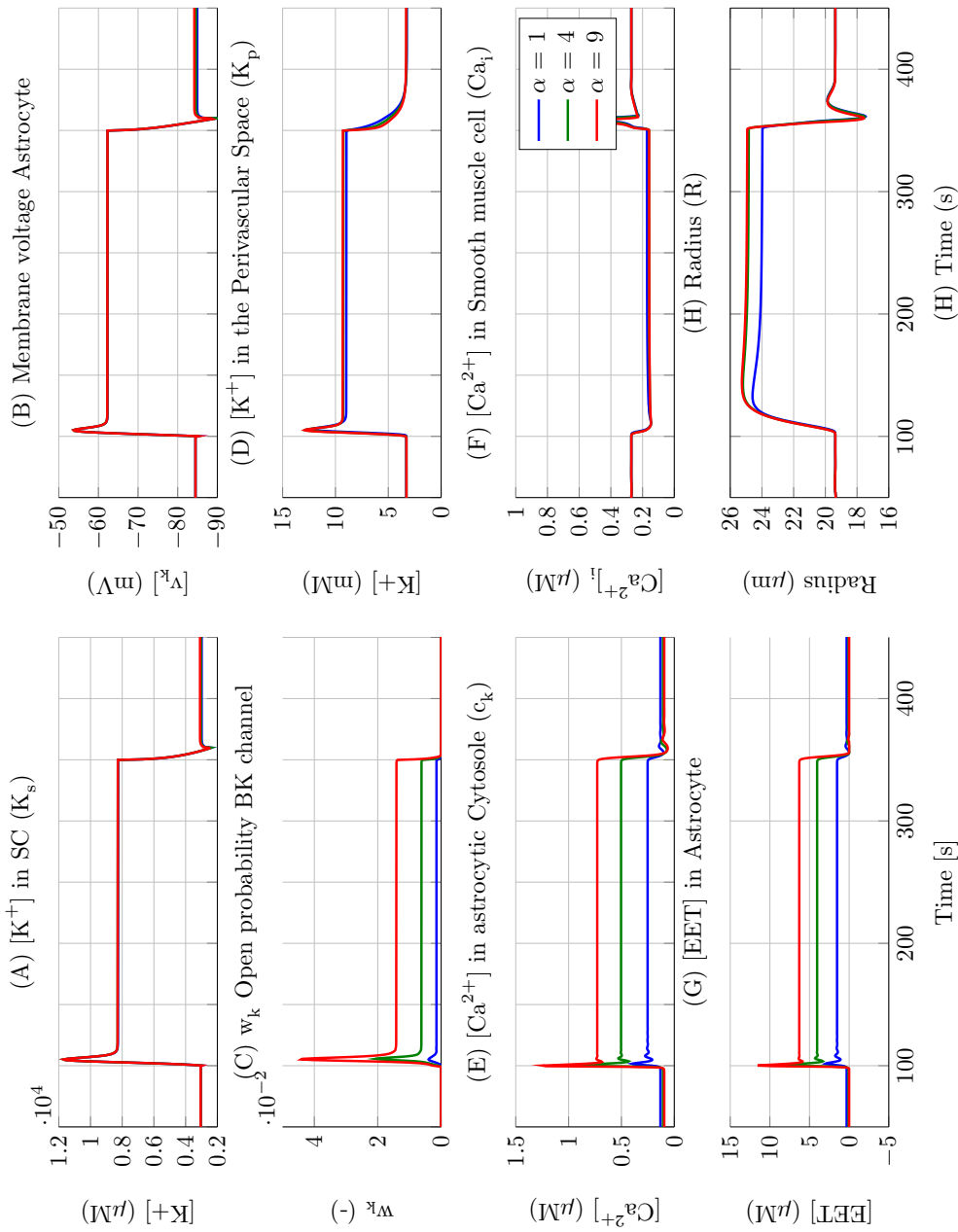


Figure 2.5: NVU model

Figure 2.6: NVU model for different value's of α to simulate high concentrations of Ca^{2+} in the astrocyte.

Chapter 3

Methods

3.1 Sensitivity BK channel

The simulations presented in figure 2.5 show that variations in c_k in the NVU model do not result in the expected radius changes according to literature. The BK channel is the channel which mediates between c_k and the radius, it is observed that a higher open probability w_k does not result in a significant increase in the potassium flux J_{BK} . Therefore the sensitivity BK channel will be investigated.

3.1.1 Experimental results by Girouard et al. (2010) vs NVU model

The work of Girouard et al. (2010) shows experiments which imply that astrocytic endfoot Ca^{2+} determines dilation and constriction in brain slices. They measured astrocytic endfoot Ca^{2+} and the diameter of adjacent arterioles in mouse cortical brain slices. Astrocytic endfoot Ca^{2+} was elevated with electrical field stimulation (EFS) or uncaging Ca^{2+} in the astrocytic endfoot. They induced moderate and high levels of astrocytic endfoot Ca^{2+} . Similar results as in Dunn et al. (2013) were found: Moderate $[\text{Ca}^{2+}]_i$ results in dilatation and high $[\text{Ca}^{2+}]_i$ results in constriction. There were no significant differences observed between elevations by EFS or uncaging Ca^{2+} , the summarized results can be found in table 3.1. In their discussion they state that the transition between

	$[\text{Ca}^{2+}]$	Radius change
Rest	124 nM	0%
low EFS	324 nM	21.3%
low uncaged Ca2+	350 nM	22.0%
high EFS	732 nM	-29.9%
high uncaged Ca2+	832 nM	-28.6%

Table 3.1: Results of experiments by Girouard et al. (2010).

evoked dilation and constriction occurs when the average endfoot $[\text{Ca}^{2+}]$ approximately doubles to 700-800 nM. This relation ship could reflect the exquisitely

high Ca^{2+} sensitivity of the astrocytic BK channel, which has been shown to exhibit a 16-fold increase in open probability with a doubling of $[\text{Ca}^{2+}]_i$ (Horrigan and Aldrich, 2002).

Replication of the experiments with NVU. A calcium dependent astrocytic BK channel is also present in the NVU model. EFS is simulated by a neural stimulus, for a high EFS the input signal is doubled (F_{input} and the amplitude of the smooth pulse function rho). The levels of uncaged Ca^{2+} are reached by releasing Ca^{2+} from the ER, this was achieved by increasing J_{\max} . Note that a neural input is given during the simulations of uncaging Ca^{2+} in figure 2.5. This is not in agreement with the experiments where only Ca^{2+} is uncaged, but without neural input there is no reaction at all. The simulations which simulate EFS are similar to the experiments. Although at the high EFS simulations $[\text{Ca}^{2+}]_i$ does not increase to high levels as in the experiments, but in both constriction is observed. The simulation of EFS gives correct results for the radius, because the neural stimulation depolarizes the membrane of the astrocyte. As result the open probability of the BK increases, so this process is not mediated by Ca^{2+} . In the simulations both, low and high uncaged Ca^{2+} , do not influence the radius of the arteriole. Figure 2.5 shows that the open probability of the BK channel w_k increases when $[\text{Ca}^{2+}]_i$ rises, but this does not influence K_p . This means that the potassium flux J_{BK_k} is not increasing with higher w_k , this is not what is expected when looking at equation 2.1. The maximum value of J_{BK_k} can be explained by that the difference between v_k and E_{BK_k} becomes smaller when w_k increases. When a higher neural stimulus is applied, the neuron will release more potassium in the synaptic cleft, the potassium concentration in the astrocyte increases. This result in a lower value for E_{BK_k} and this allows a higher concentration K_p .

3.1.2 Adaptations in the BK channel

In this section some adaptations are suggested to change the influences of the BK channel in the NVU model. The equations for the BK channel are adapted from Gonzalez-Fernandez and Ermentrout (1994) and Farr and David (2011). Donk (2013) did a parameter estimation for the BK channel in the NVU model by using experimental data from Filosa et al. (2006). The estimated value for the single channel conductance G_{BK} in the NVU model is approximately more than 15 times higher than other values from literature, see table 3.1.2. In equation 2.1 they used a general nernst potential instead of a reversal potential, which is consistent with the work of Østby et al. (2009). Although the original equations consists a reversal potential for the BK channel around -90 mV, see table 3.1.2.

	G_{BK}	v_{BK}
NVU Dormanns et al. (2015)	4300 [pS]	E_{BK}
Filosa et al. (2006) (experiment)	225.6 [pS]	-
Gonzalez-Fernandez and Ermentrout (1994)	314 [pS]	-90 mV
Witthoft et al. (2013) (numerical)	200 [pS]	-80 mV

Table 3.2: Values for the conductance and the reversal potential of the BK channel from literature.

To solve the problem described in section 3.1.1 we propose to change E_{BK} back to a constant reversal potential ν_{BK} , see equation 3.1.

$$J_{BK_k} = \frac{g_{BK}}{F} w_k (v_k - \nu_{BK}) \quad (3.1)$$

G_{BK} is set to 225.6 [pS] according to the experiments of Filosa et al. (2006), for the conversion to a specific ion conductance g_{BK} see equation 3.2.

$$g_{BK} [\Omega m^{-2}] = \frac{G_{BK} [pS] \cdot 10^{-12}}{A_{ef} [m^2]} \quad (3.2)$$

Here is A_{ef} the characteristic exchange surface of the astrocytic endfoot. The value for ν_{BK} is estimated by fitting K_p during neural stimulation, see figure 3.1. For $\nu_{BK} = 81.135mV$ the same value of K_p is reached during neural stimulation. After the neural pulse at $t = 100s$ the potassium concentration K_p (red line) increases slower than the in the original model (blue line). This makes sense because the conductance of the adapted BK channel is approximately 19 times lower and the driving force ($v_k - E_{BK}$) has the same order of magnitude.

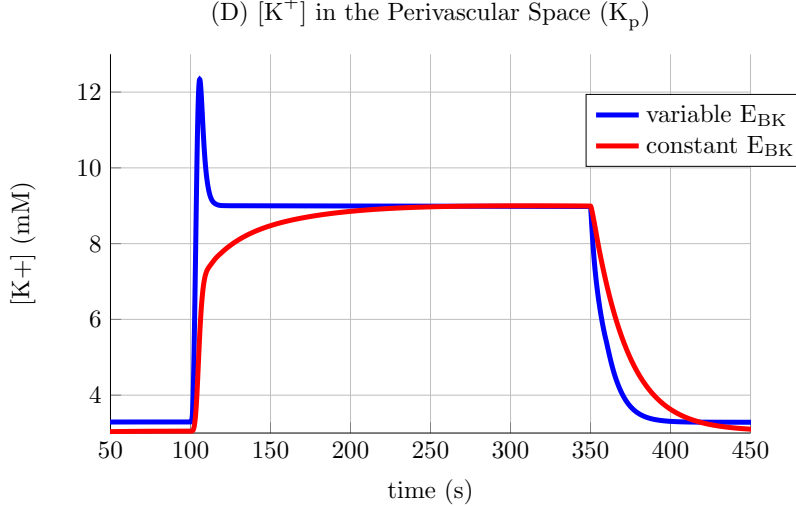


Figure 3.1: The blue line is K_p during neural stimulation in the original NVU model, the red line shows K_p where E_{BK} is set to a constant value ($\nu_{BK} = 81.135mV$) to fit the original NVU model and $G_{BK} = 225.6$ pS

3.1.3 Change the calcium dependency of the BK channel.

Figure 3.3 shows neural stimulations for different value's of α to simulate high concentrations of Ca^{2+} in the astrocyte. The BK channel is adapted as described in section 3.1.2. When $c_k = 250$ nM the radius shows dilation and for $c_k = 750$ nM it gives constriction, this is in agreement with the experiments by Girouard et al. (2010). For $c_k = 500$ nM we expect $r = r_0$ so neither constriction or dilation will occur, but in the simulation there is constriction. Therefore

the dependency of the BK channel to Ca^{2+} needs to be adapted, so that the switching point between dilation and constriction is around $c_k = 500 \text{ nM}$ similar to the paper of Girouard et al. (2010). The dependency of w_k to Ca^{2+} is described with the function v_3 . v_3 depends on 4 constants, v_5 , Ca_3 , Ca_4 , v_6 and state variable $[\text{Ca}^{2+}]_i$. v_6 and Ca_4 are adapted so that v_3 has a higher value for $c_k > 300 \text{ nM}$. For $v_6 = -13.6 \text{ mV}$ and $Ca_4 = 350 \text{ nM}$. This changes v_3 as function of Ca^{2+} , see figure 3.2. The results of the radius change will be discussed in the Results section.

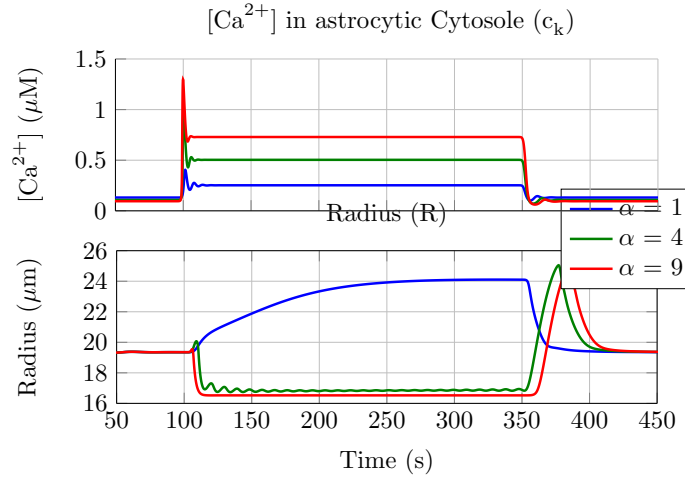


Figure 3.2: Adapted NVU model with $\nu_{BK} = 81.135$ and $G_{BK} = 225.6 \text{ [pS]}$ for different value's of α to simulate high concentrations of Ca^{2+} in the astrocyte.

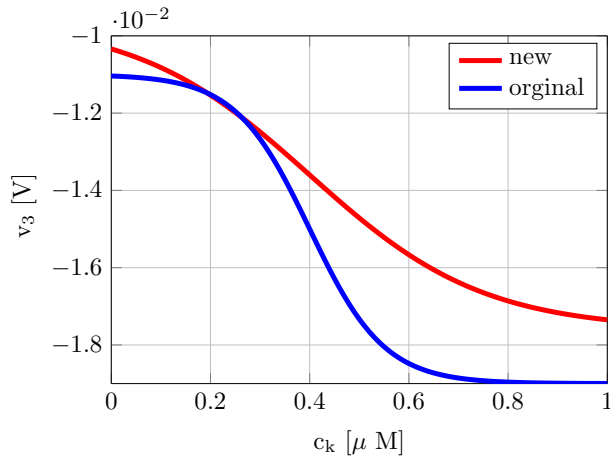


Figure 3.3: v_3 as function of c_k

3.2 Bidirectional model, TRPV4 channel.

The experiments from Dunn et al. (2013) show that TRPV4 channels are an important factor in astrocytic sensory and vasoregulatory functions. Witthoft and Karniadakis (2012) presents a bidirectional model for neurovascular coupling. In this model there is vascular regulation by a astrocytic pathway induced by neural activity and they included a signalling mechanism from the vessel to the astrocyte, via a stretch activated TRPV4 channel. This section contains a review of the bidirectional model and a proposal for an addition of a TRPV4 channel in the NVU model.

3.2.1 Bidirectional model.

The bidirectional model by Witthoft and Karniadakis (2012) consists of a neuron, astrocyte and a smooth muscle cell (SMC), the equations are based on models of Gonzalez-Fernandez and Ermentrout (1994), Bennett et al. (2008) and Farr and David (2011). The neural input is a smooth pulse of potassium and glutamate released in the synaptic cleft. The astrocyte has four different ion channels: a IP_3 -channel initiated by glutamate, a TRPV-channel, a BK-channel and a channel that transports potassium from the synaptic cleft into the astrocyte. There is an endoplasmatic reticulum (ER) present in the astrocyte where calcium is stored. The smooth muscle cell has a KIR-channel, potassium-channel, a voltage operated calcium-channel and leak-channel. The contraction model, dependent on the calcium concentration in the smooth muscle cell, according to the work of Gonzalez-Fernandez and Ermentrout (1994). Figure 3.2.1 shows an overview of the model. The bidirectional model is less complex compared to the NVU model, several compartments and channels are not present. But the glutamate induced Ca^{2+} -release pathway and the interaction between the BK and KIR channel are similar to the NVU.

TRPV4 channel

In literature it is found that the TRPV4 channels are activated by both chemical and physical stimuli: cell swelling, heat and mechanical displacement Filosa and Iddings (2013). Witthoft and Karniadakis (2012) included a mechanosensitive Ca^{2+} channel (TRPV4) at the endfoot of the astrocyte. In this model vessel dilation activates the TRPV4 channels, allowing an influx of Ca^{2+} from the perivascular space into the astrocytic cytosol. The channel is inhibited by intra- and extracellular $[Ca^{2+}]$, it has a slow decay at a low extracellular $[Ca^{2+}]$ and a fast decay in presence of high extracellular $[Ca^{2+}]$. This is in contrast with the findings of Dunn et al. (2013), where moderate intracellular $[Ca^{2+}]$ levels activate the TRPV4 channel. The open probability m_k is modeled as an ODE which always decays to the steady state value of m_∞ , see equation 3.3.

$$\frac{dm_k}{dt} = \frac{[Ca^{2+}]_p}{\tau_{TRPV}}(m_\infty - m_k) \quad (3.3)$$

Here is $[Ca^{2+}]_p$ the calcium concentration in the perivascular space and τ_{TRPV} is a time-constant. $[Ca^{2+}]_p$ and τ_{TRPV} determine the decay-rate of the open probability. The dimensions of this equations are not correct, Witthoft and

Karniadakis (2012) used $[Ca^{2+}]_p$ in μM to create a Ca^{2+} -dependent time constant. The TRPV4 channel steady state open probability m_∞ is modeled by the Boltzmann equation, see equation 3.4.

$$m_\infty = \left(\frac{1}{1 + e^{-(\epsilon - \epsilon_{1/2}/\kappa)}} \right) \left[\frac{1}{1 + H_{Ca}} \left(H_{Ca} + \tanh\left(\frac{V_a - \nu_{1,TRP}}{\nu_{2,TRP}}\right) \right) \right] \quad (3.4)$$

The first term depends on the strain ϵ , this makes the open probability of the TRPV4 channel dependent on radius of the vessel. The strain ϵ is given by $\epsilon = (r - r_0)/r_0$, the local radial strain on the arteriole. The strain on the perivascular endfoot of the astrocyte is approximately equal to local radial strain on the arteriole since the astrocytic endfoot surrounds the arteriole. $\epsilon_{1/2}$ is the strain required for half-activation. The second term consists of the voltage gating and the inhibitory behaviour based on experimental results by Nilius et al. (2004) and Watanabe et al. (2003). The inhibitory term H_{Ca} , see equation 3.5, depends on the intracellular Ca^{2+} concentration and the Ca^{2+} concentration in the perivascular space.

$$H_{Ca} = \left(\frac{[Ca^{2+}]_k}{\gamma_{Cai}} + \frac{[Ca^{2+}]_p}{\gamma_{Cae}} \right) \quad (3.5)$$

Here are γ_{Cai} and γ_{Cae} constants associated with the calcium concentrations.

J_{TRPV} is the calcium ion influx into the astrocyte given by equation 3.6.

$$J_{TRPV} = \frac{g_{TPRV} m_k (V_k - \nu_{TRPV})}{(C_{astr} \gamma)} \quad (3.6)$$

with g_{TPRV} the maximum channel conductance, V_k the membrane potential, ν_{TRPV} the channel reversal potential, C_{astr} the astrocyte cell capacitance γ a scaling factor for relating the net movement of ion fluxes to the membrane potential Koenigsberger et al. (2006) and m_k the open channel probability.

Replicate the bidirectional model

In order to have better understanding of bidirectional behaviour of the model, the model was replicated in Matlab using an ode15s solver. Instead of using the contraction model of Gonzalez-Fernandez and Ermentrout (1994) the same contraction model as in NVU is implemented. When a input signal by neuron is simulated the results of this model shows similar behaviour compared to the results of Witthoft and Karniadakis (2012). Although the membrane voltage of the astrocyte is too high: 50 mV compared to -40 mV. The potassium concentration in the perivascular space (K_p) is too low: 14 mM compared to 18 mM. The differences could be caused by:

- The input signal is not given in the paper.
- The value of $I_{\Sigma K}$ (The current due to the potassium flux from the synaptic cleft to the astrocyte.) in our simulation is probably to high. This can have two causes: A wrong input signal or the adjustment of γ . The value of γ is changed by a factor 1000 to correct for μM to mM . The change in γ may also explain the difference in $[K_p]$, since this will influence the potassium fluxes J_{BK} and J_{KIR} .

- Units in general, the paper is not very clear whether they use mM or μM , since the equations are not 'units independent' this may cause differences.
- Two mistakes were found in the paper: the signs of $I_{\Sigma K}$ and I_k are not correct.

With the addition of a TRPV4 channel they were able to prolong dilation after the neural pulse stops. This effect is caused by the opening of the TRPV4 channel by stretch, which allows an influx of Ca^{2+} into the astrocyte. This keeps the BK channel opened, even after the neural input.

3.3 TRPV implementation in NVU

The TRPV4 channel will be implemented in the NVU model, the equations for the TRPV4 channel are adapted from the model by Witthoft and Karniadakis (2012), see subsection 3.2.1.

Essential parameters for implementing TRPV4 channel in NVU What are the essential parameters for implementing a TRPV4 channel in NVU? Are those parameters available in the NVU model?

- $[\text{Ca}^{2+}]$ in the perivascular space ($[\text{Ca}_p^{2+}]$).
- $[\text{Ca}^{2+}]$ in the astrocyte.
- A contraction model to determine the strain ϵ of the arteriole.
- Membrane potential of astrocyte.
- It is necessary that there is a BK-channel on the astrocyte, the open gate probability should depend on the intracellular $[\text{Ca}^{2+}]$ in the astrocyte. Otherwise the addition of a TRPV4 channel will have no effect.

The NVU model does not contain equations for $[\text{Ca}^{2+}]$ in the perivascular space. This could be implemented in NVU model or the calcium concentration can be considered as constant.

Implementation In the NVU model the equations for ion fluxes and the membrane potential are based on the model of Østby et al. (2009). Compared to the equations of Witthoft et al. (2013), they use a different type of scaling and the Nernst potential is used instead of the channel reversal potential. But the equation for C_{ak} in the NVU model is not scaled according to the model of Østby et al. (2009), where the other ion concentrations in the astrocyte are scaled. The calcium related equations in the bidirectional model are the similar to the equations in the NVU model. Therefore the equations from the bidirectional model are used, instead of scaling the equations according to the work of Østby et al. (2009). The Ca^{2+} flux through the TRPV4 channel is given by:

$$J_{TRPV} = -1/2 \frac{I_{TRPV}}{(C_{astr}\gamma)} \quad (3.7)$$

The factor 1/2 is there because there are two positive charges for every calcium ion Witthoft et al. (2013). I_{TRPV} is the electrical current through the channel:

$$I_{TRPV} = G_{TPRV} m_k (V_k - E_{TRPV}) \cdot 10^3 \quad (3.8)$$

The reversal potential ν_{TRPV} in equation 3.7 will be replaced by the Nernst potential of the TRPV4 channel given by equation 3.9, the value for E_{TRPV} is close to the reversal potential ν_{TRPV} in the bidirectional model. The factor 10^3 is used to change the units from V to mV.

$$E_{TRPV} = \frac{R_g T}{z_{Ca} F} \ln\left(\frac{C_{a_p}}{C_{a_k}}\right) \quad (3.9)$$

Here is R_g the gas constant, T the temperature, z_{Ca} the ion valence of Ca^{2+} and F the Faraday constant. C_{a_p} and C_{a_k} are the Ca^{2+} concentration in the perivascular space and the Ca^{2+} concentration in the astrocyte respectively.

Calcium in the perivascular space

In the NVU model there is no Ca^{2+} in the perivascular space modelled, this could be an important factor since the open probability m_k depends on C_{a_p} . In the bidirectional model a simple ODE is used to describe C_{a_p} , see equation 3.10, here C_{a_p} will always decay to the steady state value $C_{a_{p_{min}}}$.

$$\frac{d[Ca^{2+}]_p}{dt} = -J_{TRPV} - J_{Ca} - Ca_{decay}(C_{a_p} - C_{a_{p_{min}}}) \quad (3.10)$$

Here is J_{Ca} the ion flux through a calcium channel from the smooth muscle cell to the perivascular space. This channel is not present in the NVU model, but in the NVU model there is a voltage operated calcium channel (VOCC) present at the smooth muscle cell connected to the extracellular space. This channel has the same function as the calcium channel in the bidirectional model. When the membrane of the smooth muscle cell hyper-polarizes the channel closes. The calcium flux through this channel is added to the ODE for C_{a_p} . Since ion fluxes are in units of $\mu M s^{-1}$ and there are different volumes for the astrocyte, perivascular space and the smooth muscle cell, scaling should be included. The volume ratio of PVS to astrocyte (VR_{pa}) and the volume ratio of PVS to smooth muscle cell (VR_{ps}) are also used in the equation for K^+ concentration in the PVS. Combining J_{VOCC} , the volume ratios and equation 3.10, results in equation 3.11

$$\frac{d[Ca^{2+}]_p}{dt} = -\frac{J_{TRPV}}{VR_{pa}} - \frac{J_{VOCC}}{VR_{ps}} - Ca_{decay}(C_{a_p} - C_{a_{p_{min}}}) \quad (3.11)$$

The value for $C_{a_{p_{min}}}$ in Witthoft and Karniadakis (2012) is $2mM$ compared to $5\mu M$ in Witthoft et al. (2013). From experiments in brain slices it is known that the calcium concentration in extracellular brain fluid is around $1.5mM$ Stringer and Lothman (1988). So it would make sense to choose for $C_{a_{p_{min}}} = 2mM$

Adapted equations.

Calcium concentrations in astrocyte. Since there is an extra calcium channel added in the astrocyte, the equations for calcium concentrations in

the astrocyte and the membrane potential of the astrocyte need to be adjusted. The calcium flux J_{TRPV} is added in the ODE for the calcium concentration in the astrocyte, see equation 3.7. The equation for c_k in the NVU model is the same as used by Witthoft et al. (2013). There is an inconsistency between the papers of (Witthoft and Karniadakis (2012) and Witthoft et al. (2013)), in one paper the TRPV4 flux is buffered, in the other paper it is not buffered. Ca^{2+} buffering is described in the work of Wagner and Keizer (1994). They show that every rate of other mechanisms that transport Ca^{2+} into or out of the cytoplasm need to be buffered (equation 37). Although the TRPV4 channels are located at the astrocytic endfoot and buffering is described in the astrocytic soma, it is unknown to what extend Ca^{2+} is buffered in the astrocytic endfoot. Since the model describes the complete astrocyte as one single point, it is chosen to include buffering for J_{TRPV} . Adapted ODE for the calcium concentration in the astrocyte.

$$\frac{dC_{a_k}}{dt} = B_{\text{cyt}}(J_{\text{IP}_3} - J_{\text{pump}} + J_{\text{ER}_{\text{leak}}} + J_{\text{TRPV}}) \quad (3.12)$$

Since the ODE for the calcium concentration in the endoplasmic reticulum (s_k) depends on C_{a_k} , should the ODE be rewritten in separate fluxes, see equation 3.13

$$\frac{ds_k}{dt} = \frac{-B_{\text{cyt}}(J_{\text{IP}_3} - J_{\text{pump}} + J_{\text{ER}_{\text{leak}}})}{V R_{E_{R_{\text{cyt}}}}} \quad (3.13)$$

Membrane voltage of the astrocyte. In the NVU model the membrane voltage of the astrocyte (V_k) is an algebraic equation instead of an ODE. For example the membrane voltage of the smooth muscle cell is described by an ODE and also Witthoft et al. (2013) used an ODE to describe (V_k). Where $\frac{dV}{dt} = \frac{1}{C} \Sigma(J_x)$ with C is the capacitance of the cell. In the NVU model the Goldman-Hodgkin-Katz equation is used, see equation 3.14

$$v_k = \frac{g_{Na_k} E_{Na_k} + g_{K_k} E_{K_k} + g_{Cl_k} E_{Cl_k} + g_{NBC_k} E_{NBC_k} + g_{BK_k} w_k E_{BK_k} - J_{NaK_k} F C_{\text{correction}}}{g_{Na_k} + g_{K_k} + g_{Cl_k} + g_{NBC_k} + g_{BK_k} w_k} \quad (3.14)$$

The new equation for V_k includes the Nernst potential, the open probability and the specific ion conductance of the TRPV4 channel:

$$v_k = \frac{g_x E_x + \dots + g_{BK_k} w_k E_{BK_k} + g_{\text{TRPV}} m_k E_{\text{TRPV}} - J_{NaK_k} F C_{\text{correction}}}{g_{Na_k} + g_{K_k} + g_{Cl_k} + g_{NBC_k} + g_{BK_k} w_k + g_{\text{TRPV}} m_k} \quad (3.15)$$

Note that this conductance is calculated from equation 3.16, including A_{ef} . To calculate g_{TRPV} we use A_{ef} , the area of the astrocytic endfeet, see equation 3.16. Donk (2013) used the same equation for calculating the conductance of the BK channel in NVU.

$$g_{\text{TRPV}} [\Omega m^{-2}] = \frac{G_{\text{TPRV}} [pS] \cdot 10^{-12}}{A_{ef} [m^2]} \quad (3.16)$$

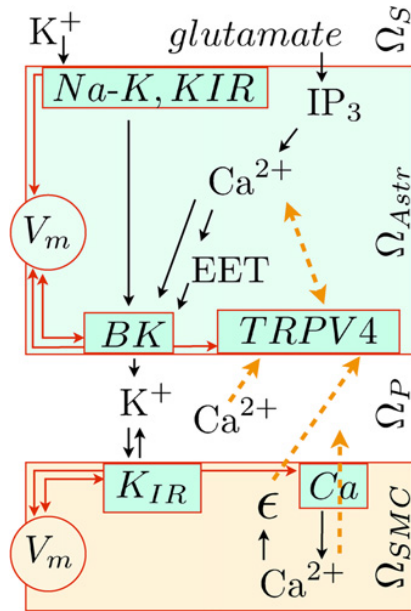


Figure 3.4: An overview of the bidirectional model. Potassium (K^+) and glutamate are released in the synaptic cleft (Ω_S). The influx of K^+ depolarizes the membrane of the astrocyte. Glutamate induces IP_3 release in the astrocyte (Ω_{Astr}), Ca^{2+} will be released from internal storage (ER) and EET is produced. Ca^{2+} and EET open the BK channel. The K^+ concentration in the perivascular space increases, this will open the KIR channel at the SMC. The out flux of K^+ hyperpolarizes the membrane of the SMC, this will close the Ca^{2+} channels. The Ca^{2+} concentration in the SMC increases and the vessel will dilate. The TRPV4 channel at the astrocyte is activated by strain (η), so the dilation of the vessel will open this channel. The influx of Ca^{2+} into the astrocyte will prolong the signalling. Dashed arrows indicate the new mechanisms introduced in the paper of Witthoft and Karniadakis (2012)

Chapter 4

Results

The simulations in this chapter are conducted with the same neural input as in 2.2. So there is a pulse from 100s to 350s and $J_{PLC} = 0.18$.

4.1 BK channel

The BK channel is adapted as described in section 3.1.2, table 4.1 shows which parameters are changed compared to the NVU model. Similar simulations are performed as in section , where different values for α are used to vary the astrocytic calcium concentration. Figure 4.1 shows the results of the simulations: moderate calcium concentration (blue line) gives dilation, high levels of calcium (red line) result in constriction of the vessel and calcium levels around 500 [nM] (green line) give oscillations around the steady state value of the radius. This result is different from the simulations in figure 2.5, where all the cases result in dilation. The higher levels of c_k (E) and EET (G) increase the open probability w_k (C). This results in a higher flux of potassium into the PVS (D). The K_p influences the calcium concentration in the SMC (F) and this determines the radius of the vessel (H). For $\alpha = 1$ the radius shows a long delay (circa 100 [s]) before reaching maximal dilation, this is not physiological. For both $\alpha = 4$ and $\alpha = 9$ the radius increases to approximately 25 μm after the neural pulse.

	NVU	Simulation
ν_{BK}	E_{BK} see eq. 2.6	81.35 mV
G_{BK}	4300 pS	225.6 pS
Ca_4	0.15 μM	0.35 μM
v_6	-15 mV	-13.57 mV

Table 4.1: The adjusted parameters of the BK channel for the simulation described in this section and the original NVU model.

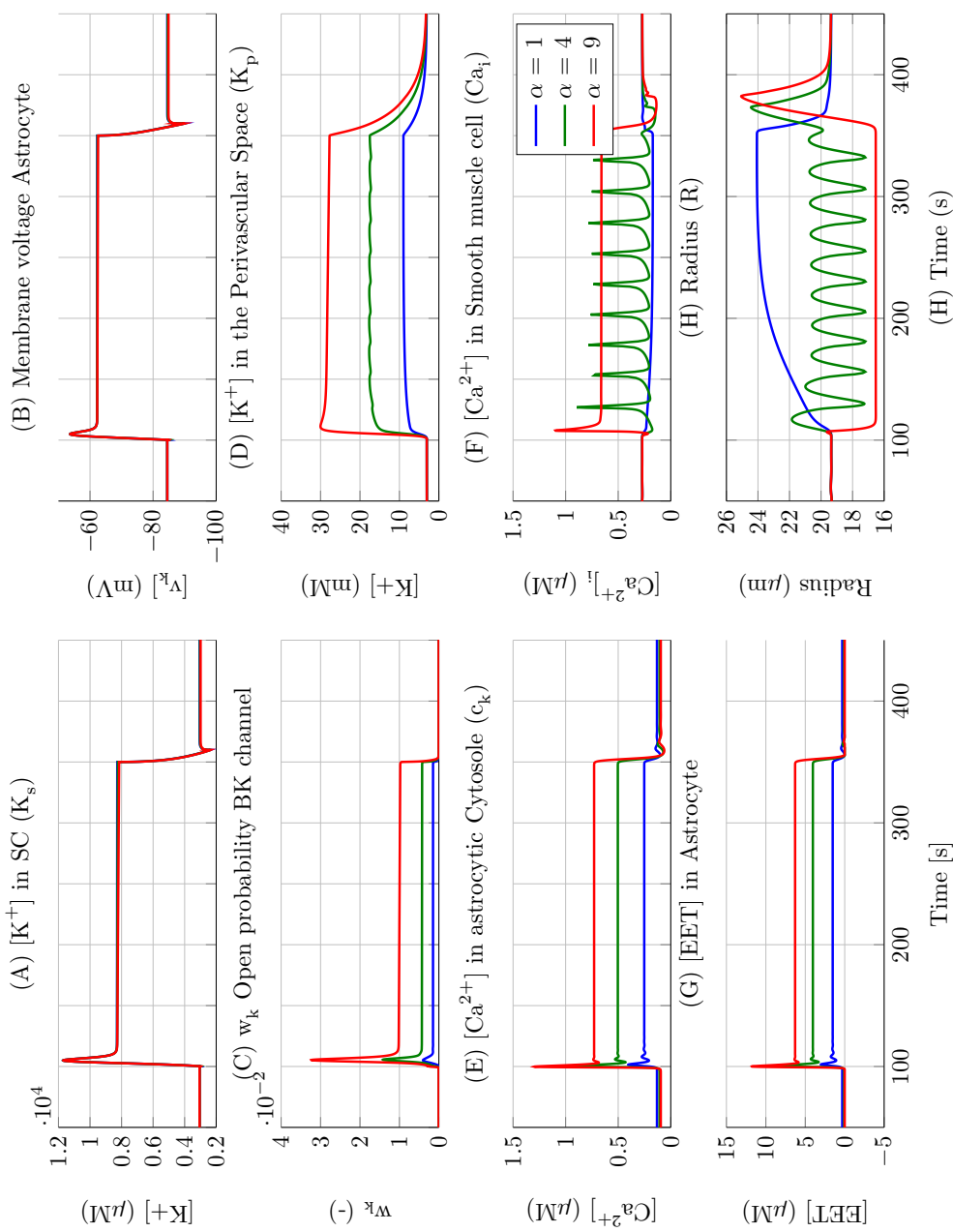


Figure 4.1: Adapted NVU model for different value's of α to simulate high concentrations of Ca^{2+} in the astrocyte. E_{BK} is considered as a constant, see table 4.1.

4.2 TRPV4

This section contains simulations with the NVU model including the changes described in chapter 3, this includes: An adapted BK channel and a stretch activated TRPV4 channel. For the TRPV4 channel two sets of parameters are used, set 1 is adapted from Witthoft et al. (2013) and set 2 is taken from Witthoft and Karniadakis (2012). Figure 4.2 shows the results of four different simulations. For set 1 and 2 there is almost no increase in c_k . For TRPV4 set 1 the membrane potential of the astrocyte increases slightly ($\pm 1 \text{ mV}$), for TRPV4 set 2 the membrane potential increases $\pm 4 \text{ mV}$ compared to the NVU model. This difference between set 1 and 2 can be explained by the difference in g_{TRPV} , see table 4.2. w_k increases which result in a higher K_p , the increase in w_k is mainly caused by the change in v_k . Compared to the NVU model the magnitude of the radius is increased and it takes around 10 seconds longer before the radius goes back to the steady state value. The TRPV4 channel reduces the delay for reaching maximal dilation compared to previous simulations with constant E_{BK} . The TRPV4 channel does not influence the calcium concentration in the astrocyte significantly, this is because the Ca^{2+} flux through the TRPV4 channel is a factor 100 smaller compared to J_{pump} and J_{IP_3} , see equation 3.12. It is unknown to which extend calcium buffering is applied to J_{TRPV} , without buffering J_{TRPV} the effect of this flux could be significant to c_k , since the value of B_{cyt} is around 0.02. To see the effect of TRPV4 without Ca^{2+} buffering equation 3.12 is changed to:

$$\frac{dC_{a_k}}{dt} = B_{\text{cyt}}(J_{\text{IP}_3} - J_{\text{pump}} + J_{\text{ER}_{\text{leak}}}) + J_{\text{TRPV}} \quad (4.1)$$

Parameter	set 1	set 2
G_{TRPV}	50 pS	200 pS
$\nu_{1\text{TRPV}}$	120 mV	120 mV
$\nu_{2\text{TRPV}}$	13 mV	13 mV
$\epsilon_{1/2}$	0.1	0.16
γ_{Ca_i}	0.01 μM	0.2 μM
γ_{Ca_e}	0.2 mM	0.2 mM
τ_{TRPV}	0.9 s^{-1}	0.9 s^{-1}
γ	834.3 $mV\mu M^{-1}$	1970 $mV\mu M^{-1}$
C_{astr}	40 pF	40 pF
κ	0.1	0.04

Table 4.2: Parameter setting for the TRPV4 channel, set 1 is adapted from Witthoft et al. (2013) and set 2 is taken from Witthoft and Karniadakis (2012)

Figure 4.3 shows simulations without Ca^{2+} buffering for J_{TRPV} . For set 1 c_k increases significantly (35%) during neural input due to J_{TRPV} . This results in a higher w_k and an increase in K_p . For TRPV4 set 1 the delay for the radius reaching the maximum dilation is decreased to 15 seconds. Compared to the NVU the dilation is still prolonged for approximately 10 seconds longer after the neural input ends. TRPV4 set 2 gives oscillations during neural stimulation. Also for $\alpha = 4$ in figure 4.1 oscillations were observed, but the frequency is

higher. In figure 4.1 oscillations were only found in the PVS and SMC (including radius), in figure 4.3 the oscillations are also present in the astrocyte (c_k , EET and w_k). This shows clearly the bidirectional behaviour of the TRPV4 channel, the feedback from the vessel to the astrocyte.

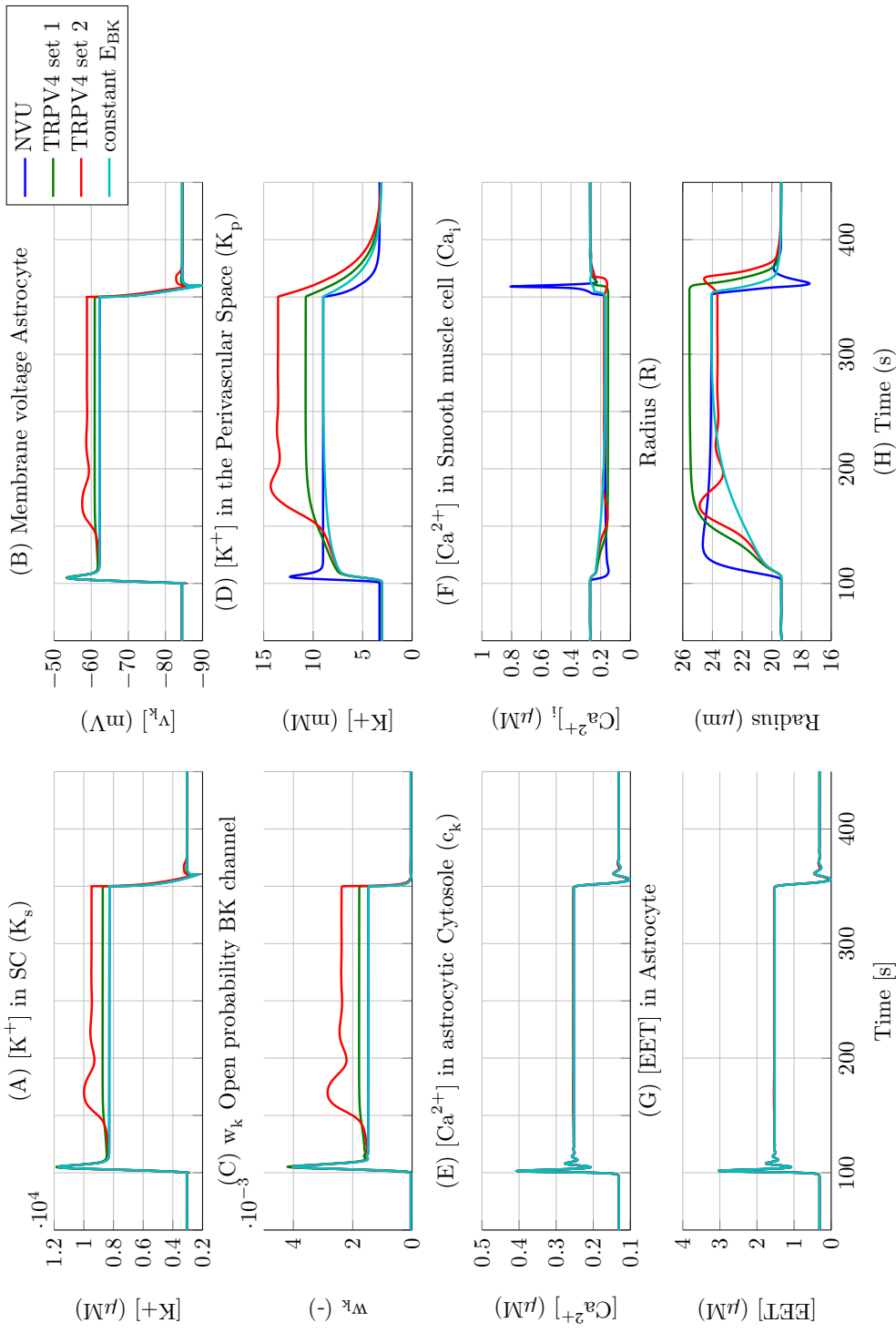


Figure 4.2: The results for simulations with TRPV4 channel. Blue line = Original NVU model; light blue line = Constant E_{BK} , green line = TRPV4 set 1; red line = TRPV4 set 2.

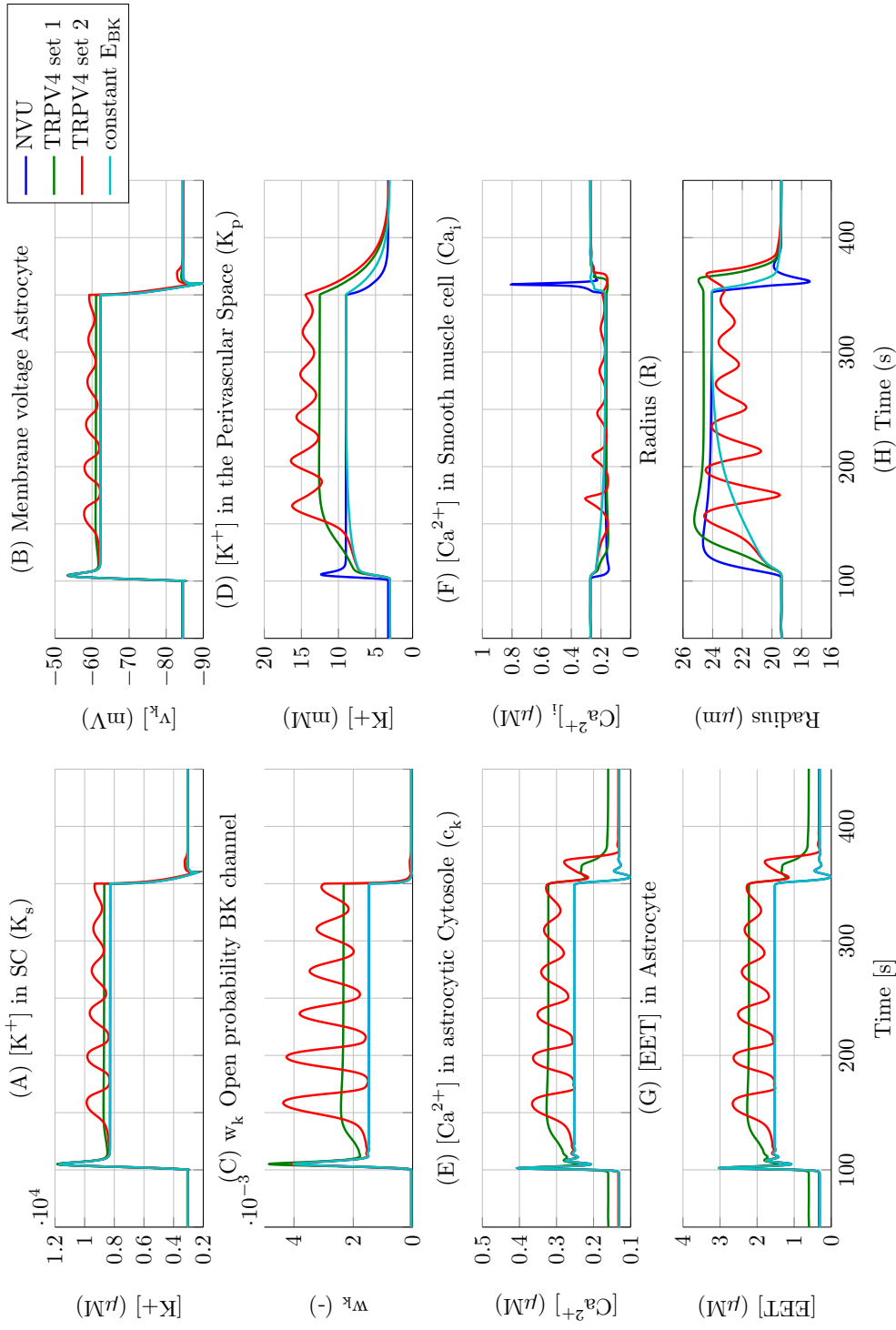


Figure 4.3:

Chapter 5

Discussion

5.1 BK channel

Changing the Nernst potential in equation 2.6 back to a constant reversal potential resulted in a model where the calcium concentration in the astrocyte is an important factor. The magnitude of the conductance of the BK channel is derived from experiments to a more realistic value. Moderate levels of c_k result in dilation and high levels result in constriction of the artery (figure 4.1). In the original NVU model both levels of c_k result in dilation, which is inconsistent with the results of Dunn et al. (2013) and Girouard et al. (2010). Using a reversal potential is correct when $\frac{c_e}{c_i} = \text{constant}$, in this case $c_e = [K_p]$ and $c_i = [K_k]$, during neural stimulation this fraction is not constant. So this solution is less physiological than using the Nernst potential and in contradiction with the Goldman-Hodgkin-Katz current equation, which is similar to the equations used in the NVU model. A possible explanation is that the NVU describes the whole astrocyte in one single point, a lumped parameter model without spatial gradient in $[K_k]$. So the potassium flux from the SC into the astrocyte has immediately an effect on the potassium concentration in the astrocytic endfoot where the BK channel is located. This is not physiologically, a delay of this effect could already provide a solution for this problem. This delay could increase the difference $v_k - E_{BK}$ so that the potassium flux J_{BK} also increases. After a neural pulse the radius of the adapted model increases slower compared to the NVU model, see the blue line in figure 4.1(H). When a TRPV4 channel is added the delay is smaller but still significant (± 10 seconds), see the difference between the blue and green line in figure 4.2(H). In the work of Farr and David (2011) a similar problem is described, a non-physiological delay of 25 seconds before reaching maximum dilation, note that similar equations are used for the BK channel. Witthoft et al. (2013) introduces a KIR channel at the astrocytic endfoot to solve this delay. Their results suggest that KIR channels take account for the fast responds to neural input and the BK channel is responsible for sustaining the response. It would be interesting to see the effect of this KIR channel implemented in the NVU model.

5.2 TRPV4 channel

A TRPV4 channel is added to the NVU model. For both sets of parameters, the addition of a TRPV4 channel prolongs dilation after the neural input is stopped. The signal is prolonged 10 seconds longer than in the NVU model, see figure 4.2. For TRPV4 set 1 the magnitude of the radius increases during stimulation, this is caused by an increase in w_k , due to the higher v_k and/or c_k , results in a higher K_p . For TRPV4 set 2 the magnitude of radius decreases compared to the NVU model. The addition of a TRPV4 channel does not result in constriction, because the c_k does not reach high enough levels, even when J_{TRPV} is not buffered at all. Calcium buffering is an unknown factor, the quantity of calcium buffering in the astrocytic endfoot and in the soma is most likely not the same. Experiments from Dunn et al. (2013) shows that the presence of an TRPV4 agonist GSK results in an average increase in endfoot $[Ca^{2+}]_i$ of $154 \pm 23\text{nM}$. Figure 4.3 shows that c_k increases with 80 nM in addition with a TRPV4 channel without buffering J_{TRPV} (set 1). When buffering is included there is almost no increase in c_k , see figure ???. This could be an argument to not buffer the J_{TRPV} flux. Although during the experiments the calcium concentration was measured in the astrocytic endfoot, this not an option in the current NVU model since it is a lumped parameter model. The TRPV channel is adapted from Witthoft and Karniadakis (2012), although their model has similarities to the NVU model, it is less extensive.

Bibliography

- K. M. Dunn, D. C. Hill-Eubanks, W. B. Liedtke, and M. T. Nelson, Proceedings of the National Academy of Sciences **110**, 6157 (2013).
- H. Girouard, A. D. Bonev, R. M. Hannah, A. Meredith, R. W. Aldrich, and M. T. Nelson, Proceedings of the National Academy of Sciences **107**, 3811 (2010).
- K. Dormanns, E. van Disseldorp, R. Brown, and T. David, Journal of theoretical biology **364**, 49 (2015).
- A. Witthoft and G. E. Karniadakis, Journal of theoretical biology **311**, 80 (2012).
- H. Farr and T. David, Journal of theoretical biology **286**, 13 (2011).
- I. Østby, L. Øyehaug, G. T. Einevoll, E. A. Nagelhus, E. Plahte, T. Zeuthen, C. M. Lloyd, O. P. Ottersen, and S. W. Omholt, PLoS computational biology **5**, e1000272 (2009).
- J. M. Gonzalez-Fernandez and B. Ermentrout, Mathematical biosciences **119**, 127 (1994).
- M. Bennett, L. Farnell, and W. Gibson, Journal of theoretical biology **250**, 172 (2008).
- M. Koenigsberger, R. Sauser, J.-L. Bény, and J.-J. Meister, Biophysical journal **91**, 1663 (2006).
- J. A. Filosa, A. D. Bonev, S. V. Straub, A. L. Meredith, M. K. Wilkerson, R. W. Aldrich, and M. T. Nelson, Nature neuroscience **9**, 1397 (2006).
- C. Hai and R. A. Murphy, Annual review of physiology **51**, 285 (1989).
- F. T. Horrigan and R. W. Aldrich, The Journal of general physiology **120**, 267 (2002).
- K. E. Donk, L. V. D. (2013).
- A. Witthoft, J. A. Filosa, and G. E. Karniadakis, Biophysical journal **105**, 2046 (2013).
- J. A. Filosa and J. A. Iddings, American Journal of Physiology-Heart and Circulatory Physiology **305**, H609 (2013).

- B. Nilius, J. Vriens, J. Prenen, G. Droogmans, and T. Voets, American Journal of Physiology-Cell Physiology **286**, C195 (2004).
- H. Watanabe, J. Vriens, A. Janssens, R. Wondergem, G. Droogmans, and B. Nilius, Cell calcium **33**, 489 (2003).
- J. L. Stringer and E. W. Lothman, Experimental neurology **101**, 132 (1988).
- J. Wagner and J. Keizer, Biophysical Journal **67**, 447 (1994).

.2 Appendix B: Documentation for NVS



3rd year Internship Report

May 25th - August 25th 2015

Dominic ROBERTS

University Supervisor:

Pierre CHAINAIS

Institution Supervisor:

Tim DAVID

Acknowledgements

I want to thank Tim, for remembering me after all these years and for taking me on.

I also want to thank all of the BRATS and UCHPC team for treating me so well throughout my stay. In particular, I want to thank Kon and Kathi for cheerfully putting me under their wing, and keeping an eye on me.

Finally, thank you Moritz, Eva, James, Aaron, Liz, Allannah, Stuart, Sweetlin, William, Henry and anyone else I may have forgotten for the good times.

Introduction

The primary foci of the third-year DAD (Decision Making and Data Analysis) course at *L'Ecole Centrale de Lille* are machine learning and its applications, applied mathematics, and basic principles of software engineering. For data scientists, this last domain may appear off-topic as successful data processing is first and foremost determined by well-chosen machine learning algorithms and data cleansing.

However, code used to implement such techniques inevitably becomes complex, due to the scale or diversity of the data used. If the code is re-used often on datasets of a similar nature, such tasks may also become repetitive. Basic, but well-designed software is a useful tool for avoiding such complications.

Indeed, machine learning is not the only domain in which complexity and repetitiveness become issues for researchers: my end-of-year 3-month internship, from May 25th to August 25th 2015, at the UCHPC centre in the University of Canterbury, Christchurch, New Zealand was an excellent opportunity for discovering how software can benefit researchers working in the biomedical sector.

This experience not only enabled me to build on the previous experience in software engineering I gained during my gap year but learn about working in a research-oriented environment rather than a corporate one. The following report details the nature of the work I carried out during my internship and how I believe I have benefitted from it.

Contents

Acknowledgements	2
Introduction	3
1 Introduction	5
1.1 UCHPC	5
1.2 BRATS	5
1.3 Medical/socio-economical context	5
1.4 Context of the internship	5
1.5 NVU	6
2 User interface of the NVS	7
2.1 Individual .ini files	7
2.2 Connections file	9
2.3 Configurations file	10
3 Software architecture	10
3.1 C code	12
3.1.1 Basic description	12
3.1.2 Issues of numerical stability with the forward Euler method	12
3.1.3 Implementation of the ODE solver	13
3.2 Topological sorting	14
4 Output and plotting	16
4.1 HDF5 files	16
4.1.1 Description	16
4.1.2 Chunking	16
4.2 Plotting	17
4.3 Comparing results with existing simulation code	19
5 Assessment of the internship	20
5.1 Work environment of UCHPC	20
5.2 My role in the organization	20
5.3 My internship	21
5.4 Work experience	21
Conclusion	22
Bibliography	23

1 Introduction

1.1 UCHPC

UCHPC (University of Canterbury High Performance Computing), formerly Bluefern, is a facility established offering computing services to research groups and companies in New Zealand. It was founded in 2006 by the University of Canterbury and several other main New Zealand universities including the Victoria University of Wellington and the Auckland University of Technology. Benefiting from a partnership with the government-funded New Zealand Science Infrastructure (NeSI) which provide similar services, it acquired new supercomputing material in 2011.

UCHPC's main aim is to facilitate supercomputer access to researchers. In practice, mainly researchers from the Chemistry, Physics and Engineering departments of the University of Canterbury use its services. Its 9 employees are mainly permanent IT consultants and developers responsible for maintaining the supercomputer hard- and soft-ware.

Despite my internship contract being signed with UCPHC, the work I did was more closely linked to the work of the Brains Trust Research team.

1.2 BRATS

When Timothy David was chosen to be the director of UCHPC in 2006, his position enabled him to found a research group focused around his main research interests: studying blood flow in the human brain by elaborating neurophysiological models. This research group, mainly consisting of University of Canterbury PhD students and researchers, shares the same offices as UCHPC. The BRATS team fully exploit their proximity to UCHPC as they require considerable computational power to simulate their models.

1.3 Medical/socio-economical context

As developed countries' populations age, neurovascular diseases are becoming more and more of a concern as they tend to affect older people([1]). The financial burden of these diseases is massive: for instance, in 2015 \$226 billion is expected to be spent on caring for individuals with Alzheimer's disease in the United States ([2]).

Research aiming to better understand these diseases and their effects on the human brain is thus justified in the eyes of research grant-awarding organisations such as the Neurological Foundation of New Zealand and Lottery Health New Zealand, enabling BRATS to acquire financial resources to carry out its research.

1.4 Context of the internship

Studying effects of neurovascular disease on humans at a microscopic level is a difficult task. Indeed, as the brain has a complex structure, *in situ* monitoring of behaviour of blood flow in the brain often requires overly intrusive techniques. While important parameters can be estimated by non-intrusive methods, in a majority of cases, research is therefore only feasible via computational methods.

Since the creation of BRATS, its students, interns and researchers have produced a large amount of model simulation code. As this code has become

more and more complex, simulating models has become increasingly prone to typing mistakes. Furthermore, vital parameters are often declared deep in the code and in several different places. As different team members sometimes work on different versions of the same model and reviewers from scientific journals suggest changes to existing model versions, the lack of modularity of the code was also an issue.

The BRATS team realized that all of these factors made their code impractical. One of the team came up with the idea of writing a programme named that would automatically generate simulation code using a template system. This programme would only need to receive a bare minimum of input as the syntax in the simulation code would be handled by the template system.

This programme is called the Neuro-Vascular Simulator (NVS), whose aim is to provide a user-friendly interface to a programme simulating models whose variables' evolutions are determined by coupled ordinal differential equations (ODEs).

Upon my arrival, the main structure of the NVS programme was already laid out. However, it was incomplete for several reasons: notably, it had no error-handling capabilities and was not versatile enough to handle differently structured inputs. Completing the programme was the main task of my internship.

1.5 NVU

The main biological model used to test the NVS was the Neuro-Vascular Unit (NVU), a biological model commonly encountered in BRATS' work and in other scientific publications regarding the human brain. As shown in Figure 1, the NVU describes the interaction between

- Neurons
- Astrocytes
- Endothelial cells
- Smooth Muscle cells
- Lumens (insides of blood vessels)

Each component of the NVU interacts with at least one other component. Studying the interaction between these components enables better understanding of how ion concentrations in these components influence behaviour of blood vessel walls in the brain.

The neuron receives stimulus from an external source. This stimulation affects ion concentrations inside the neuron, which in turn influence the ion concentrations in its neighbouring components, and so on until the physical structure of the blood vessel wall is affected.

It is no easy task to simulate the evolution of the ion concentrations and other variables describing the state of each component: fully describing behaviour of these variables in each component requires defining many parameters, intermediary variables and ordinal differential equations. For instance, the NVU model involves 26 state variables and 76 intermediary variables. For the NVS to be user-friendly, it was thus necessary to provide it with an easily approachable interface.

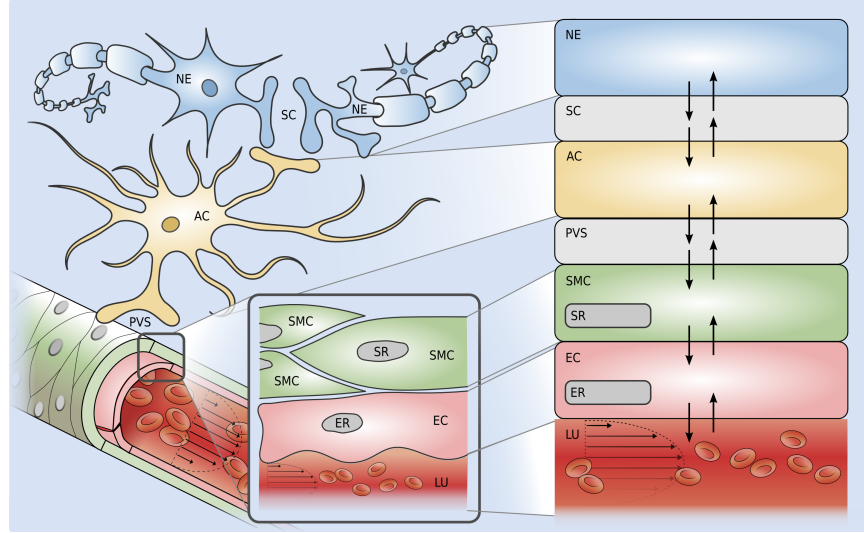


Figure 1: Overview of the NVU model, consisting of NE (neuron), AC (astrocyte), SMC (smooth muscle cell), EC (endothelial cell). The behaviour of intermediary components and lumens were not studied.

2 User interface of the NVS

2.1 Individual .ini files

In order to prevent the aforementioned typing mistakes when making changes to a model or its components, it was decided to require users to put all details of each component of a model in one individual .ini file.

An .ini file is a text file split into sections specified by headers written with the syntax [{header}]. Each header can contain properties and values written with the syntax {property} = {value}, or more headers to make nested structures.

As shown in Figure 2, all component NVS .ini files are defined by a unique identifier and by properties in the following sections:

- The [initial] section contains initial values for state variable values.
- The [parameters] section contains intrinsic parameters to the component. The nature of these parameters can be varied: for instance, chemical and physical constants featuring in differential equations can be defined as parameters as well as mechanical constants conditioning blood vessel wall movement and constants defining the external stimulus applied to the neuron. Users may specify the units of their parameters by inserting them after the parameter value, separated by a comma.
- The optional [input] section contains variables to which input from an external source will be assigned.
- The [algebraic] section contains algebraic variables, which are functions

```

identifier = example

[initial]
state_var_1 = 0
state_var_2 = 1

[parameters]
a = 2
b = 3

[input]
input_var =

[algebraic]
alg_var_1 = state_var_1 + state_var_2 - a
alg_var_2 = alg_var_1 - input_var

[ode]
dstate_var_1_dt = alg_var_1 * 3 + input_var
dstate_var_2_dt = -dstate_var_1_dt

```

Figure 2: Example of a component NVS .ini file

of parameters, state variables or other algebraic variables. Algebraic variables can be useful as intermediary variables for avoiding long differential equations as well as transformations of state variables for plotting purposes.

- The [ode] section contains the system of ordinal differential equations that define the interaction between the component’s state variables.

.ini files can be conveniently accessed by Python using the configobj module and their simple structure lends itself well to complex mathematical models. Furthermore, users do not have to master a programming language to fill out .ini files. However, some complex algebraic variables may require sophisticated functions such as piecewise functions. In these cases, users must use the syntax of the Sympy module as it is used to process the equations in the .ini files.

Despite their convenience, .ini files are not completely foolproof : it is still possible to make syntax errors, such as forgetting to close brackets, which are caught by the Sympy module. More complex errors such as missing headers and nonsensical equation order (i.e. including a variable in the right-hand side of an equation that was not declared higher up in the file) are caught and communicated to the user using assert statements. These hand-written statements are quite strict on users and also produce errors in case of redundancies, such as parameters that were declared but not used in any equations. This was to prevent sloppy declarations that could increase the file size unnecessarily.

In practice, allowing users to make such mistakes could have been avoided by providing a graphical user interface that would limit the possible number of mistakes and syntactical errors a user could make. However, this option was judged to be overly complex given that most users are likely to have enough computer programming experience to be aware of likely errors, and, more obviously, for time and financial constraints.

```

identifier = connections

[endothelialcell]
V_coup_i = smoothmusclecell.V_coup_i
J_IP3_coup_i = smoothmusclecell.J_IP3_coup_i
J_Ca_coup_i = smoothmusclecell.J_Ca_coup_i
R = wallmechanics.R
h = wallmechanics.h

[smoothmusclecell]
Ca_j = endothelialcell.Ca_j
I_j = endothelialcell.I_j
v_j = endothelialcell.v_j
K_p = astrocyte.K_p
R = wallmechanics.R
h = wallmechanics.h

[astrocyte]
J_KIR_i = smoothmusclecell.J_KIR_i
J_Na_n = neuron.J_Na_n

[wallmechanics]
Ca_i = smoothmusclecell.Ca_i

```

Figure 3: The connections file for the NVU model

After the user creates individual .ini files for each component of the model, a “connections” .ini file must be created in order to specify the nature of the interaction between each model.

2.2 Connections file

As described in Figure 3, the connections file contains one section for each component of the model. In each section, one or more equations are present:

- the right-hand side describes the inputting component and the variable it will input using class-attribute style syntax (i.e. {module}.{variable}). In some cases, the user will want the input to be constant, in which case a numerical value can be specified instead.
- the left-hand side describes the variable in the input’s recipient component to which it will be assigned.

```

input_f = """Piecewise(( F_input * g_ab / (g_a * g_b) * (1 - (t - t_0_neuron) / delta_t)**(bet - 1)
    *((t - t_0_neuron) / delta_t)**(alpha - 1) ,
    (t > t_0_neuron) & (t < t_1_neuron) ),
    (-F_input,
    (t >= t_2_neuron) & (t <= t_3)),
    (0, True ))"""


$$input_f = \begin{cases} \frac{F_{input}g_{ab}}{g_ag_b} \left( \frac{1}{\delta t} (t - t_0neuron) \right)^{\alpha-1} \left( 1 - \frac{1}{\delta t} (t - t_0neuron) \right)^{\beta-1} & \text{for } t > t_0neuron \wedge t < t_1neuron \\ -F_{input} & \text{for } t \geq t_2neuron \wedge t \leq t_3 \\ 0 & \text{otherwise} \end{cases}$$


```

Figure 4: Code for a piecewise function in an .ini file (top) and the corresponding LaTeX output (bottom)

Again, the connections file is not foolproof : error-handling is included in the Python code that processes it. For instance, it is necessary to verify right-hand sides of equations under each section to make sure the inputting module contains the specified variable.

Once each .ini file and the connections file have been examined individually, the whole set of .ini files is examined for consistency. For instance, several .ini files may contain identical identifiers.

Users can check they filled in the .ini files correctly with a .tex file that is automatically generated for each .ini file if it is considered to be syntactically and mathematically correct. As shown in Figure 4, this provides users with a prettier presentation of each model.

When designing the interaction between the connections file and the .ini component files, it can be observed that there is a slight code duplication issue: instead of creating a connections file, it would have been feasible to simply specify information in each .ini file. However, it was decided to enter all links between the .ini files in the same file in order to preserve modularity.

2.3 Configurations file

The configurations .ini file is used for defining parameters related to the configuration itself, such as overall simulation time and timestep for the differential equation solver. It is presented to the user in much the same way as the other two types of .ini file.

Users can thus input their model to the NVS software using easily configurable input files. In order to explain how these input files enable simulation of the model it is necessary to delve into the architecture of the NVS software.

3 Software architecture

As shown in Figure 5, a Python script processes the .ini files and extracts the information contained in them. This information is passed to Mako templates which generate C and Matlab files that simulate the model and output results to HDF5 files. An example of a MATLAB Mako template is illustrated in Figure 6 and the MATLAB code generated from it in Figure 7.

Mako templates are a useful tool for automatically generating large chunks of code with recurring design patterns. However, syntax for indicating Mako template instructions in code may conflict with the syntax of the code itself. For instance, the '%' symbol can be used to write comments in Octave/Matlab

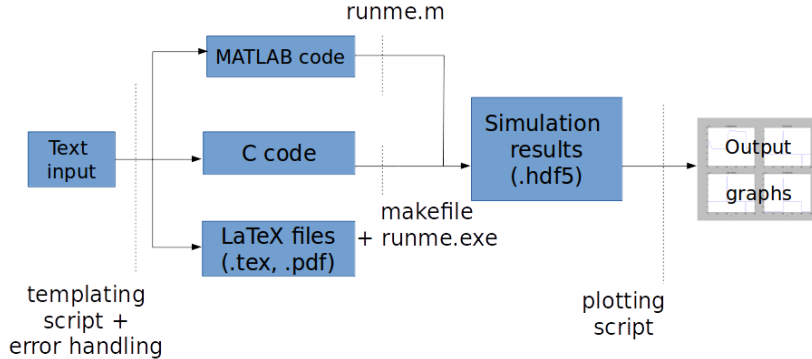


Figure 5: Layout of the NVS software

```
% for id, component in model.components.iteritems():
[f_ode_${id}, f_alg_${id}, info.components.${id}] = ${id}();
% endfor
```

Figure 6: A piece of MATLAB template code. Note that lines preceded by '%' are Python code

but is key to writing Mako control statements. Confusions such as these were taken into account when writing code templates.

Using these templates, the information extracted from the .ini files is stocked in instances of Python classes representing

- individual components of a model, containing all attributes specified in the corresponding .ini file
- the overall model, whose attributes are the individual components.

Both of these Python classes' initialization methods are lengthy and contain the bulk of the error-handling. The latter Python class also contains methods for generating the LaTeX files and the C and Matlab files.

Generating code in C and in MATLAB is key to the usefulness of the NVS as the two languages complement each other well:

- MATLAB code is readable and easily configurable, meaning it is well-adapted to quickly testing and prototyping models and verifying they gives satisfactory and consistent results.

```
[f_ode_wallmechanics, f_alg_wallmechanics, info.components.wallmechanics] = wallmechanics();
[f_ode_endothelialcell, f_alg_endothelialcell, info.components.endothelialcell] = endothelialcell();
[f_ode_neuron, f_alg_neuron, info.components.neuron] = neuron();
[f_ode_astrocyte, f_alg_astrocyte, info.components.astrocyte] = astrocyte();
[f_ode_smoothmusclecell, f_alg_smoothmusclecell, info.components.smoothmusclecell] = smoothmusclecell();
```

Figure 7: A piece of MATLAB code generated from the MATLAB template in Figure 6.

- However, C has the advantages of being far faster and will turn out to be essential if significant computational power is required. C is also an important programming language for the BRATS team as it is the only language that will work with its supercomputers. Furthermore, it is one of the only languages enabling code parallelization. This is especially important as the BRATS team plan to run several bits of NVS-generated code in parallel in order to simulate a system modelled by a collection of neurovascular units.

3.1 C code

The C code makes use of the forward Euler method to simulate state variables. This was so the ODE solver could be quickly implemented. However the forward Euler method presents several drawbacks.

3.1.1 Basic description

The Euler method is a basic way for describing behaviour of a variable whose evolution is conditioned by an ordinary differential equation.

As described in [3], let $t = (t_0 + nh, n \in \mathbb{N}) \in \mathbb{R}^{\mathbb{N}}$ be an increasing sequence of real numbers. Given an ODE with an initial condition:

$$y'(t) = f(t, y(t)), y(t_0) = y_0 \quad (1)$$

We can approximate the value of y at $t_1 = t_0 + h$ using a 1st order Taylor series expansion, assuming y is of class \mathcal{C}^2 :

$$y(t_1) = y(t_0 + h) = y(t_0) + y'(t_0)(t_1 - t_0) + O((t_1 - t_0)^2) = y_0 + f(t_0, y_0)h + O(h^2) \quad (2)$$

Applying the same reasoning to successive values of t yields the sequence

$$y(t_{n+1}) \approx y_n + f(t_n, y_n)h \quad (3)$$

which is an approximation of the function y with an error which is $O(h^2)$ for each timestep. This is known as the Euler forward method.

3.1.2 Issues of numerical stability with the forward Euler method

The main pitfall of the Euler forward method is its behaviour when faced with certain types of ODEs. As detailed in [4], when using the Euler forward method to simulate solutions to such ODEs, if the step size is too large, the generated sequence $(y(t_0), y(t_1), \dots)$ may be numerically unstable and diverge. To illustrate stability issues, let us consider the system:

$$y' = \lambda y, \lambda \in \mathbb{R} \quad (4)$$

Using the forward Euler method for this particular system with a step size $h \in \mathbb{R}_*^+$ yields the generated sequence (y_0, y_1, \dots) so that for all $n \in \mathbb{N}$

$$y_{n+1} = (1 + h\lambda)^n y_n \quad (5)$$

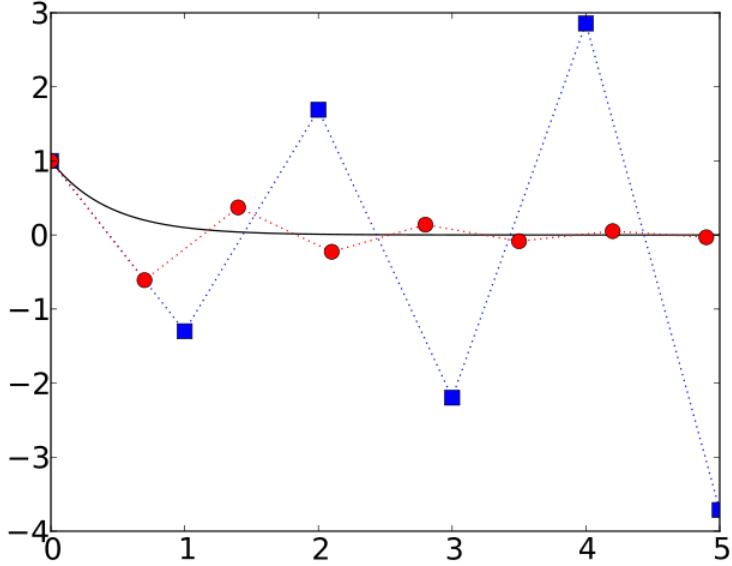


Figure 8: Illustration of the Euler method when applied to the system $y' = -2.3y$ with step sizes $h = 1$ (blue) and $h = 0.7$ (red)

The solution for the system is the function $y : t \rightarrow e^{-\lambda t}$, which converges to 0 when $t \rightarrow +\infty$. For the sequence $(y_n)_{n \in \mathbb{N}}$ to have the same property when $n \rightarrow \infty$, h must be chosen so that $|1 + h\lambda| < 1$. If this is not the case, as shown in Figure 8, the forward Euler method yields an unstable solution.

In practice, this problem was simply avoided by choosing a very small step size. However, doing so increased the necessary computation to simulate the ODEs.

A more sophisticated ODE solver such as a more sophisticated Runge-Kutta method would allow a more accurate and less lengthy simulation. Implementing this will probably be the next step of the development of the NVS.

3.1.3 Implementation of the ODE solver

The usage of the Euler solver method to update the values of the state variables is detailed in Algorithm 1. As algebraic variables are functions of state variables, they are updated at the start of each iteration using the new values of the state variables.

Two vectors u and u_{next} of length $\{\text{number of state variables}\}$ are allocated memory and populated with the initial values of state variables. For each timestep dt , u will contain the current state variable values and u_{next} will be populated using the forwards Euler method to generate the next vector of variable values.

Another vector alg of length $\{\text{number of algebraic variables}\}$ is allocated memory and will be successively populated with algebraic variable values.

Finally, the vector du of length {number of state variables} will contain the values of the right-hand sides of the ODEs.

Algorithm 1 Layout of C simulation code in the NVS

```

Initialisation :  $u, u_{next}, alg, du, dt$ 
while simulation is still running do
    populate  $alg$ 
    populate  $du$ 
     $u_{next} = u + du * dt$ 
    write  $u$  to output file
    write  $alg$  to output file
     $u \leftarrow u_{next}$ 
    clear  $alg$ 
end while
```

Output:

- output file containing state variable values
 - output file containing algebraic variable values
-

It was necessary to continually overwrite a vector containing state and algebraic variables for each timestep as one large vector containing all values over all timesteps would be too large for memory. Luckily, HDF5 files (detailed in a later section) have rapid write access meaning computational speed was not compromised.

Algebraic expressions and right-hand sides of ODEs are calculated component by component. As algebraic expressions may depend on algebraic expressions belonging to other modules, the order in which the components are processed must respect inter-module algebraic variable dependencies. Likewise, algebraic expressions may depend on other algebraic expressions belonging to the same module, meaning individual components processing order must respect intra-module algebraic variable dependencies. The order in which components and algebraic expressions inside components are processed can be determined by a topological sorting algorithm.

3.2 Topological sorting

Inter-module algebraic variable dependencies can be modelled by a directed graph like the one in Figure 9.

A topological sort of a directed graph is an ordering of its vertices that respects dependencies. Several such orders may exist: for instance, two possible topological sortings of the graph structure on Figure 8 are:

- Neuron, Astrocyte, Wall Mechanics, Smooth Muscle Cell, Endothelial Cell
- Wall Mechanics, Neuron, Astrocyte, Smooth Muscle Cell, Endothelial Cell

If the directed graph contains a directed cycle then it is impossible to topologically sort the graph. Several implementations for topological sorting exist. In this case the Kahn algorithm (1962) ([5]), detailed in Algorithm 2, was used.

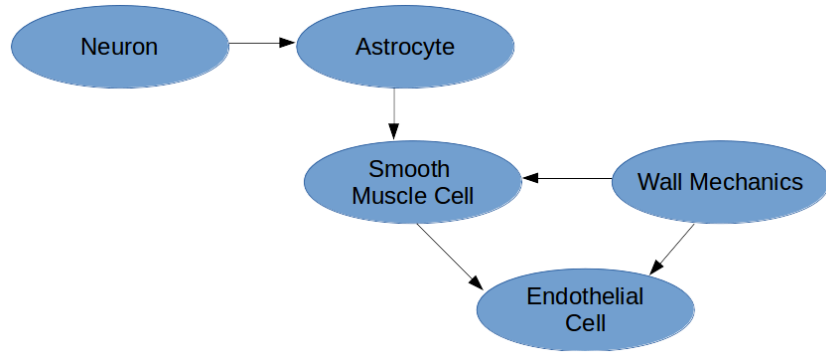


Figure 9: Graph structure of the NVU modules. If an arrow goes from A to B, it means A is dependent on B.

Algorithm 2 Kahn-topsort algorithm

Input : Directed graph $G = (N, V)$ with nodes N and vertices V

Initialisation : empty list N_{sorted}

```

while  $N$  contains nodes with no incoming vertices do
  take any node  $n_0 \in N$  with no incoming vertices
  remove  $n_0$  from  $N$  and its outgoing vertices from  $V$ 
  add  $n_0$  to tail of  $N_{sorted}$ 
end while
if  $N \neq \emptyset$  then
  Error: graph contains directed cycle
else
  pass
end if
  
```

Output: N_{sorted}

The topological sorting algorithm is only applied at one point in the NVS code, in the file nvs.py before the C templates are generated. The sorted list of components and sorted lists of algebraic variables are passed to the templates which can then initialize variables, calculate algebraic expressions and right-hand sides of ODEs and pass algebraic variables to other components while respecting both intra- and inter-module dependencies.

Once the algebraic variables and right-hand sides of ODEs are calculated at each iteration, the algebraic and state variable values can be outputted to an HDF5 file and plotted.

4 Output and plotting

4.1 HDF5 files

4.1.1 Description

HDF5 (Hierarchical Data Format) is a file format well-adapted for containing large amounts of numerical data. It was chosen to output simulation data into this format because of the short time it takes to write to it compared to writing to more traditional .txt files as well as its ubiquity compared to other similar data formats such as ADIOS. However, such advantages come at a price and writing to an HDF5 file is a complex process. Despite this, once created, accessing HDF5 files is relatively easy thanks to high-level APIs in Python.

An HDF5 file is composed of

- groups, whose role is analogous to folders in a file system
- datasets, which are arrays containing data elements contained in groups

In the case of the NVS, two datasets were necessary, one containing values for each state variable every n timesteps of the simulation and the other containing the algebraic variable values.

Each dataset is described by

- a dataspace, describing the dimensions of the array
- a datatype, describing the nature of the objects in the array (in our case, doubles)

As mentioned earlier, there is often not enough memory to contain the results of the entire simulation. Thus, data is periodically written to HDF5 to hyperslabs (chunks of the dataset) and is immediately deleted from memory if it is no longer needed for the simulation.

4.1.2 Chunking

One of the reasons HDF5 is well-adapted for stocking data is its chunking capabilities ([6]), which allow for optimized reading and writing access. Chunking allows partitioning of a dataset along certain dimensions. As illustrated in Figures 10 and 11, accessing data inside of a chunk inside of a chunked dataset can be faster than accessing the same data in a contiguous version of the same dataset.

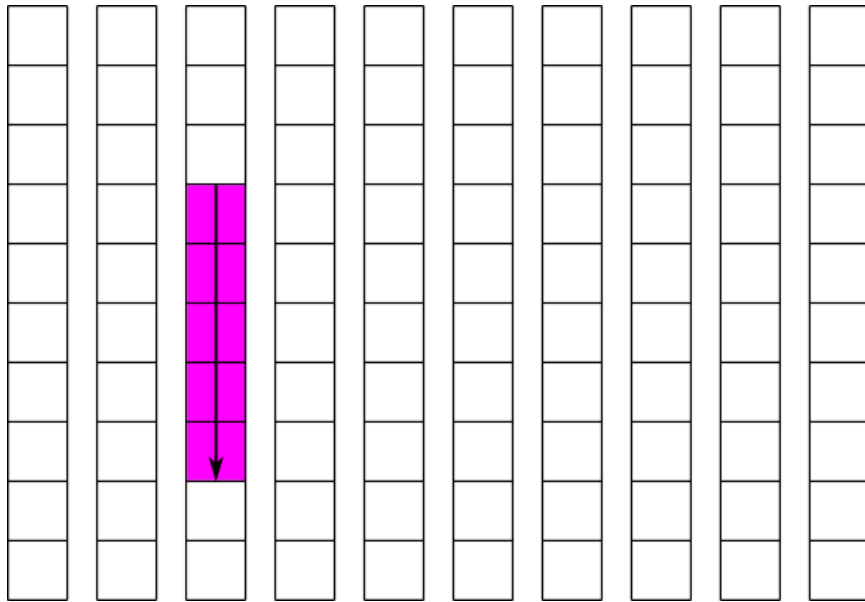


Figure 10: Accessing a chunk of memory in a vertically chunked HDF5 file. As the memory is vertically chunked, access is rapid.

In particular, chunking is essential when writing data to the dataset for each timestep. Data was thus written to datasets in horizontal chunks as one chunk represents all variable values for one timestep.

4.2 Plotting

Once full, the HDF5 files can be accessed via a Python script to plot the variables using the matplotlib module. This Python script allowed users to make limited choices concerning plotting: all state and/or all algebraic variables can be plotted at once by adding ‘state’ and ‘algebraic’ respectively as command-line arguments to the Python script. Names of individual variables can added and plotted in the same way.

Users simulating biological models will likely want to gain a global overview of the behaviour of the state and algebraic variables. As this would mean displaying a potentially large number of variable graphs to the user, deciding how to do so required some forethought: in particular, the NVU model we simulated contained 26 state variables and 76 algebraic variables. After some experimentation, it was decided to plot the variables in groups of 16 subplots per figure as shown in Figure 12. On figures where fewer than 16 variables are left to plot, the layout of the remaining subplots was organized so that there would be as few gaps as possible.

This plotting system has its limitations, however, particularly when a prime number of subplots are required as one subplot will be left unused, introducing an unaesthetic gap in the figure. Furthermore, the plotting options presented to the user are limited: individual plot colour cannot be chosen and variables

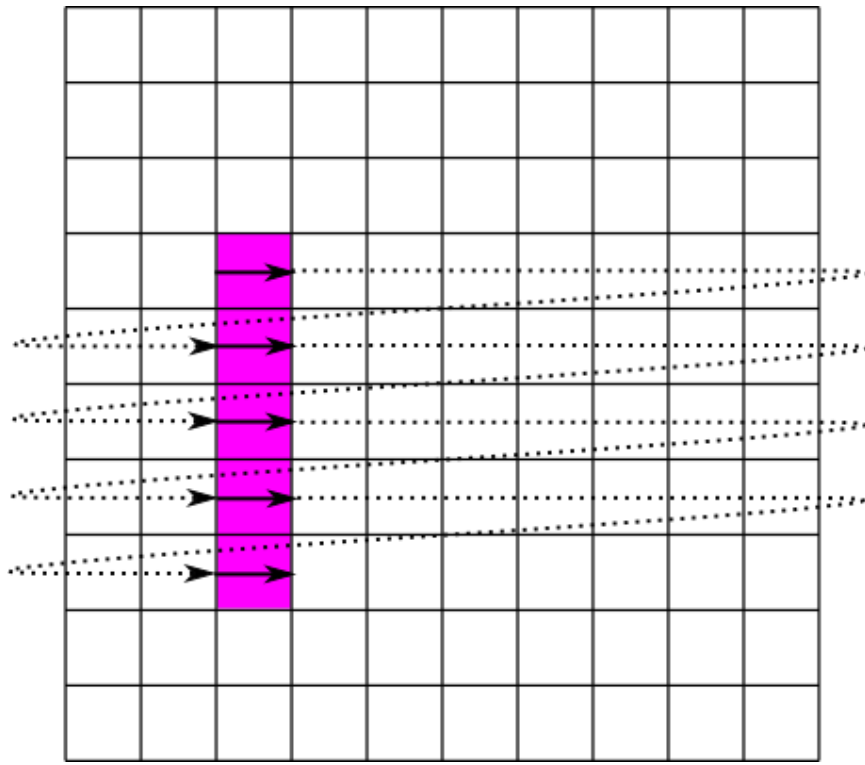


Figure 11: Accessing a chunk of memory in a non-chunked HDF5 file. Access is inefficient as the chunk of memory is not contiguous in the HDF5 file.

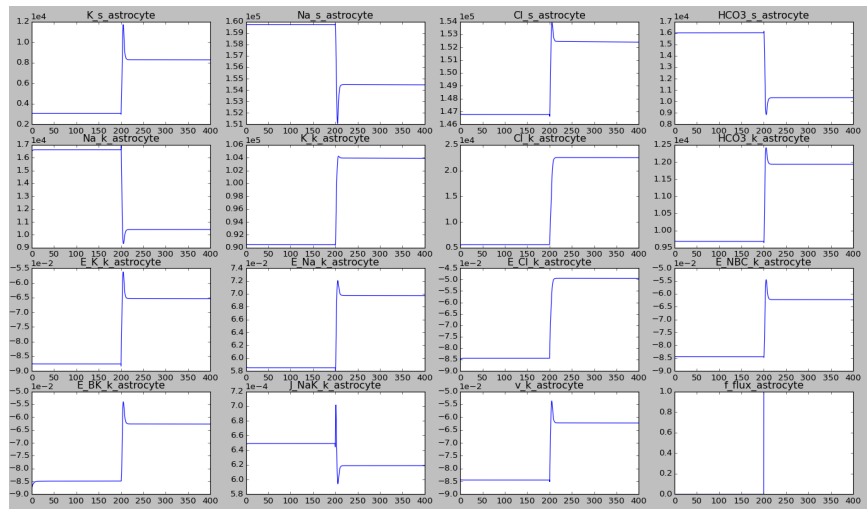


Figure 12: 16 algebraic variables belonging to the astrocyte component are plotted using the Python plotting script

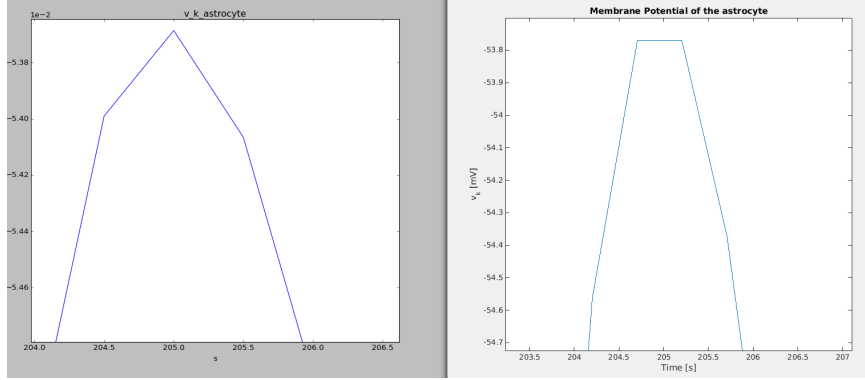


Figure 13: zoom-in of the Membrane Potential of the Astrocyte, when simulated for 500s and plotted both from the C code (left) and the MATLAB code (right)

are grouped by component and by type but the order in which they are plotted cannot be specified. Nevertheless, it was overall appreciated by BRATS team members as a pretty way of simultaneously displaying graphs of many variables.

4.3 Comparing results with existing simulation code

In order to check output was consistent with expected results, the values of the plotted variables were compared to values generated by previously written MATLAB code. Loose consistency could be evaluated at a glance by visually comparing plotted output by both sets of results.

A more qualitative comparison of results by mathematically comparing individual variable values at each timestep was tricky to obtain, as MATLAB differential equation solvers use adaptive timesteps. As illustrated in Figure 13, this meant that the two solvers were often “desynced” when confronted with differential equations for which the solution was a function containing steep curves.

However, significantly modifying our differential equation solver was not necessary as our results were only judged to differ by around 1e-4 units from the previously written code.

5 Assessment of the internship

Being part of the UCHPC/BRATS team for an extended period was an opportunity to reflect on the workplace, how I contributed to their work and what experience I gained.

5.1 Work environment of UCHPC

The offices of UCHPC/BRATS were an extremely pleasant place to work in. While its open-office layout sometimes made for a noisy environment in which it was hard to concentrate, it made for a collaborative and relaxed atmosphere. This made it easy for BRATS team members to ask each other questions and to keep up to date with progress on current tasks.

The office culture differed strongly from the corporate culture I experienced during my last two internships: office hours were extremely flexible, particularly for BRATS PhD students who often worked from home or entered and exited the office at varying hours. As peak access times for the UCHPC supercomputers were generally between 8 a.m. and 5 p.m., however, the UCHPC staff could generally not afford such flexibility.

Despite the office desks being split into two BRATS/UCHPC halves, there was no social separation between the two groups. A videoconferencing/meeting room is present next to the offices, used by UCHPC for regular videoconferences with other members of its NeSI partners but also by BRATS for catch-up meetings and for collaboration with other biomedical researchers in New Zealand universities.

5.2 My role in the organization

The UCHPC/BRATS team regularly take on interns from the University of Canterbury and from universities throughout the world, particularly from Germany and the Netherlands as the director has contacts in these institutions. Interns are mainly undergraduate biomedical engineers and help with implementing models developed by the BRATS PhD students, who act as the interns' supervisors. However, other interns such as myself are brought on to work on other topics such as software development. The work I did with the BRATS team does not quite match the description of what was written on my contract: I did not directly contribute to the development of neurovascular coupling models, but my work with the NVS should indirectly help BRATS team members prototype and simulate systems defined by their models more quickly.

Interns are generally very satisfied with their internships as they feel their supervisors actively help them to learn about their relevant subject area as well as assigning them specific tasks to do. Indeed, my supervisor was willing to gloss over my code and point out mistakes and clumsiness. I greatly valued this feedback as I realize that reading code, particularly code written by inexperienced developers, can be quite a chore. Furthermore, a wide range of expertise in many different areas is within reach of BRATS' interns: in particular, UCHPC's team are well-qualified to answer any computer-science related questions.

5.3 My internship

My internship was part of a project initiated by a BRATS team member who subsequently changed universities but who continued to work on the project. As such, we held regular Skype meetings to discuss issues that arose during development.

Thanks to my gap year, during which I was exposed to many different software engineering situations, I was already familiar with the majority of the necessary technologies and programming concepts required of me: my previous experience in Python programming, using GitHub, code templating and error handling were particularly useful. I was thus able to complete most of the work evoked earlier in this report without major difficulties, worked generally autonomously and was given a large degree of freedom while being loosely guided. Indeed, from time to time I needed reminding of the bigger picture, which my supervisor helped me with by suggesting priorities in my day-to-day task list. In critical stages in development such as the first test of NVS on the NVU model, my supervisor and I pair programmed in order to improve code quality and to watch out for any bugs.

5.4 Work experience

I particularly gained from learning about numerical simulation and its related issues, such as stability and stiffness, which I believe are crucial for confronting the mathematics obtained by theoretical arguments to the realities of producing results using limited computational resources. With the blessing of my supervisor, I also took a week off my duties with the BRATS team to follow the High-Performance Computing course at the University of Canterbury. Despite it not being directly related to my internship in the end it enabled me to better apprehend the C programming language and gave me insight on parallel computing issues. Both aspects of this experience should be useful in any career linked with manipulating large amounts of data, where fast programming languages and optimization via code parallelization are key.

Generally speaking, the task I was assigned during my internship was not especially new to me as the 6-month web development internship I did during my gap year was based on a similar software programming experience. However, I had never spent any time in a research environment, which I found quite a different experience to working in a corporate environment : in particular, there was more emphasis on the quality of work output. In my experience of working in companies, the main concern was functionality of the output rather than its quality, which is understandable given the differences between the aims of both types of institutions.

Despite my previous experience in writing scripts and software engineering, I was never able to discuss software engineering concepts in detail with my supervisors in previous internships either because it was not judged sufficiently relevant to my task or because my supervisors were not competent in the area. As the end result of this internship is software that is expected to be used by the following generation of PhD students and interns needing to simulate systems of ODEs, it was important that I learn a few extra concepts in software engineering, such as out-of-source build, in order for my software to make sense to software engineers.

Conclusion

I presented the concepts behind the NVS and gave a live demonstration of the software capabilities at a seminar to representatives from the Mechanical Engineering, Mathematics and Computer Science departments of the University of Canterbury a few days before the end of my internship period. It received a warm reception from attendees who agreed that it would be a useful tool for research communities that aim to model systems with a similar degree of complexity to BRATS neurophysiological models.

Current BRATS members are pleased with the current version of the NVS software. I hope that future BRATS PhD students and researchers can also benefit from it. If this is the case and BRATS is interesting in maintaining and updating the NVS software, improvements can still be made to it: in particular, more sophisticated differential equation solvers can be implemented, the code can be parallelized in order to improve simulation speed and systems involving higher-order or partial differential equations can be simulated.

In any case, the experience I gained during my internship at UCHPC will be invaluable to me as it allowed be to hone my software development skills, as well as exposing me to an environment I expect will be similar to the one I will be in during my PhD in the University of Illinois at Urbana-Champaign for the next four years.

Bibliography

- [1] Alzheimer's association (2015) <http://www.alz.org/facts/>
- [2] Xing Li Wang, David A. Scott (2006) Molecular Mechanisms of Tobacco-induced Diseases, p253
- [3] Michael Zeltkevic (1998) http://web.mit.edu/10.001/Web/Course_Notes/Differential_Equations_Notes/node3.html
- [4] Stephan Houben (2002) http://www.win.tue.nl/casa/meetings/seminar/previous/_abstract020220_files/talk.pdf
- [5] Lydia Sinapova (2014) http://faculty.simpson.edu/lydia.sinapova/www/cmsc250/LN250_Weiss/L20-TopSort.htm
- [6] HDF5 Group (2015) <https://www.hdfgroup.org/HDF5/doc/Advanced/Chunking/>